THE PRODUCTION OF NOVEL GLASS-CERAMICS FROM PROBLEMATIC UK WASTES USING BORATES

CHRISTINE JOAN DIMECH

A thesis submitted in fulfilment of the requirements for the degree of

DOCTOR of PHILOSOPHY

IMPERIAL COLLEGE LONDON

DEPARTMENT OF MATERIALS

London 2009

Abstract

Incineration of waste is increasing in the UK as landfill resources diminish. Municipal waste incineration produces waste residues; bottom ash, fly ash and air pollution control (APC) residues. The present research project focuses on APC residues, which are a hazardous waste arising from cleaning of incineration flue gases. APC residues must be pre-treated before disposal at hazardous landfill or placed in permanent secure storage. The aim of this research project was to produce novel glass-ceramics from optimised combinations of waste materials to provide a stabilised, safe material of value and to provide an alternative to disposal. Pre-treatment of the APC residues by washing was necessary to remove soluble chloride phases. Electrostatic precipitator (EP) dust and soda-lime glass cullet were combined with the washed APC residues as sources of glass forming oxides and borate. An optimised borate-containing silicate glass was produced from the wastes, from which dense, sintered glass-ceramics and bulk glass-ceramics were successfully fabricated. A powder sintering method was used to produce a dense sintered material from washed APC residues, EP dust and glass cullet. It was determined that the use of commercially available sodium borate (Neobor®) could be used to replace the waste source of borate to produce a sintered material of equal mechanical and physical properties. The main crystalline phases of all heat treated materials were wollastonite and gehlenite. The resulting mechanical and physical properties of the glass-ceramics and sintered materials indicated they would be acceptable as construction materials. The results of the research project indicate that thermal treatment is a convenient technology for the safe utilisation of a problematic waste (APC residues from municipal waste incineration) in new products of potential commercial interest.

Table of Contents

ABSTRACT **2**

TABLE OF CONTENTS **3**

LIST OF FIGURES **8**

LIST OF TABLES **15**

1 LITERATURE SURVEY **19**

1.1 Introduction 19
1.2 The Current Situation 20
1.3 Landfill 22
1.3.1 UK Situation 22
1.3.2 European Legislation 23
1.4 Incineration 26
1.4.1 The incineration process 26
1.4.2 Incineration of Waste Legislation 28
1.4.3 South East London Combined Heat and Power (SELCHP) 30
1.4.4 Incineration Residues 31
1.4.4.1 Bottom ash 31
1.4.4.2 Fly Ash 33
1.4.4.3 APC Residues 34
1.4.5 Disposal and Reuse of APC Residues 37
1.4.6 Stabilisation and solidification 38
1.4.6.1 Thermal treatments 40
1.4.7 Dioxins and furans 45
1.5 Silicate Glasses 46
1.6 Glass-ceramics 49
1.6.1 Glass-Ceramic Production 50
1.6.2 Glass-Ceramics in Waste Management 53
1.7 Borates 57

1.8 Borates in Glass 58

2 RESEARCH AIMS AND OBJECTIVES 61

2.1 Aims 61
2.2 Objectives 62
2.3 Research Methodology 63

3 MATERIALS AND EXPERIMENTAL PROCEDURES 66

3.1 Materials 66
3.1.1 Pre-processing of Wastes 67
3.1.2 Pre-Treatment of APC Residues 67
3.1.2.1 Washing of APC Residues 68
3.1.2.2 Calcination of APC Residues 68
3.2 Characterisation 69
3.2.1 Particle Size Analysis 69
3.2.2 X-Ray Fluorescence and X-Ray Diffraction 69
3.2.3 Scanning electron microscopy 69
3.2.4 Transmission electron microscopy 70
3.2.5 Thermo-gravimetric differential thermal analysis (TG/DTA) 71
3.3 Glass-Ceramics from Non-Vitrified Wastes 72
3.3.1 Processing routes 72
3.3.2 Formation and sintering of powder compacts 72
3.3.3 Use of sodium borate as EP dust replacement 74
3.4 Vitrification of wastes 75
3.4.1 Production of melts 75
3.5 Glass-Ceramics from Vitrified Wastes 79
3.5.1 Differential thermal analysis 79
3.5.2 Optical heating microscopy 79
3.5.3 Determination of nucleation temperature and time 81
3.6 Determination of physical and mechanical properties 82
3.6.1 Linear Shrinkage 82
3.6.2 Water Absorption 83

3.6.3 Density and Porosity 83
3.6.4 Wear resistance 84
3.6.5 Microhardness 84
3.6.6 Bending strength 84
3.6.7 Modulus of Elasticity 85
3.6.8 Coefficient of Thermal Expansion 85
3.6.9 Granular Leach Test 86

4 SINTERED MATERIALS FROM RAW MATERIAL POWDERS 87

4.1 Introduction 87
4.2 Characterisation of Material 87
4.2.1 APC Residues 87
4.2.2 WAPC residues 90
4.2.3 APC residues from other UK EfW facilities 94
4.2.4 Electrostatic precipitator (EP) dust 96
4.3 Characterisation of sintered materials 98
4.3.1 Sintering linear expansion and shrinkage 99
4.3.2 Densification of sintered samples containing EP dust 102
4.3.3 Microstructure analysis 102
4.3.3.1 TEM analysis of sintered material SB2 107
4.4 Characterisation of sintered materials containing Neobor® 111
4.4.1 Linear expansion and density 111
4.4.2 Water absorption 113
4.4.3 Microhardness 117
4.4.4 Distilled water leach test 117
4.4.5 Microstructure analysis 118
4.5 Chapter Summary 128

5 GLASS AND GLASS-CERAMICS FROM VITRIFIED APC RESIDUES 129

5.1 Introduction 129
5.2 Glass melts 129
5.2.1 Optimisation of the addition of WAPC residues 131

5.2.2 Effect of borate addition 132
5.3 WAPC residues from other UK EfW facilities 135
5.4 Mechanical and physical properties of Glasses 137
5.4.1 Vickers microhardness 137
5.4.2 Bending strength 138
5.4.3 Modulus of elasticity 138
5.4.4 Distilled water leach test 139
5.5 Powder sintering of glass 141
5.5.1 Densification of powder compacts during sintering 141
5.5.1.1 Effect of heating rate 144
5.5.1.2 Effect of powder particle size 148
5.5.2 Nucleation and crystallisation studies of glasses 153
5.6 Microstructure of sintered glass-ceramics 157
5.6.1 SEM analysis of sintered glass-ceramic 157
5.6.2 TEM analysis of sintered glass-ceramic 162
5.7 Mechanical and physical properties 162
5.7.1 Bending strength 162
5.7.2 Modulus of elasticity 163
5.7.3 Density and porosity 163
5.7.4 Leach test of sintered glass-ceramic 164
5.7.5 Wear resistance and Microhardness 164
5.7.6 XRD analysis 166
5.8 Bulk crystallisation 166
5.8.1 Nucleation and crystallisation analysis of glass GB6 167
5.9 Microstructure of bulk glass-ceramic 167
5.10 Mechanical and physical properties 179
5.10.1 Microhardness 179
5.10.2 Density and porosity 180
5.11 Chapter Summary 180

6 CONCLUSIONS 182

7 FURTHER WORK 186

7.1 Optimisation of APC residue washing pre-treatment.....186
7.2 Large scale production.....187
7.3 Mechanical properties of sintered material containing Neobor®.....187
7.4 Porous aggregate.....188
7.5 The use of glass in solid oxide fuel cell technology.....188
7.6 Thermal shock of glass and glass-ceramics.....189
7.7 Economic viability of processes and large scale production trials.....189

8 APPENDIX 1.....198

List of Figures

Figure 1-1: Energy from Waste (EfW) Incinerator..... 28

Figure 1-2: Schematic of silicate glass structure showing randomly orientated tetrahedra containing a network modifier..... 48

Figure 1-3: Glass-ceramic processing routes a) conventional method b) modified conventional method c) petrurgic method as defined by P. McMillan [1]..... 52

Figure 1-4: SEM image of a glass-ceramic formed from vitrified municipal incinerator fly ash showing dark areas of residual glass phase, bright nucleation sites and crystalline phase (grey) [33]..... 57

Figure 2-1: Methodology diagram showing lines of investigation for the development of novel glass-ceramic materials from waste materials..... 64

Figure 3-1: Overview of glass-ceramic processing routes developed and investigated in this project..... 73

Figure 3-2: Image of a glass powder compact showing position of height and diameter measurements..... 81

Figure 4-1: XRD trace of crystalline phases in as-received APC residues..... 89

Figure 4-2: Secondary electron SEM micrograph of as-received APC residue..... 89

Figure 4-3: Secondary electron SEM micrograph of soft agglomerates of washed APC residues..... 92

Figure 4-4: XRD trace showing crystalline phases in APC residues washed at different liquid to solid ratios..... 93

Figure 4-5: TG-DTA results for as-received APC residues heated at 10^{o}C/min to 1200^{o}C showing associated weight loss, endothermic and exothermic changes. 95

Figure 4-6: TG-DTA results for washed APC residues heated at 10°C/min to 1200°C showing associated weight loss, endothermic and exothermic changes. 95
Figure 4-7: XRD patterns of as-received APC residues from different UK EfW facilities ('noise' past 55 2θdegrees are not significant features). 97
Figure 4-8: XRD patterns of WAPC residues from different EfW facilities washed at a L/S ratio of 20. 97
Figure 4-9: XRD pattern of EP dust showing main crystalline phases. 98
Figure 4-10: Sintering temperature versus change in linear dimension for samples containing different concentrations of EP dust. 101
Figure 4-11: Sintering temperature versus bulk density for samples containing different concentrations of EP dust. 101
Figure 4-12: XRD pattern of sample SB2 sintered at 950°C for 2 hours. 105
Figure 4-13: Material SB2 sintered at 900°C for 2 hours showing early stages of bladed crystal formation. 105
Figure 4-14: Material SB2 sintered at 950°C for 2 hours showing bladed crystals and cubic crystalline matrix. 106
Figure 4-15: Material SB4 sintered at 950°C for 2 hours showing well-developed crystalline structure composed of a high percentage of cubic crystal phase (x1000). 106
Figure 4-16: Material SB2 sintered at 1000°C for 2 hours showing bladed crystals and pore voids. 107
Figure 4-17: TEM bright field image of sample SB2 sintered at 950°C for 2 hours (x30,000) and X-ray diffraction patterns. Area 1 is a single crystalline phase whilst area 2 corresponds to a polycrystalline area. 109

Figure 4-18: TEM bright field image of sintered sample SB2, area 2, polycrystalline matrix (x30,000) showing homogenously distributed crystals of < 0.5µm.....110
Figure 4-19: Center dark field (-g) diffraction pattern from polycrystalline area 2 in Figure 4-17. Inset image shows crystalline diffraction pattern. 1000mm camera lens.....110
Figure 4-20: EDX spectrum of crystalline area rich in titanium (area 1 in Figure 4-18).....111
Figure 4-21: Macrograph of sintered samples NB1-4 heat treated at different temperatures a)950^{o}C b)1050^{o}C c)1100^{o}C d)1150^{o}C.....114
Figure 4-22: Plot of linear expansion versus sintering temperature of samples containing different concentrations of sodium borate. 115
Figure 4-23: Plot of density versus sintering temperature of samples containing different concentrations of sodium borate. 115
Figure 4-24: Plot of water absorption versus sintering temperature for samples containing different concentrations of sodium borate. 116
Figure 4-25: XRD patterns of samples NB2 and NB4 sintered for 2 hours at1150^{o}C. 116
Figure 4-26: Secondary electron SEM micrograph of sintered sample NB2 fracture surface showing interconnected pores. 119
Figure 4-27: Secondary electron SEM micrograph of sintered sample NB4 fracture surface showing closed porosity. 119
Figure 4-28: SEM secondary electron image of polished surface of sample NB4 and individual EDX element maps for Na, Al, Si, Ca, Mg, K, Zn, Cr, Fe, Ti (x500) light areas show presence of element, dark areas show absence. 120

Figure 4-29: SEM secondary electron image of polished surface of NB2 and individual EDX element maps for Na, Al, Si, Ca, K, Cr, Cl (x500)) light areas show presence of element, dark areas show absence. 122
Figure 4-30: Schematic showing fracture path with crack deflection in a glass-ceramic. 124
Figure 4-31: SEM micrograph of a fracture surface of sample NB4 sintered at 1150^{o}C for 2 hours (gold coated x2500). 126
Figure 4-32: EDX element spectrum for sample NB4 point 1, sintered at 1150^{o}C for 2 hours (gold coated). 126
Figure 4-33: EDX element spectrum for sample NB4 point 2, sintered at 1150^{o}C for 2 hours (gold coated). Peaks without labels are gold. 127
Figure 4-34: Backscattered SEM macrograph of fracture surface of sample NB4 sintered at 1150^{o}C for 2 hours (gold coated x2500). 127
Figure 5-1: XRD patterns of glasses G4 and GB6 showing halos from short range period order. 134
Figure 5-2: DTA traces of powdered glasses G4 and GB6 heated to 1200^{o}C. 135
Figure 5-3: Macrograph of vitrified WAPC residues from other UK EfW facilities: a) Portsmouth b) Marchwood c) SELCHP (November) 137
Figure 5-4: SEM micrograph of typical GB6 glass powder morphology <75μm. 142
Figure 5-5: OHM images showing effect of heating rate on sample G4 morphology after sintering at 850^{o}C. 143
Figure 5-6: OHM images showing effect of heating rate on sample GB6 morphology after sintering at 810^{o}C. 144
Figure 5-7: Plot of relative change in height (ΔH/Ho) during sintering of G4 and GB6 glass powder compacts at different heating rates (small particle size <45μm). 147

Figure 5-8: Plot of relative change in diameter (ΔR/Ro) during sintering of G4 and GB6 glass powder compacts (small particle size <45μm).....147
Figure 5-9: SEM micrographs of polished cross sections of: A) G4 glass sintered at 5°C/min, B) G4 glass sintered at 20°C/min, C) GB6 glass sintered at 5°C/min, GB6 glass sintered at 20°C/min to a final temperature of 850°C.....148
Figure 5-10: Plot of relative change in height (ΔH/Ho) during sintering of G4 and GB6 glass powder compacts (45-75μm). 150
Figure 5-11: Plot of relative change in width (ΔR/Ro) during sintering of G4 and GB6 glass powder compacts (45-75μm).....150
Figure 5-12: Secondary electron SEM micrographs of polished sections of sintered GB6 specimens, heating rate: 5°C/min a) <45μm grain size b) 45-75μm grain size and sintered G4specimens heating rate: 5°C/min c) <45μm grain size d) 45-75μm grain size. 151
Figure 5-13: DTA traces of GB6 glass powdered and bulk, heated to 1200°C.....154
Figure 5-14: Plot showing crystallisation peak heights versus nucleation temperature for sintered glass-ceramic from glass GB6. 156
Figure 5-15: DTA traces showing crystallisation peaks of sintered glass-ceramic from glass GB6, following different nucleation temperature hold times. 156
Figure 5-16: A) Secondary electron SEM micrograph of sintered glass-ceramic PC fracture surface showing porosity size and distribution (x100). B) Secondary electron SEM micrograph of sintered glass-ceramic PC fracture surface showing typical bladed crystal formations (x1000). 157
Figure 5-17: SEM micrographs of sintered glass-ceramic polished samples sintered at 850°C for A) 1hr B) 3hr (x1000).....159

Figure 5-18: TEM bright field image of the glass-ceramic specimen sintered at 850^{o}C (x80,000). Area 1 is crystalline, area 2 is a residual amorphous phase.....160

Figure 5-19: TEM morphology of crystal particles using centre dark field technique with - $\vec{g}$ diffraction beam. Diffraction pattern inset.....160

Figure 5-20: Selected area diffraction pattern from region 2 in Figure 5-18 showing the amorphous structure of the glassy phase.....161

Figure 5-21: EDX spectrum of Ca and Si rich crystalline area 1 indicating the presence of substituted elements.....161

Figure 5-22: EDX spectrum of amorphous area 2 depleted in Si and Ca. 161

Figure 5-23: XRD pattern showing crystalline phases within glass-ceramic from glass GB6 sintered at 850^{o}C, heating rate:5^{0}C/min, hold time: 2hrs. 166

Figure 5-24: DTA traces of powdered and bulk glass GB6 showing crystallisation peaks. 168

Figure 5-25: Macrograph of bulk glass-ceramics heated at 1^{o}C/min 15 min dwell. Upper row showing internal fracture surfaces, lower row showing external surfaces. 169

Figure 5-26: SEM micrographs of the glass-ceramic heated to 850^{o}C, 900^{o}C and 1000^{o}C, 15 minute dwell (polished surfaces) magnification x100. 172

Figure 5-27: SEM micrographs showing the crystalline phase forming in the glass-ceramic, heat treated at 850^{o}C. A) polished surface B) polished and HF acid etched, magnification x500.....173

Figure 5-28: XRD patterns of glass GB6 after heat treatment at indicated temperatures with a heating rate of 1^{o}C/minute for a hold time of 15 minutes.....174

Figure 5-29: Secondary electron micrograph of the bulk glass-ceramic heat treated at 1000^{o}C for 1 hour. 174

Figure 5-30: SEM micrographs of polished surfaces of the bulk glass-ceramic heat treated at stated temperatures for 4 hours (x50) showing the effect of temperature on crystalline morphology. 176

Figure 5-31: Secondary electron SEM micrograph showing the polished surface of a glass-ceramic treated at 1000^{o}C for 4 hours (A) showing positions of EDX point analysis (B). 177

Figure 5-32: Backscattered SEM micrograph of bulk glass-ceramic (1000^{o}C) (A) showing EDX point analysis and associated element spectrums (B).....178

List of Tables

Table 1-1: Management options for municipal waste 2007/2008 21

Table 1-2: Typical UK APC residue chemical composition. 35

Table 1-3. UK municipal waste APC composition from SELCHP EfW Facility. 36

Table 1-4. Summary of APC residue thermal treatments showing process, composition, peak treatment temperature and final product..... 41

Table 1-5: Properties of glass and glass-ceramic materials..... 53

Table 1-6. Typical glass-ceramics produced from incinerator fly ash; compositions and properties..... 56

Table 1-7: Compositions of some commercial borosilicate glasses 59

Table 3-1. Batch mixes for powder sintering. 75

Table 3-2 Batch mix compositions for trials using Neobor® as an additive. 75

Table 3-3: Batch compositions for experimental glass melts..... 78

Table 3-4: Batch compositions for optimisation of WAPC content in melts..... 78

Table 3-5: Batch compositions for optimisation of EP dust in melts 78

Table 4-1 Elemental composition of APC residues, WAPC residues and EP dust. ... 88

Table 4-2: Chloride content of WAPC residues washed at different L/S ratios determined by ion chromatography (original chloride content of APC residues 21wt%)..... 91

Table 4-3: ICP elemental analysis of APC residues washed at L/S ratio 20..... 92

Table 4-4: Vickers microhardness values for sintered samples S5, SB1-4.....100

(Standard deviations in square parentheses).....100

Table 4-5: Batch mix compositions for sodium borate trials 112

Table 4-6: ICP-AES analysis of leach test leachate liquors for sample NB4.....117

Table 5-1: Results of preliminary glass melt investigation.....130
Table 5-2: Results of increasing WAPC residue addition to glass batch mixes melted at 1400^{o}C.....132
Table 5-3: Result of increasing EP dust addition to glass batch mix.....133
Table 5-4: XRF analysis of glass GB6 (1400^{o}C, 25 minutes).....140
Table 5-5: ICP-AES analysis of glass leach test samples. 141
Table 5-6: Shrinkage measurements during sintering of GB6 and G4 powder compacts for a particle size <45μm at different heating rates. 145
Table 5-7: Shrinkage measurements during sintering of GB6 and G4 glass powder compacts for particle size 45μm-75μm. 149
Table 5-8: ICP-AES analysis of sintered glass-ceramic leach test samples.....164
Table 5-9: ware speed values (Wd) obtained from each sample tested. 165
Table 5-10: Microhardness values for bulk glass-ceramics. 179
Table 6-1: Summary of properties of the products produced from thermal treatment of APC residues in combination with other wastes.....185

List of Abbreviations

APC	Air Pollution Control Residues
BAT	Best Available Techniques
EDX	Energy Dispersive X-Ray
EfW	Energy from Waste
EP	Electrostatic Precipitator
MSW	Municipal Solid Waste
PPC	Pollution Prevention and Control
PVC	Polyvinyl Chloride
SELCHP	South East London Combined Heat and Power
SEM	Scanning Electron Microscopy
TEM	Transmission Electron Microscopy
TGDTA	Thermo-gravimetric Differential Thermal Analysis
WAC	Waste Acceptance Criteria
WAPC	Washed Air Pollution Control Residues
XRD	X-Ray Diffraction
XRF	X-Ray Fluorescence

Publications and Presentations

This research was presented at conferences and published as listed below;

Presentations:

- *Development of Novel Glass-Ceramics from Problematic UK Wastes Using Borates*. Waste And Resource Management Network (WARMNET) Conference, Nottingham UK, July 2005
- *Development of Novel Glass-Ceramics from Problematic UK Wastes Using Borates.* Junior EuroMAT, Lausanne Switzerland, September 2006

Posters:

- *Development of Novel Glass-Ceramics from Problematic UK Wastes Using Borates.* GSEPS Research Day, Imperial College London, July 2006
- *Development of Novel Glass-Ceramics from Problematic UK Wastes Using Borates*. Department of Materials Research Day, Imperial College London 2007

Publication:

- C. Dimech, C., C. R. Cheeseman, S. Cook, J. Simon, A. R. Boccaccini. *Production of Sintered Materials from Air Pollution Control Residues from Waste Incineration*. Journal of Materials Science (2008) 43: 4143–4151.

1 Literature survey

1.1 Introduction

This research was carried out in response to the growing problem of disposal of hazardous waste in the UK. With the implementation of the European Landfill Directive, UK hazardous waste must be disposed of at dedicated landfill sites with appropriate pre-treatment to meet European Waste Acceptance Criteria (WAC). Landfilling of hazardous and non-hazardous waste however, is no longer a sustainable disposal solution due to dwindling land resources and the rising cost to the waste producers. This research focuses on air pollution control (APC) residues, which are a hazardous waste arising from cleaning of flue gases during the incineration of municipal waste. Being a hazardous waste they must be treated prior to being disposed of in hazardous landfill. As the amount of municipal waste being incinerated increases so too will the production of APC residues.

A potential solution to sending hazardous waste, such as APC residues, to landfill or permanent storage is to reuse them to produce a non-hazardous, material of value. The aim of this research is to develop a technically feasible process for producing glass-ceramic materials from APC residues to provide an attractive alternative to disposal or storage. There has been relatively little research into the reuse of APC residues compared to bottom ash and fly ash, which are the other residues from municipal waste incineration. Research into stabilisation and reuse options becomes increasingly important with the increase in the number of municipal waste incineration facilities and the concurrent increase in APC residue production.

Glass-ceramics are polycrystalline, inorganic solids formed by the controlled heat treatment of suitable silicate glasses [1]. The high temperatures required to produce glass-ceramics make it a potentially suitable process for treating hazardous waste. Thermal treatments have been investigated for a range of silicate wastes often with additives such as (soda-lime) glass cullet, to tailor the chemical composition of the glass in order to conveniently alter its crystallisation behaviour.

The thesis is organised in the following manner; Chapter 1 reviews the literature related to the management of municipal waste in the UK, APC residues and the thermal treatment of silicate wastes. The methodology of approach to the research project is explained with a statement of aims and objectives in Chapter 2. The experimental procedures and techniques used are detailed in Chapter 3, which is followed by two chapters containing the results and discussion of the investigations; Chapter 4 concerning sintered materials from raw material powders, and Chapter 5 considers the development glass and glass-ceramics from vitrified APC residues and combinations of wastes. The conclusions and recommendations for further work are given in Chapter 6 and Chapter 7, respectively.

1.2 The Current Situation

Each year approximately 400 million tonnes of waste are produced in the UK, 28.5 million tonnes of which is municipal solid waste (MSW) [2]. MSW can be classified as waste originating from households, civic amenity sites, business offices and light industrial activity within a local authority area. Surveys carried out by the Department

for Food, Environment and Rural Affairs (DEFRA) have shown that the production of total municipal waste has increased steadily each year since 1996/97 by an average of 3 per cent [3]. This trend is likely to continue for the foreseeable future placing an increasing strain on landfill sites and consequently the environment.

Once MSW has been collected, there are a number of management options available, including recycling, landfill, thermal treatment or composting. Municipal waste, which is unsuitable or simply not diverted for recycling or composting will be disposed of, either by landfill or incineration. The Municipal Waste Management Statistics 2007/2008 produced by DEFRA [2, 3] illustrates the burden placed on landfill and the under use of alternative management options. The proportion of the waste managed by each option in that year is shown in Table 1-1.

Table 1-1: Management options for municipal waste 2007/2008

Disposal option	Percentage of total municipal waste collected
Landfill	54%
Incineration with Energy from Waste (EfW)	11%
Recycled/composted	34%
Other	<1%

Source: DEFRA. [2]

1.3 Landfill

1.3.1 UK Situation

Landfill has historically been the most used method of waste disposal in the UK because it is relatively cost effective and easy process compared to incineration or recycling [4]. Many years ago there was little concern about the effect that landfilling of waste might ultimately have on the environment and sites were not at a premium. Landfill sites are basically excavations in the ground which are lined to prevent leachates from escaping (although in practise no liner can completely prevent leaks), into which waste is deposited immediately upon arrival at the site. It is general procedure to cover the waste with soil each day or at regular periods during the day to prevent pests. Once full the landfill will be capped and landscaped. The degradation of organic waste within the landfill generates methane and carbon dioxide. Landfill gases will need to be vented from the landfill during its lifetime and if it is collected it can be used to generate electricity and heat. Leachate also forms and is a combination of biodegradation liquid, rain water and liquid waste [5]. Landfills are classified as hazardous, non-hazardous or inert and accept waste applicable to the classification based on the European Waste Catalogue and the Waste Acceptance Criteria. These are further explained in section 1.2.2.

Landfill still accounts for the majority of municipal solid waste disposal in the UK with 65 million tonnes of waste landfilled in 2007 [6]. However, it is becoming a scarce resource with existing landfill facilities becoming full and a very limited

number of new sites available due to lack of space. It is predicted that there is six and a half years of landfill use left at sites for non-hazardous wastes in England and Wales based on waste production and management in 2007 [6]. Public opposition has increased over time as information concerning the environmental damage caused by landfilling, such as the release of 'green house' gases and the release of liquid leachates to surface and ground waters, has become widely available and understood. Consequently there is now a general view that there should be a shift towards more sustainable methods of waste disposal. Between 2006 and 2007 the UK saw a decrease of 5% in the use of landfill and a 22% decrease since 2001 [6].

Legislation is another driving factor behind the move away from landfill as changes are made to limit environmental damage and encourage the use of alternative waste management options such as energy from waste (EfW) incineration. The legislation currently affecting landfill operation is explained in section 1.2.2.

1.3.2 European Legislation

The landfilling of hazardous waste in the UK is subject to European directives. The directives control what can be sent to landfill and any pre-treatments that may be required to reduce the hazardous nature of the waste. The aim is to minimise the environmental impact of hazardous waste disposal and encourage alternative waste management options. The directives and associated guidance for the landfilling of waste are outlined below [5, 7]:

- **EC Landfill Directive (1999/3/EC)**

The directive came into force in July 2002, and was incorporated into UK legislation under The Landfill (England and Wales) Regulation 2002. The directive requires that all landfill sites should be classified as, hazardous, non-hazardous or inert, and each will accept appropriate wastes. The wastes are classified as municipal, hazardous, non-hazardous or inert. The aim is to reduce the environmental impact that a landfill, and the waste it contains, has on the environment during its lifetime. Provisions are made within the directive to cover the siting and long-term maintenance of landfills. A number of deadlines were set for the termination of certain wastes being sent to landfill or prerequisite treatment prior to landfilling [8]:

- From July 2007 hazardous liquids e.g. corrosive, flammable, explosive or infectious will be banned from landfill. Non-hazardous liquids will be banned by 2007.
- From 16 July 2005 the co-disposal of hazardous and non-hazardous waste in landfill was banned.
- Any waste that does not meet the requirements set out in the waste acceptance criteria will be banned.

Further provisions are made covering classification of waste through the European Waste Catalogue (EWC) and Waste acceptance criteria (WAC) [7, 9].

- **European Waste Catalogue (2000/532/EC)**

The EWC lists all wastes according to the industry they originate from and classifies them as, hazardous or non-hazardous to the environment. Air pollution control (APC) residues are listed within the EWC as a hazardous waste under section 19 and coded as 19 01 07* 'solid waste from gas treatment'. If mixed with fly ash it is coded as 19 01 13* 'fly ash containing dangerous substances' [10].

- **Waste Acceptance Criteria**

The Waste Acceptance Criteria (WAC) is the procedure put in place to determine whether waste can be accepted for landfilling. The WAC came into force on 16th July 2005 and sets out the leaching limit values for all hazardous waste going to landfill. For hazardous waste there are numerical limits placed on organic content and leachable components. Testing methods are specified and it is the waste producer who is responsible for assessing waste using the WAC before transfer and disposal. Non-hazardous waste does not need to meet any specific criteria [11].

- **The Revised Waste Framework Directive**

The Revised Waste Framework Directive was signed by the European Parliament in November 2008 and came into force on the 12th December 2008. The Directive sets out a framework for waste management in the EU, promoting both reuse and recycling, including energy recovery from waste incineration as a recovery activity within a revised waste management hierarchy [12]. The UK has two years in which to

transpose it into law. This change in waste management will drive the use of EfW incineration facilities and the production of incineration residues including APC residues.

1.4 Incineration

1.4.1 The incineration process

The advantages of incineration of waste in a modern EfW facility over landfill are the sterilisation of waste, the reduction in volume, elimination of methane production and the ability to reclaim energy. The actual reduction in volume of waste depends on the composition, which may vary by region and season, and the efficiency of the individual facility. A reduction of up 90% by volume is possible in an efficient system. There are approximately eighty three [6] incineration facilities in the UK processing a range of wastes, including municipal waste, clinical waste, animal residues and sewage sludge [13]. There are currently twenty municipal waste incinerators, or EfW facilities, in operation in the UK with further facilities under construction which process only municipal waste [13, 14]. The incinerators have a system in place that allows the recovery of energy, and in some cases heat, from waste.

There are a number of different methods of waste incineration including mass burn, fluidised bed, pyrolytic and rotary kiln incinerators. Mass burn systems are commonly used for the incineration of MSW with energy recovery in the UK. Figure 1-1 shows a typical EfW facility [5]. The EfW facility supplying the APC residues for this research project uses a mass burn system with a moving grate. Such facilities operate

continuously except for maintenance shut downs (the use of multiple furnaces negates the need for complete shut down). Waste is delivered by trucks and stored in bunkers that can hold up to three day's deliveries [15]. Waste is transferred by crane to a feed chute that channels the waste onto the moving incineration grate within the combustion chamber. Waste is ignited on the grate by contact with hot combustion gases and the fire intensified by introducing primary air from below. This primary air is often drawn from the storage bunkers to prevent odours escaping from the plant. The combusting waste moves along the grate allowing the waste to be mixed and ash to fall. The heat generated by combustion is used to heat steam via a boiler. This steam can be used to provide heat or hot water to the local community. In the UK plants generate electricity using a steam turbine. It is estimated that a modern EfW facility can generate 500 kWh of electricity for every tonne of waste input [16]. A complete explanation of the function of EfW incinerators can be read in 'Waste Treatment and Disposal' by P. Williams [15].

The air pollution control systems within incineration facilities are of most importance for this project. Flue gases leave the combustion chamber carrying with them particulates. The gases include CO_2, NO_x, SO_2, HCl and H_2O, all of which are harmful to the environment apart from water vapour. Modern EfW facilities are equipped with air pollution control technology such as electrostatic precipitators and bag filters to remove particulates, scrubbers using slaked lime ($Ca(OH)_2$) to remove acid gases from the flue gas and activated carbon scrubbers to capture heavy metals and organic compounds such as dioxins and furans [17]. The process of incineration with air pollution control technology will ultimately produce bottom ash, fly ash and air pollution control (APC) residues and gases.

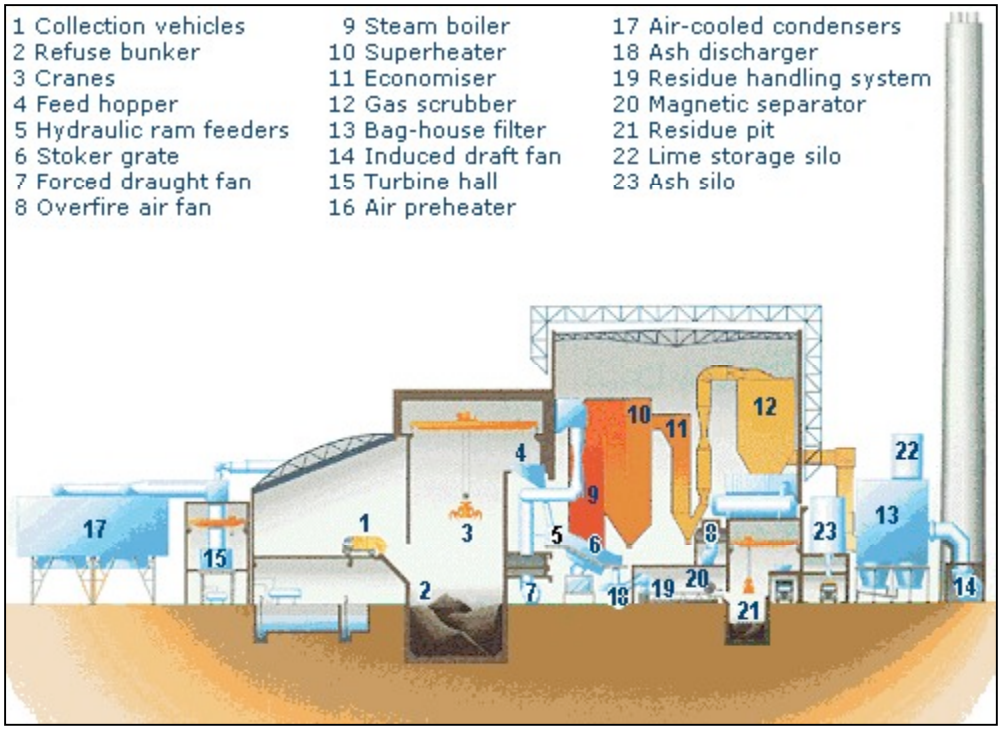


Figure 1-1: Energy from Waste (EfW) Incinerator
Source: Environmental Services Association www.esauk.org [5]

1.4.2 Incineration of Waste Legislation

Incineration of wastes is subject to a number of legislative controls. Those of most significance in relation to the incineration of municipal waste are outlined below:

- **Waste Incineration Directive (2000/76/EC)**

The aim of this directive is to reduce the pollution caused by the incineration of waste; in particular emissions to groundwater, surface water, air and soil through emission limits, operational protocols and technical stipulations such as types of particulate filtration systems. The aim is to limit and control the release of heavy metals, dioxins, NOx, SO_2 and particulates. The directive came into force in the UK in December 2002 [18].

- **Combined Heat and Power Directive (2004/8/EC)**

This European directive was introduced in December 2003 and aims to encourage the increased use of EfW incineration as a means to supply electricity to national grids across Europe, and heat in suitable areas. No specific targets for energy generation have been set, however, member countries are obliged to enable the easy connection and distribution of EfW electricity via the national grid based on transparent and non-discriminatory criteria. Member states will also be required to report on progress and incorporate the directive into national law by 21st February 2006. The UK incorporated the directive into UK law on 21st February 2004 [19].

- **Integrated Pollution Prevention and Control (IPPC) Directive (96/61/EC)**

This European directive was implemented into UK legislation via The Pollution and Prevention Control Act 1999. The aim of the directive is to limit pollution from point sources within European member countries. As well as this it aims to ensure efficiently run operations limiting waste generation, noise pollution and accident avoidance. The directive achieves this by regulating industrial activities, such as incineration of waste, using permits to operate. The issuing of permits is based on the best available techniques (BAT). This means that an incinerator will need to be using the techniques and equipment that are currently the best available, in terms of environmental protection, in order to be issued a permit. Pollution prevention and control (PPC) permits are available for all new incineration plants and those being modernised as from 31st October 1999. By October 2007 all waste management facilities, including landfills, will be required to hold a PPC permit. The BAT

information is determined by European experts and is available in BAT reference documents (BREFS) [7, 18].

- **EC Landfill Directive (1999/3/EC)**

This directive was explained in detail in section 2.1.1. It also applies to the incineration of municipal waste due to APC residues being classed as hazardous according to the EWC and so, subject to WAC at landfill. The WAC criteria came into force on 16th July 2005 and the onus is placed on the APC residue producer to treat the residues in an appropriate manner or find an alternative disposal/recycle route [7, 18].

1.4.3 South East London Combined Heat and Power (SELCHP)

The SELCHP incinerator began operating in 1994. The plant was built by a consortium of public and private organisations including the local London boroughs of Lewisham and Greenwich [20, 21].

SELCHP is a mass burn EfW facility that processes up to 420,000 tonnes of municipal waste per annum supplied by the surrounding boroughs of Lewisham, Bromley, Greenwich and Westminster. At times waste from other boroughs may be incinerated by SELCHP to keep waste input and plant efficiency high, partly due to increasing levels of recycling of household waste by the public. The facility produces electricity which is used to run the plant and excess is sent to the national grid.

Modern air pollution technology is employed including semi-dry lime and activated carbon gas scrubbers, electrostatic precipitators and bag filters.

1.4.4 Incineration Residues

1.4.4.1 Bottom ash

Bottom ash consists of burnt out, unburned and non-burnable residues that are collected from the bottom of the stoker grate [4]. Grate siftings are the finer fractions of ash that fall through the stoker grate during the combustion process and are combined with the bottom ash. Bottom ash accounts for approximately 25wt% of the incoming municipal waste. Processing of the bottom ash occurs to remove ferrous metals and/or the addition of water to cool the ash. Bottom ash is heterogeneous in nature as MSW composition varies between, and within countries, and between seasons of the year. For example areas that have high levels of materials recycling are altering the MSW input and consequently the combustion residue compositions. In winter the composition of municipal waste can vary due to road salting and extra plastics during the Christmas season.

Despite this variation in composition a number of options exist for the reuse of bottom ash rather than disposal at landfill. This is partly due to bottom ashes containing fewer heavy metals in lower concentrations than fly ash or APC residues as they are generally volatilised during combustion to later condense and combine with particulate residues [22]. If combustion does not take place in optimum conditions then this is likely to result in a higher heavy metal content in the bottom ash. Bottom ashes are used as an aggregate in road construction and filler in concrete

constructions in many countries [23]. Some countries, such as Sweden and Germany do not recycle bottom ash, or only in limited amounts, because of variations in bottom ash chemical composition due to different technologies and processes used, and legislation concerning what constitutes hazardous waste and leachate values [23, 24].

A more scientific approach to the recycling of bottom ashes has been used to develop glass and glass-ceramics. There are well established vitrification and glass-ceramic technologies, which are covered, in greater detail in chapters 3, 4 and 5. Vitrification of bottom ash, and other incinerator residues, is attractive because the process produces an inert glassy product by encapsulation, incorporation or volatilisation of heavy metals and hazardous elements. Melting or vitrification of bottom ashes produces various glassy slags and can be achieved using various technologies including electric furnaces and plasma melting [25].

Glass-ceramics can be produced from bottom ash by a number of methods to create products suitable for aggregates and building materials. It has been shown, for example that glass-ceramics produced by powder sintering are useful building materials although there are variations in properties, which limit their applications in the marketplace. For example, Appendino *et al* [26] produced a low-cost, sintered glass-ceramic with properties comparable to commercial tiles apart from a low Vickers hardness which eliminated their use as floor tiles. A further glass-ceramic produced by a different powder sintering route also possessed insufficient hardness due to porosity [27]. Such problems may be overcome by optimisation of processes with further dedicated research. Bottom ash was used in combination with fly ash and tincal ore waste (from boron processing) as a replacement for Portland cement by

Kula *et al* [28]. It was determined that these wastes in combination could successfully be used as a replacement for up to 25wt% Portland cement with the combined action of tincal waste and bottom ash having positive effect on compressive strength of Portland cement.

1.4.4.2 Fly Ash

Fly ash is composed of particulates removed from the incinerator flue gases by electrostatic precipitators. They are collected prior to the air pollution control processes outlined earlier in section 1.4.1. Fly ash resembles a grey powder, finer than bottom ash as it has been carried from the combustion chamber by flue gases. Fly ash is listed as a hazardous substance in the EWC and therefore has to be disposed of at a dedicated landfill site with suitable pre-treatment. It contains heavy metals such as lead, copper and mercury. These heavy metals are volatilised during combustion and become incorporated into fly ash particles as the temperature falls. Heavy metal concentrations depend on the presence of fluorine and chlorine which affect the heavy metal compounds formed and their presence in bottom ash or fly ash [29]. The fly ash contains less carbon and calcium oxides than APC residues as they are removed from the gas stream prior to treatment with activated carbon or lime.

A common method of treatment is to mix the ash with cementitious material to form monoliths prior to landfilling, since fly ashes do not contain such high levels of calcium (which could leach), as they have not been subjected to lime scrubbing treatments. There has also been research into the reuse of municipal waste fly ash for the production of glass and glass-ceramics [30-34].

1.4.4.3 APC Residues

APC residues are a product of the cleaning processes that the flue gases are subjected to prior to discharge to the atmosphere as outlined above. They consist of a mixture of fly ash, lime, activated carbon (and the condensed gaseous emissions) and particulates from the bag filters. APC residues account for approximately 3% by weight of the input of municipal waste [35]. Approximately 128,000 tonnes of APC residues are produced from MSW incineration each year in the UK with the twenty EfW facilities producing approximately 95% of UK APC residues [13]. The output of APC residues is expected to increase in the future by approximately 40,000 tonnes per annum [13].

The residues are hazardous and must be disposed of at dedicated hazardous landfill sites according to the EU Landfill Directive, EWC and WAC. The following codes apply to APC residues according to the classifications stated in European Waste Catalogue (2002) [36]:

10 01 18* wastes from gas cleaning containing dangerous substances.
10 01 19* wastes from gas cleaning, other than those mentioned in; 10 01 05, 10 01 07 and 10 01 18.

APC residues can contain a wide range of elements (refer to Table 1-2 and Table 1-3), varying between incineration facilities, with the main constituents being O, Si, Ca, Al, Cl, K, Na, S and Fe, mainly as oxides. APC residues are an environmental hazard due to their heavy metal and highly mobile alkaline salt content, in particular calcium, sodium, and potassium oxides and chlorides. If disposed of in landfill and exposed to

liquids, these oxides will form highly alkaline leachate that has the potential to pollute soil, ground waters and surface waters. Table 1-3 shows the typical chemical species present in a UK derived APC residue greater than 1% by weight. The sample used for this research project was taken from the SELCHP EfW facility in London, UK. The weight percentages will vary over time according to season and content of input.

Table 1-2: Typical UK APC residue chemical composition.

Element	Total Metals (mg/kg)*
Aluminium	10,000-24,000
Arsenic	10-210
Barium	70-400
Calcium	30-35wt%
Cadmium	100-150
Cobalt	9-14
Chromium	12-200
Copper	350-600
Iron	3000-5200
Mercury	<1-16
Potassium	9000-24,000
Magnesium	4000-6000
Manganese	350-500
Molybdenum	2-13
Sodium	13,500-20,500
Nickel	15-35
Phosphorus	1500-3000
Lead	2500-3500
Antimony	200-500
Selenium	<1-6
Tin	200-800
Titanium	900-4000
Thallium	<1
Vanadium	<30
Zinc	4000-8500
Bromine	1000-2000
Fluorine	100-1500
Chlorine	16wt%

*Aqua regia digest
Source; Resource Recovery Forum, 2004 in Rani et al [13].

The calcium oxides can be attributed, at least in part, to the lime scrubbing. Polyvinyl chloride (PVC) is responsible for the vast majority of chloride species present in combustion residues and gases; removing PVC through processing for recycling therefore reduces the chloride concentration within the combustion products. In this way, removal of PVC from the waste stream is advantageous for the environment. A reduction in the content of PVC however, reduces the calorific content of the waste and less energy will be derived per tonne of waste burned. There is an ongoing drive in the UK towards households recycling as much of their waste as possible, including plastics so it is possible that a reduction in APC residue chloride content will occur over time.

Table 1-3. UK municipal waste APC composition from SELCHP EfW Facility.

Chemical species	% weight
Aluminium oxide	3
Calcium oxide	53
Chlorides	21
Potassium Oxide	4
Sodium oxide	5
Silicon dioxide	5
Sulphur trioxide	5
Zinc oxide	1
Others	3

Source: XRF analysis carried out by independent materials analysis laboratory CERAM for author as XRF facility not available in university department.

The composition of APC residues varies between countries according to their input waste and the incineration and air pollution control technology used. Chloride levels are particularly variable. The presence of PVC in municipal waste is greater in more

developed and westernised countries where it is used extensively in food packaging. As mentioned previously the amount of PVC o be incinerated is being reduced through recycling efforts in the UK. The UK APC residues being studied contain approximately 21% chlorides. This is comparable to 23% in Korea [37], <18% in Belgium [38] and 9% and 12% in China.

1.4.5 Disposal and Reuse of APC Residues

Incineration of waste has not always involved the reclamation of energy and air pollution legislation has become increasingly stringent over recent decades. Therefore research into uses of APC residues has a relatively short history compared to other wastes such as bottom ash. APC residues are currently disposed of rather than recycled, as there is no technology currently established specifically for this waste. Up until 16 July 2005 APC residues were disposed of in hazardous waste landfill. After this date the residues were subject to the WAC and needed to be treated to meet the criteria for hazardous landfill or be placed in permanent storage [39]. As APC residue is a highly alkaline dry powder it can be used to neutralise acidic liquid wastes prior to landfill [40, 41]. By mixing with waste water or other solution a solidified product is achieved, which can be more easily handled than a dry powder for placement in landfill [13]. Treatment of residues in this way does not meet the WAC limits for disposal at hazardous waste landfill but they can currently be disposed at a UK treatment plant that has derogation of the WAC limits [13, 42]. Prior to the introduction of WAC 12% of UK APC was used for waste neutralisation whilst 88% of APC residue was being landfilled in bags or mixed with water to form

a solid waste [41] . APC residues are also disposed of by storage in sealed containers in disused, UK salt mines [43, 44].

There has been relatively little research into the stabilisation for disposal and reuse of APC residues compared to bottom ash and fly ash. This may be because APC residues contain more hazardous elements than bottom ash and until recently air pollution control abatement systems varied between facilities which led to a wide variation in chemical composition. As the number of EfW facilities increases however, so too will the amount of APC residue needing treatment and disposal therefore research into possible re-use becomes increasingly important. The introduction of new EfW facilities and the refurbishment of older facilities to meet current standards have meant that air pollution control systems in the UK facilities are extremely similar in terms of hardware and technology.

Research into APC residue management can be divided into two groups: those that aim to reduce or stabilise the hazardous nature of the APC residues and those that aim to produce a useful inert material or product that has a market value.

1.4.6 Stabilisation and solidification

A traditional approach of stabilisation and solidification using cement has been found to be unsuitable for APC residues as the high soluble salt content is only partially immobilised within the cement matrix [38, 45-47]. The addition of the APC residues to cement has also been found to cause false-set of cement, which is undesirable, as the cement needs to be mixed to regain a workable consistency. Carbonation of the

set cement was carried out to gauge long-term durability. It showed that leaching of heavy metals and sulphates was not achieved and increased with time [45]. Sulphates and chlorides also failed to be immobilised by cement solidification and carbonation investigation carried out by Todorovic and Ecke [48]. This is important as carbonation is a naturally occurring phenomenon of cement and durability of the stabilised waste was not addressed in all of the literature.

Earlier, unpublished research by Pollution Prevention Resource Centre (PPRC) showed that heavy metals could be retained in a cement matrix but they too failed to completely immobilise calcium phases. It has also been recently demonstrated that chloride phases are not immobilised by solidification with cement [49]. This is due to heavy metal solubility being influenced by pH whilst salts such as Cl, K and Na are not, being free to diffuse out into solution. However, the PPRC planned to use the concrete monoliths as shore protection devices where release of soluble salts is not regarded as a hazard to the environment [50]. The disparity in results could be due to variation in APC composition or type of cement used, but full experimental details are currently unavailable. The main disadvantages of solidification and stabilisation processes are the increase in volume due to the added binders and the incomplete retention of leachable species.

Rather than try to immobilise the APC residues as-received, research has looked to completely extract the mobile fractions leaving a stabilised solid residue, which can then be disposed of safely in landfill. Different washing processes have been investigated with varying wash durations and liquid to solid ratio. In each case distilled water was used as the washing medium. Both Rouchotas [51] and Wand *et al*

[52] determined that a liquid to solid ratio (L/S) of twenty was adequate to remove 95% of chlorides and large amounts of calcium, potassium and sodium in excess of 50%. Chimenos *et al* [53] and Abbas *et al* [54] used lower L/S ratios of three and two respectively with a repeated wash process. These processes appear, in comparison over complicated for significantly less chloride removal. Repeated washings add to the expense of the process although there is less wash water to dispose of. However, optimum washing times for the removal of soluble salts in all cases was found to be between one and two hours. The recycling of APC residues must be as economical as possible so shorter processing times and limited secondary waste streams are desirable. Washed APC (WAPC) residue, if not disposed of, can be used to produce potentially useful materials via various thermal treatments. Such methods are outlined below, and are most relevant for the present research project.

1.4.6.1 Thermal treatments

Thermal treatment of wastes can be achieved by vitrification and sintering. Sintering can be carried out using vitrified materials (using the crushed/powdered vitrified product) or non-vitrified material such as WAPC residues. Table 1-4 lists a summary of research into thermal treatments of APC residues.

The use of vitrification circumvents the problem of leachable species as they can be incorporated in the glass matrix and the technology is well established having been applied to other wastes. Early investigation into the vitrification of APC residue treatment was carried out in 1994 by Corning Inc. in collaboration with Pollution Prevention Resource Centre (PPRC) [55]. They succeeded in vitrifying APC residues

with the addition of glass cullet to form an amorphous green glass capable of retaining 99.5% of the heavy metals present in the APC residues. Prior to vitrification, the APC residues were washed to remove soluble chlorides to limit hazardous gas emissions during thermal treatment. Full details and main conclusions are not known, as the research paper was not published. Pre-treatment of APC residues by washing was also used in more recent research to remove chlorides [37]. It was found that the pre-treatment led to a lower vitrification temperature compared to untreated material when no other additives were used in the batch. The resulting glass-ceramic of 3330kg.m^{-3}, prepared by melting, possessed favourable mechanical properties (fracture toughness of 1.6 MPam$^{1/2}$) making it suitable for structural and wear resistant materials.

Table 1-4. Summary of APC residue thermal treatments showing process, composition, peak treatment temperature and final product.

APC treatment	Composition of material	Peak temperature	Product produced
Sintering [52]	WAPC	800-900^{o}C	Pellets for landfill
Sintering [56]	APC	850^{o}C	Powder for landfill
Vitrification [55]	WAPC, soda lime cullet	unknown	Amorphous green glass
Vitrification [57]	APC, silica	Unknown (electric arc)	Amorphous black glass – road aggregate
Vitrification [37]	WAPC	850-950^{o}C	Glass-ceramic
Sintering [58]	APC/WAPC, clay	1170^{o}C	Lightweight aggregate
Sintering [59]	WAPC	1210^{o}C	Building products
Vitrification [60, 61]	APC, silica, sodium carbonate	1400^{o}C	Glass for reuse/disposal
Sintering [62]	APC, bottom ashes	900^{o}C	Road aggregate
Calcination [63]	WAPC, calcium phosphate gel	900^{o}C	Mineral filler in cement or road aggregate

Vitrification was successfully used in the USA with APC residue from a refuse derived fuel energy recovery facility. The residues were vitrified without pre-treatment, with the addition of silicate additives to give a dense black glass. The process was not without problems as the high treatment temperature caused the evolution of HCl gas at a rate of 1kg/hour [57]. HCl gas is produced near to glass transition temperatures [64]. Such a process would require additional emission clean-up costs. The research by Corning Inc and Kim & Kim [37, 55] has shown that the production of harmful gas emissions during vitrification was minimised by washing the APC residues. A glass containing APC residues from Bavaria, again without pre-treatment was produced from APC residues [60, 61]. A number of pure chemical additives were added, as 100% APC residue did not form a glass melt. A balance between no glass formation and dilution was found to be 38wt% APC residues, 50wt% SiO_2 and 12wt% Na_2O. The batch mix was also influenced by aiming to reduce melting time and temperature to limit heavy metal evaporation. As with the research by Kim & Kim it was observed by De Casa *et al* that washing of APC residues also lowered the temperature required for thermal treatment compared to that of untreated residues due to a relative increase in the CaO content [37, 59].

It should be noted however, that although removing chlorides helps prevent gas production, it is also possible to incorporate them into a glass matrix. Chloride-containing radioactive wastes are routinely vitrified in a number of glass systems such as phosphate and borosilicate glasses as well as glass-ceramics [65]. Research has shown that there is a limit to the amount of chlorides that can be incorporated successfully into a silicate glass at a level of 20 wt% or less [66, 67]. For concentrations higher than 20wt% a phase separation of liquid calcium chloride

and/or the evolution of chloride containing gas occurs [64, 66, 68]. A chloride containing fly ash and bottom ash mix was vitrified in a CaO-Al_2O_3-SiO_2 glass system by Siwadamrongpong *et al* [68]. Their work showed that the incorporation of chlorides depends on the availability of non-bridging oxygens; the greater the number the more chlorides can be incorporated in a bonded state with Ca^{2+} ions. It is not clear whether such a relationship would be applicable to different glass systems as investigation into the incorporation of chlorides into silicate glass containing boric acid (H_3BO_3) showed the critical factor was the molar ratio of boric acid to chlorides [69].

Washing of APC residues was used by Quina *et al* [58] to enhance the process of producing lightweight aggregate. The washing procedure involved a two-batch extraction of soluble compounds at a liquid to solid ratio of 10 for 10 minutes to effectively increase the proportion of oxides Fe_2O_3, SiO_2 and Al_2O_3 in the washed APC residue. When combined with clay and sintered at 1170^{o}C for 8 minutes the high proportion of oxide compounds decomposed causing bloating and the formation of spherical lightweight aggregate pellets. There is no mention however, of the fate of chloride compounds as the washing is purely investigated to increase bloating. The maximum amount of expansive clay that can be replaced by washed APC residues is 10% which is low compared to other thermal treatments.

Washing of APC residues has been used prior to calcination by Nzihou & Sharrock [63]. The APC residues were washed in water with a calcium phosphate gel added to separate out the soluble chlorides and retain heavy metals in the solid phase by forming metal cations substituting for calcium. The treated residue was then calcined

at 900°C as it was found that this further reduced leaching of metals by forming an insoluble crystalline structure. There was no certain end product from this research but it was suggested that the stabilised, calcined material could be used in cement blocks or as road base.

A further variation of a washing procedure for APC residues was to wash them in an iron oxide ($FeSO_4$) solution at a liquid to solid ratio of 5 for 24 hours (the wash water was recycled) [62, 70]. After drying, the treated APC residues were combined with bottom ashes at a ratio of 1:9 then heated at 900°C in a controlled atmosphere for 45 minutes. It was found that sintering did not occur but that leaching of metals was as expected for bottom ashes and the APC residues were stabilised. Again, the suggested use of the treated residues was in road construction. The applicability of the heat treatment for all APC residues as an effective process for preventing leaching of metals varied between sources of residues.

The use of APC residues in the production of marketable materials should not only be of benefit in environmental terms, *i.e.* the preservation of scarce resources and pollution prevention, but in financial terms as well. An example cost analysis based on a small scale, electric arc vitrification pilot plant showed that the cost of residue treatment was less than the market value of products such as: aggregate for air blasting, architectural blocks as well as tiles and glass wool products [57].

This literature search has shown that there are a number of possible treatments for APC residues. However, only those involving thermal treatments, in particular vitrification, show promise for providing a recycling route. Vitrification is a high-cost

process compared to solidification or stabilisation methods of APC residue treatment but this may be balanced by its superior long-term stability [39]. It is also clear that the composition of APC residues is inconsistent, varying between and within countries and through the year. This makes the successful application of any one treatment method to any APC residues hard to predict, although wide research helps to isolate problematic residue constituents making prediction more accurate.

1.4.7 Dioxins and furans

APC residues contain organic toxins polychlorinated dibenzo-*p*-dioxins and dibenzofurans. Dioxins and furans are generated during the incineration of waste as the temperature of flue gases decrease (250-450^{o}C) [71]. The carbon and lime that are used to clean the flue gases provide a surface on which the dioxins and furans condense. These toxins are of concern, as they are known to be carcinogenic and therefore hazardous to health. The presence of dioxins and furans in APC residues could make the disposal or reuse problematic. Research has been carried out to address the detoxification of APC residues. The dioxins and furans can be destroyed at high temperatures (above 700^{o}C) [72, 73]. Ward *et al* used a sintering process to heat fly ash and APC residues to 850^{o}C to detoxify as well as de-volatilise the heavy metal content [73]. However, this may be too expensive in practice unless the sintered material is used in appropriate applications rather than disposed of in landfill, as suggested in the paper. APC residues and fly ash can be added to cement but without such a detoxifying pre-treatment leaching of dioxins and furans is possible [74, 75]. High temperature treatment can cause solidification of APC or fly ash residues and blocking of equipment requiring the addition of additives prior to heat treatment [72].

Thermal treatments of APC residues, such as sintering and vitrification are energy intensive but negate the need for thermal pre-treatment as the processes occur at temperatures capable of removing dioxins and furans. Reuse or stabilisation options carried out at low temperatures, such as incorporation into cementitious materials may become less attractive if a high energy pre-treatment were required.

1.5 Silicate Glasses

Glass has been manufactured for thousands of years. It is believed that the Egyptians were responsible for developing early techniques and compositions from around 1500 B.C. [76]. The development of glass making occurred in many countries such as Italy, China, France and Syria over the centuries, through shared and independently discovered technology. Uses of glass in products as known today, such as plate glass and optics are relatively modern, first being developed in the 17^{th} and 19^{th} centuries respectively [76, 77]. Glass is an important material being used in industry for applications such as glazing, containers, glassware for cooking and chemical containment, and car windscreens [78]. Glass research continues today in order to meet the increasing technological demands placed upon it.

A glass can be defined as a solid produced by the fusion of materials which are cooled without crystallisation. Glass is amorphous, which means it lacks any long-range ($\geq$1000 atomic diameters) [79], periodic atomic order; a characteristic shared by liquids. Due to this, a glass can also be described as a super-cooled liquid. A number of elements are capable of forming glass solely or in combination with other suitable

oxides. Such elements are known as network-formers or glass-formers and include the oxides of silicon (SiO_2), boron (B_2O_3), phosphorus (P_2O_5), germanium (GeO_2) and arsenic (As_2O_5).

Glass-formers form bonds with oxygen as a tetrahedral arrangement, or triangular in the case of boron. A lattice of ions forms, identical to that of the crystalline oxide forming the glass, but distortion of bond angles during rapid cooling gives rise to the lack of long-range order in the network [1, 77].

Commercial glasses are based on silica. In a glass made up of silica (SiO_2), each silicon atom is surrounded by four oxygen atoms to form a tetrahedral structure (SiO_4). A three-dimensional glass structure is achieved by the joining of tetrathedra at their corners. The distances between silicon and oxygen atoms and between two oxygen atoms are the same as in crystalline forms of silica and leads to short-range order. The lack of long-range order within a glass is achieved by the random variation in the positions of neighbouring tetrathedra. The angle between two silicon ions (via a corner oxygen ion Si-O-Si) can vary between 120 and 180^o as well as rotations of the tetrahedra at shared corner oxygen atoms, lead to long-range disorder [78, 80].

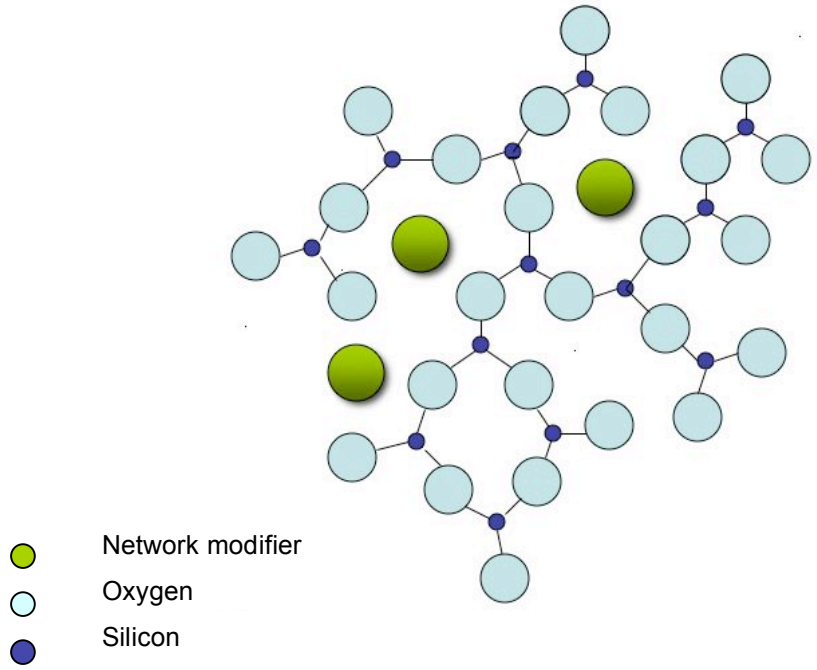


Figure 1-2: Schematic of silicate glass structure showing randomly orientated tetrahedra containing a network modifier.

Network modifiers are alkali/alkaline oxides that add positive ions to the structure, interrupting the bonds between polyhedra by attaching to an oxygen making it non-bridging. This leaves the network non-continuous and weakened (Figure 1-2). Network modifier oxides are incapable of producing a glass network alone. Examples include: sodium (NaO_2) and calcium (CaO).

The majority of commercial glasses are based on silica. The most common silicate glass is soda-lime glass, the main component of which is sand (SiO_2). The approximate composition of soda-lime glass is 75% SiO_2, 15% soda (Na_2O or Na_2CO_3) and 10% lime (CaO) [76]. It is possible to make a pure silica glass (vitreous silica) however, this requires extremely high furnace temperatures and so is prohibitively expensive to produce on a large scale. Vitreous silica possesses extremely good chemical resistance, mechanical strength and low thermal expansion. The addition of soda lowers the melting temperature and viscosity but also lowers the

mechanical strength and increases thermal expansion. The hardness and chemical durability is improved by adding lime to the batch mix [76, 77].

A common silica based glass for technical applications is borosilicate glass. Such glass contains up to 80% silica, 7%-13% boric oxide (B_2O_3), 2%-8% soda, potassium oxide (K_2O) and aluminium oxide (Al_2O_3). Borosilicate glass possesses high chemical and thermal shock resistance (due to a lower thermal expansion than silicate glass) so it is used for applications such as laboratory ware, cooking dishes, lamps and in the chemical industry [76].

1.6 Glass-ceramics

Glass-ceramics are polycrystalline solids that are formed by the controlled thermal treatment of a suitable parent glass [1]. Heat treatment causes the nucleation and growth of one or more crystal phases from the amorphous glass. When viewed under a microscope, the crystalline phases are easily distinguishable from a residual amorphous glass phase, hence the name glass-ceramic.

Glass-ceramics have benefits over traditional polycrystalline ceramics. Zero porosity can be achieved due to the parent material being a glass and therefore dense. It is also for this reason that uniformity of properties within the glass-ceramic are achievable [81]. Glass-ceramics can also possess properties that exceed those of the parent glass and they can be even better than the properties of some conventional ceramics such as mechanical strength, chemical durability and thermal shock resistance [1].

1.6.1 Glass-Ceramic Production

There are a number of methods available to produce glass-ceramics. Figure 1-3 graphically represents three commonly used methods of glass-ceramic production; the conventional method, the modified conventional method and the petrurgic method as described by P. McMillan [1].

The conventional method requires the preparation of a homogenous glass, shaped as required. In order for microcrystalline phases to develop there must be a period of nucleation followed by a period of crystal growth at a higher temperature. This stage requires careful control to achieve a homogeneous distribution of fine-grained crystals which are desirable for good mechanical strength. Nucleation is achieved by heating the parent glass at a controlled rate to a pre-determined nucleation temperature where it is held until the required number of nuclei has formed. Nucleation can be homogeneous if it occurs throughout a single phase glass, or heterogeneous if nuclei form at existing interfaces caused by, for example, phase separation, contaminant particles, colloids or bubbles. Nuclei form within the glass due to differences in free energy.

When there is a close overlap of nucleation and crystal growth temperatures then nucleation and crystallisation can be achieved with a single-stage heat treatment. This is known as the modified conventional method. Freshly molten glass can be taken directly to nucleation temperature without first cooling to room temperature. This is known as the petrurgic method.

Additives may be needed to provide adequate nucleation sites. These are known as nucleating agents. Examples of such agents are TiO_2 and P_2O_5. Nucleating agents are soluble within the glass but upon cooling or reheating are able to precipitate and act as nucleation sites from which crystal growth can take place [1]. Following nucleation the temperature is increased to allow optimal growth of crystalline phases and held at temperature until the desired degree of crystallinity is reached. The heating schedules for nucleation and crystallisation vary for individual glass compositions and the stages can be altered to control nuclei and crystal growth as well as improve processing times and costs.

Glass-ceramics can be formed from glass that has been cooled, powdered and compacted to the required shape by pressing, extrusion, hot-pressing or slip-casting. Controlled heating to initiate nucleation is similarly required although nucleation will take place at the particle boundaries. Dense glass-ceramics can be formed by this method as viscous sintering during the following stage of crystal growth leads to the closure of pore spaces [80].

The thermal expansion, durability, strength and other properties of a glass-ceramic can be controlled by varying the crystal size and type, bonding between grains, crystal orientation and degree or percentage of crystallinity. These, in turn, are determinable by changes to parent glass composition, choice of nucleating agent and heat treatment schedule [81].

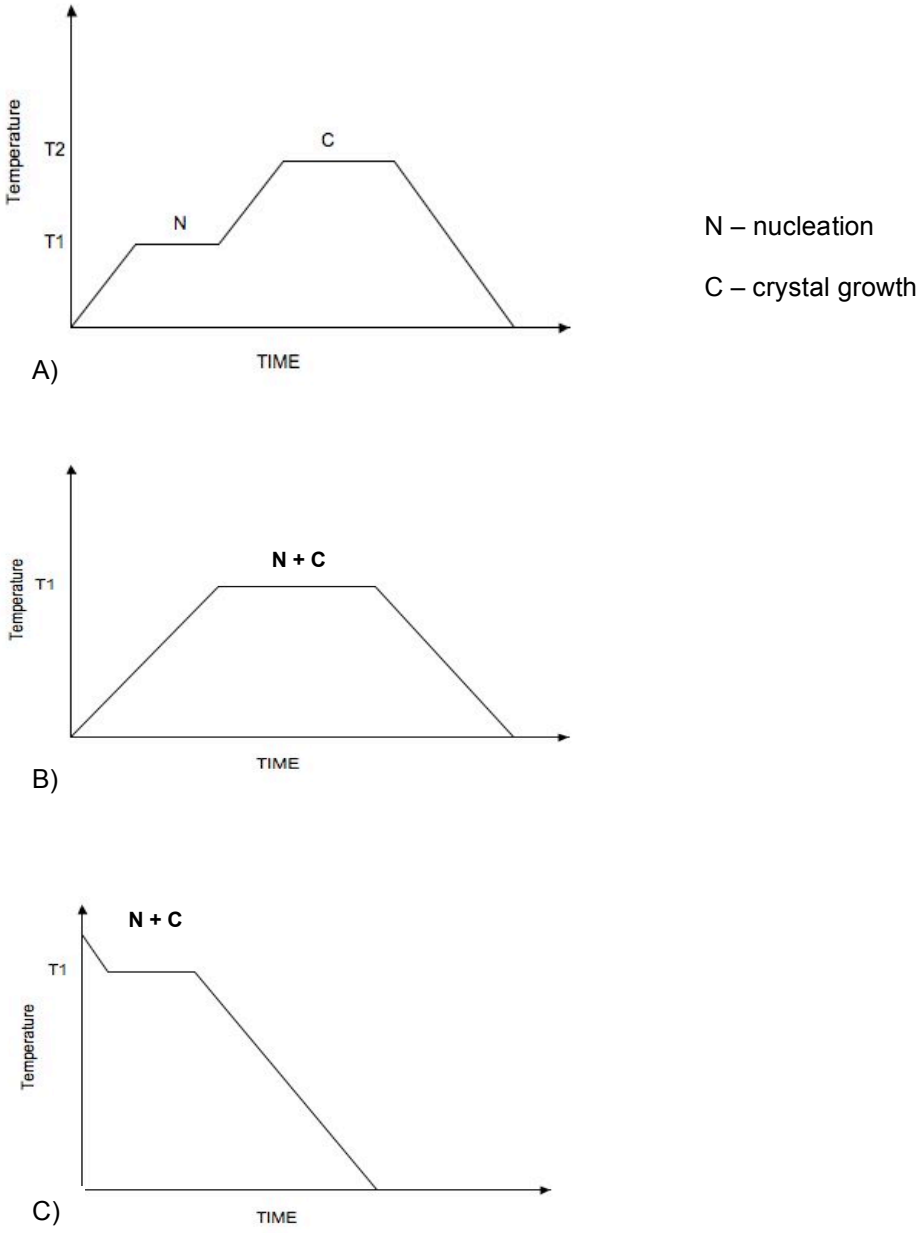


Figure 1-3: Glass-ceramic processing routes a) conventional method b) modified conventional method c) petrurgic method as defined by P. McMillan [1].

Glass-ceramics have a range of favourable physical, mechanical, chemical, thermal and dielectric properties, as well as controllable microstructures that make them excellent engineering materials [82]. Glass-ceramics can be mass produced using glass forming techniques for applications ranging from ovenware and tableware,

electrical insulators, tiles and architectural cladding [83]. Glass-ceramics are also used for highly technical applications. For example, radomes for aircraft and missiles are fabricated from glass-ceramics as they are able to meet the requirement for thermal shock resistance and mechanical strength for high-speed flight in dense atmospheres. Dielectric properties are also essential to prevent distortion of radar signals [1]. Glass-ceramics have been used in nuclear reactor rods to combine the neutron-absorbing characteristics of technical boron-containing glass with the high refractoriness and low thermal expansion of ceramics by conversion of the parent glass to a glass-ceramic [1]. Table 1-5 shows a range of mechanical and physical properties for a selection of commercial glasses and glass-ceramics.

Table 1-5: Properties of glass and glass-ceramic materials.

Properties	Density ($kg.m^{-3}$)	Young's modulus (GPa)	Bending Strength (MPa)	Thermal expansion ($x10^{-6o}C^{-1}$)	Use	Ref.
Soda lime glass	2480	74	50	8.5	Bottles, glazing	[78, 80]
Borosilicate glass (pyrex)	2230	65	55	4	Lab ware, cook ware	[78, 80]
Fotoceram glass-ceramic	2410	87	148	10.3	Automotive precision parts	[82]
Macor glass-ceramic	2520	-	104	9.4	Electrical insulator	[82]
Wollastonite	2720	-	440	6.2	Building material	[82]
Slag Sital	-	93	90-130	6.5-8.5	Cladding, roads	[82]

1.6.2 Glass-Ceramics in Waste Management

The sintering and vitrification of waste to form glass-ceramics are well-established technologies. They have been applied to many types of silicate waste and combinations of wastes of wide ranging chemical compositions. Such wastes include

coal fly ash [84, 85], wastes from mining and quarrying, e.g. borates, gold and slate [86-88], metallurgical waste from zinc and steel processing [89, 90], waste glass [91] and the bottom ash and fly ash from municipal waste incinerators [30-34]. Glass-ceramics are used to encapsulate waste in an inert or less hazardous form, as in the case of radioactive waste [65], or to produce products with market value, such as floor and wall tiles.

Thermal treatments of APC residues to produce stable materials, including glass-ceramics have been relatively limited compared to other waste streams (discussed in section 1.4.6.1). However, extensive research has been carried out into other silicate waste streams.

Fly ash from municipal waste incineration has been used to produce glass-ceramics by vitrification followed by the conventional two-stage method of nucleation followed by crystallisation. This has been achieved without the addition of additives to the as-received fly ashes [92, 93]. In other research, additives have been used. Park *et al* have carried out a number of investigations into the thermal treatment of fly ashes to produce chemically stable, diopside based glass-ceramics using SiO_2, TiO_2 and MgO as additives [94, 95]. SiO_2 is added to promote glass formation and to lower viscosity in wastes with a low level of glass-forming oxides. This may also be achieved by the addition of silicate glass waste, as used by Romero *et al* [96, 97] and Cheng [98]. The addition of sand can also be used to increase the SiO_2 content [98, 99]. Feldspar waste has also been used for this purpose by Boccaccini *et al* and Karamanov *et al*, which ultimately led to gehlenite crystalline phases due to the aluminium content of feldspar waste [34, 99]. TiO2 can be added in low amounts

(typically <2wt%) as a nucleating agent whilst additives such as MgO and $Mg(OH)_2$ are used to achieve a desired crystalline phase such as diopside or gehlenite, respectively [94, 98].

The powder method of crushing and milling of a parent glass followed by heat treatment of the powder compacts, with or without additives is used to produce sintered glass-ceramics. This processing route is favourable when a parent glass composition exhibits surface rather than bulk, nucleation and crystallisation [30, 100, 101].

Another silicate waste produced from incineration of waste is bottom ash which is similar to fly ash in composition but contains less heavy metals due to these elements being incorporated into fly ash as they condense from flue gases. As with fly ash, it is possible to produce glass-ceramics with and without additive materials. Cheeseman *et al* produced a dense sintered ceramic material from bottom ash without additives composed of diopside and wollastonite crystalline phases [27]. Other investigations into bottom ash have employed sintering of vitrified bottom ash. It was found that it was not necessary to use additives using this process as the addition of binders with the intention of improving processing of green bodies was in fact detrimental leading to swelling [102].

In a recent review paper, Wu *et al* have reported more than 100 glass-ceramic systems developed from silicate wastes [103]. Some further examples are included in Table 1-6. Figure 1-4 shows the typical microstructure of a glass-ceramic containing diopside as a main crystalline phase obtained from MSWI fly ash [32, 33].

Coal ash has also been a focus of glass-ceramic research. Coal ash is produced as a waste stream from the burning of coal in thermal power stations. As with the other silicate wastes already discussed it is possible to process coal ash with and without additives. Erol *et al* produced glass-ceramics of zero porosity by sintering powdered parent glass. Those glass-ceramics produced without any additives produced a superior material in terms of crystal structure, chemical durability and mechanical properties compared to samples containing red mud and silica [104]. The petrurgic method was used by Francis *et al* to produce glass-ceramics from a combination of coal ash and soda-lime glass (20-60wt%) [105]. The resulting glass-ceramic was a dense black material containing plagioclase and augite crystalline phases. It was found that at an increased cooling rate the magnetic crystal phase, magnetite formed.

Table 1-6. Typical glass-ceramics produced from incinerator fly ash; compositions and properties

Material	Main crystalline phase	Density $kg.m^{-3}$	Bending strength MPa	Thermal expansion coefficient (10^6 $^oC^{-1}$)	Reference
MSWI fly ash	Diopside	2890	N/A	N/A	[33]
MSWI fly ash	Diopside	2780	127	6.2	[94]
MSWI fly ash	Diopside	2890	N/A	6.5	[31]
MSWI fly ash	Augite	2740	N/A	6.0	[30]
MSWI fly ash	Ferrobustanite	2650	58	7.9	[99]

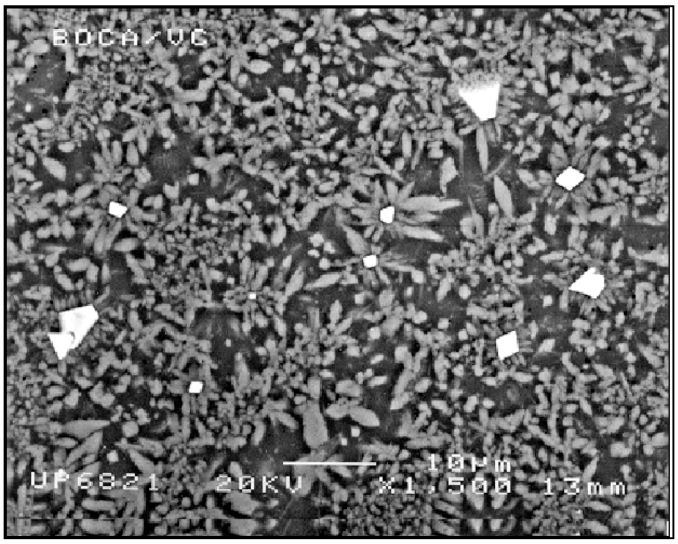


Figure 1-4: SEM image of a glass-ceramic formed from vitrified municipal incinerator fly ash showing dark areas of residual glass phase, bright nucleation sites and crystalline phase (grey) [33]

1.7 Borates

A section on borates is included here as this group of compounds was used in this research project with the aim of improving the thermal behaviour of the APC residues. Boron is the fifth element in the periodic table. It does not exist on its own but occurs naturally combined with oxygen and other elements to form borates (inorganic salts) and boric acid H_3BO_3. More than eighty species of borate ores are mined around the world [106]. The main ores mined are boric acid, tincal ($Na_2B_4O_7 \cdot 10H_2O$), Kernite ($Na_2B_4O_7 \cdot 4H_2O$), Ulexite ($NaCaB_5O_9 \cdot 8H_2O$) and Colemanite ($Ca_2B_6O_{11} \cdot 5H_2O$). These ores are refined using a range of methods to produce many different boron based products. Such products include; plant fertilizers, detergents, fire retardants, wood treatments, radioactive waste containment, glass and ceramics [106].

Boron containing wastes arise from the process of mining boron. The reuse of tincal waste has been investigated by researchers in Turkey as this is an important region for boron mining. Tincal waste is a source of SiO_2, B_2O_3, CaO and MgO and research has shown that it can be used as an additive in production of cements, wall tiles and glazes to stabilise, improve mechanical properties, decrease water absorption and reduce production costs (through reduced processing temperatures and replacement of commercial batch materials) [28, 86, 107, 108].

1.8 Borates in Glass

Boric oxide (B_2O_3) is a glass-forming oxide, capable of forming a glass without additives. The resulting glass however, is soluble in water. Vitreous boric oxide structure consists of triangular units rather than the tetrahedral ones formed in silicate glasses [77]. The structure of vitreous boric oxide is described by Shelby (2005) as being planar but forming a 3 dimensional structure as would a piece of crumpled paper, rather than that of silica which is truly 3 dimensional [80]. However, borates can also be used in multi-component glasses.

Boric oxide in various forms is commonly used as a batch ingredient in a wide range of glass compositions to improve the material properties of glass such as mechanical strength, chemical resistance and thermal shock as was discussed in section 1.5. Boric oxide was used in glass as far back as the 19th century by Michael Faraday in his research on optical glasses [77]. By far the largest use of borates nowadays is in special glass production. Examples of such glasses are fluorescent tubes, ovenware, laboratory glass, fibreglass and liquid crystal displays where special qualities, such as

those mentioned above, are desired. Table 1-7 shows typical chemical compositions of some commercial borate-containing glasses.

Table 1-7: Compositions of some commercial borosilicate glasses
[77, 80]

Glass	SiO_2	Na_2O	CaO	K_2O	MgO	Al_2O_3	B_2O_3
Heat resisting glass (labware)	81	4				2	13
Fibre glass (E glass)	54.5	0.5	17.5		4	15	8.5
Sealing glass	75	4		2		2	17

The addition of boric acid to a glass batch can act as a fluxing agent, lowering the melting temperature of glass and the melting time, improving furnace output and in turn reducing energy consumption. Boric acid (H_3BO_3) and anhydrous borax ($Na_2B_4O_7$) are commonly used in glass production as fluxes due to their low melting temperatures. They contain boric oxide which is liquid at 500^oC [77]. Introducing a component, such as boric acid to a glass batch helps to reduce the melt temperature of the entire batch by helping to dissolve remaining batch particles and providing a liquid to aid mixing [80]. Initial mixing of batch components prior to heating is also important to prevent segregation of ingredients, which inhibits the melting process. The addition of water to a glass melt can also help to reduce the viscosity, aiding mixing and accelerating melting time [80]. It is possible to introduce water by the addition, and heating of H_3BO_3.

In this research project boric acid has been considered (using electrostatic precipitator (EP) dust) as an additive to glass-ceramic silicate compositions to investigate whether its use can improve melting temperature, melting time, heat resistance, chemical

durability and/or mechanical strength of the parent glass and the glass-ceramics produced thereafter, or directly from nonvitrified powders. EP dust comes from the fume abatement systems of fibreglass production as explained in Chapter 3. Such a residue is classed as a hazardous waste and there is currently no reuse option for it. A similar waste was used to produce sintered glass-ceramics when first vitrified in combination with glass from cathode ray tubes and feldspar mining residue [109]. The waste was derived from the lime used to neutralise the acidic fumes produced in a vitrification plant and had a similar chemical composition to EP dust used in this research, with high levels of CaO, SiO_2 and B_2O_3. A glass-ceramic containing wollastonite and sanidine was produced by powder sintering of the parent glass. The wastes were chosen with the aim of producing a wollastonite based glass-ceramic to replicate Neoparie ceramics.

2 Research Aims and Objectives

This research was carried out in response to the growing problem of disposal of hazardous waste in the UK. With the implementation of the European Landfill Directive, as discussed in the previous chapter, hazardous waste must be disposed of at dedicated landfill sites with appropriate pre-treatment to meet European Waste Acceptance Criteria. This is an increasingly costly disposal route for producers of hazardous waste and a drain on the finite landfill resources within the UK.

2.1 Aims

The ultimate aim of the research project was to investigate the use of problematic UK wastes, including APC residues from municipal EfW facilities combined with selected additives, to produce novel and useful glass-ceramic materials exhibiting physical properties making them suitable for industrial applications. The disposal of APC residues is a major waste management problem in the UK and overseas. There is currently no use for APC residues which are disposed of at hazardous landfill sites. Therefore, a re-use method is sought as an alternative to costly and environmentally harmful disposal methods. In particular there is a potential for the production of glass-ceramics for industrial applications including building materials and machine components where mechanical strength and wear-resistant properties of glass-ceramics are beneficial.

The energy intensive production of glass-ceramics must be justified with the development of materials with sufficiently attractive properties to be considered for commercial exploitation. Therefore optimisation of processing, e.g. minimising the temperature of fabrication and simplification of process technology constitutes the core of the experimental programme of this project.

2.2 Objectives

The following objectives were defined to achieve the project aims:

- Characterise and understand the thermal behaviour of APC residues from UK municipal EfW facilities and of suitable waste additives, in particular boron containing electrostatic precipitator (EP) dust and soda lime glass cullet.
- Study the fundamental mechanisms involved in silicate glass-ceramic processing from chosen combinations of waste residues by the sintered powder route with the aim to optimise processing parameters (e.g. attainment of highest possible density at the lowest possible processing temperature in materials with the highest possible content of APC residues).
- Investigate and optimise the use of borates in the production of glass-ceramics from APC residues.
- Understand how variations in APC residue composition affect the processing conditions, microstructure and resultant, relevant silicate glass-ceramic properties.
- Characterise the physical, mechanical and other relevant engineering properties of glass-ceramics produced in order to identify and develop viable opportunities for commercial exploitation.

2.3 Research Methodology

A number of routes of investigation were proposed for the development of novel glass-ceramic materials from combinations of APC residues and other wastes. Figure 2-1 shows the three processing routes that were explored (full details of the techniques used are explained in Chapter 3). The research steps were categorised as inputs, processes and products. The main input, and focus of the research were APC residues in an as-received state. The APC residues were then pre-treated by washing to reduce the chloride content and facilitate thermal treatment without the formation of chloride gases. Following washing of the APC residues, EP dust and glass cullet were added in optimised combinations to reduce processing temperatures and improve the mechanical and physical properties of the materials produced.

The experimental processes can then be divided into those processes based on a parent glass, obtained by melting the residues (vitrification) or based on powder sintering without a vitrification step. A number of glasses were fabricated to derive an optimised composition, in terms of waste content and thermal behaviour, in particular the ability to crystallise to a homogeneous microstructure. The optimised parent glass was also characterised as a product of the research as it may exhibit aesthetic properties of interest. A single glass composition was used to produce a glass-ceramic via the powder sintering method. The bulk glass was milled and pressed to form a powder compact (green body) then heat-treated using a heat schedule determined by thermal characterisation of the parent glass. Sintered samples were characterised by a range of analytical techniques (refer to Chapter 3).

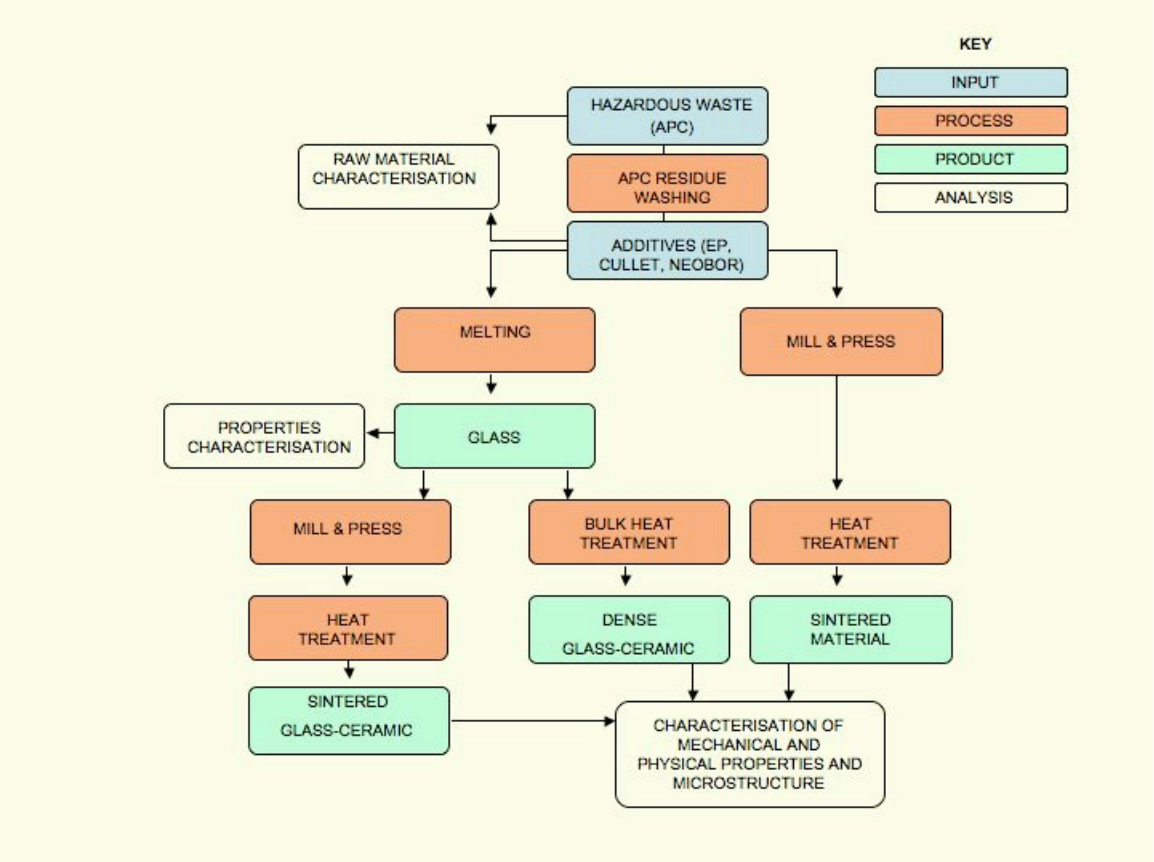


Figure 2-1: Methodology diagram showing lines of investigation for the development of novel glass-ceramic materials from waste materials.

The same parent glass was also used to produce dense bulk glass-ceramic material by selected thermal treatments. Bulk samples were heat-treated using a different heat schedule, which was derived by characterisation and thermal analysis of the parent glass and devitrified samples.

The process outlined in Figure 2-1 does not contain a vitrification stage. The washed APC (WAPC) residues were milled with glass cullet and/or EP dust then pressed to form green bodies. These samples were then heat treated according to results of thermal characterisation and analysis of sintered samples. Several compositions were

investigated in a logical process to optimise the mechanical and physical properties of the resulting sintered product. A further sintered material was produced via the same experimental procedure replacing EP dust with a commercially available source of borate to determine whether a waste stream was replaceable if supply ceased. This is an important aspect to consider if the present materials developed from combinations of wastes would reach commercial exploitation.

In total five optimised materials were produced from combinations of the aforementioned wastes; a parent glass, bulk dense glass-ceramic, sintered porous glass-ceramic and two powder sintered materials (without a vitrification stage).

3 MATERIALS AND EXPERIMENTAL PROCEDURES

3.1 Materials

Chemical and physical experimental analysis was carried out on the following selected waste materials: APC residues, EP dust and crushed soda-lime glass cullet.

The APC residues were sourced from the SELCHP EfW facility (www.selchp.com, London, UK), storage silo 2 on the 9th March 2005. The APC residues were stored in airtight plastic sacks at room temperature.

The EP dust was supplied by Rio Tinto Minerals Ltd (London, UK). The EP dust was stored at room temperature in a sealed plastic bag. The EP dust was crushed using a mortar and pestle prior to use due to clumps formed by compaction. EP dust was chosen as an additive as it contains boron as well as being a problematic waste. EP dust is listed as hazardous waste under the EWC. In addition to EP dust, sodium tetraborate pentahydrate ($Na_2B_4O_7 \cdot 5H_2O$) was used as a commercial source of boric oxide (B_2O_3) in experimental batch compositions for comparison purposes. This chemical was supplied by Rio Tinto Minerals Ltd. Further characterisation of this commercial product was not necessary since all relevant information was available from the supplier.

Building aggregate company, Day Aggregates (London, UK) supplied the recycled crushed soda lime cullet which was produced from glass of mixed colour collected from bottle banks in London.

3.1.1 Pre-processing of Wastes

The APC residues, EP dust and glass cullet were received direct from the producers without any treatment. APC residues did not require any processing prior to washing as the as-received state is a fine free-flowing powder. The EP dust was ground using a pestle and mortar to break up the large agglomerations caused by compaction on the electrostatic precipitator. This treatment was to facilitate accurate weighing for batch mixes. The glass cullet was received crushed to an average particle size of 5mm. Prior to use the cullet was washed in distilled water and dried in an oven at 105^{o}C for 24 hours. The glass cullet was milled in 50g batches in a Tima mill for a duration of 2 minutes to produce a powder that could be easily weighed for use in batch mixes (and subsequent milling to desired particle size).

3.1.2 Pre-Treatment of APC Residues

Two methods of pre-treatment of APC residues were investigated. The objective of pre-treatment was to reduce the chloride content of the as-received APC residues and so facilitate the thermal treatment required to produce glass-ceramics. The pre-treatments were washing with distilled water to remove soluble compounds and calcination to release volatiles. These two methods of pre-treatment are outlined below.

3.1.2.1 Washing of APC Residues

APC residues were washed in distilled water at liquid to solid ratios: 5, 10, 20 and 40 to form WAPC residues. For example, a liquid to solid ratio of 20 required 20ml distilled water for every 1g of APC residues. A washing ratio of 20 was selected based on chloride removal, the literature search (Chapter 1) and previous research carried out at Imperial College [51]. The APC residues were weighed then added to the corresponding amount of distilled water in a glass beaker. The beaker was covered to prevent evaporation or spillage and the contents stirred for two hours using a magnetic stirrer at a medium speed. The liquor was filtered under vacuum using a 542 Whatman filter paper using a buchner flask and funnel. The filtered solids were dried for 24hrs at 105°C then crushed using a pestle and mortar. The washed APC powder was stored in a sealed plastic container.

3.1.2.2 Calcination of APC Residues

APC residues were heated in a fireclay crucible at 770°C for 6 hours using an electric furnace (Lenton). The calcination temperature was determined by TG/DTA analysis of as-received APC residues. The heating duration was based on the literature search of calcination of fly ashes (Chapter 1). The calcined APC (CAPC) residues were crushed to a powder using a mortar and pestle and stored in an airtight plastic container.

3.2 Characterisation

3.2.1 Particle Size Analysis

Mean particle size and range of APC and washed APC residues were measured using a Malvern Mastersizer laser particle analyser with a 300mm lens (1.2-600μm detectable particle size range). Distilled water was used as the transport medium.

3.2.2 X-Ray Fluorescence and X-Ray Diffraction

X-ray fluorescence (XRF) was used for quantitative elemental analysis of raw materials, WAPC residues and glass samples. Analysis was carried out by CERAM (Stoke-on-Trent, UK) [110].

Crystalline phases in raw materials and thermally treated samples were analysed by means of X-ray diffraction (XRD) for bulk and powdered samples. A Philips PW1700 series automated powder diffractometer and Cu Kα radiation with a secondary graphite crystal mono-chromator was used. The 2θ range was 5^{o} to 100^{o} with a step size of 0.04^{o} and 1.4 second scan time.

3.2.3 Scanning electron microscopy

A JEOL JSM 840 scanning electron microscope (SEM) was used to examine the microstructure and elemental compositions of glass-ceramic batch materials and their fusion products with a voltage of 20kV applied. Secondary electrons were used to

produce images and perform elemental analysis. The microscope was equipped with a backscattered electron detector. Chemical composition of samples was acquired using energy dispersive X-ray (EDX) analysis.

Powdered samples of the batch materials were mounted on stubs and carbon coated. Solid samples were set in resin, manually ground using silicon carbide grit papers (320, 800, 1200 and 4000) then polished to a 1μm finish using diamond paste. Solid samples for fracture surface observation were mounted on stubs. All samples were coated with carbon or gold. The coatings are conductive and are required to allow the flow of electrons away from the sample surface. If the surface of the sample becomes charged the image generated will be of poor quality. Gold, being a superior conductor to carbon, was used to produce high quality images. Carbon coating was used where possible for EDX, as carbon has few electrons, unlike gold which has many, so reducing the likelihood of signal interference. EDX analysis was used to determine the composition of phases present in a specimen using a high-energy focused beam of electrons to generate X-rays characteristic of the elements within the specimen. Chemical composition is determined by comparing the intensity of X-rays from known standards with those from the specimen.

3.2.4 Transmission electron microscopy

Transmission electron microscopy (TEM) was used to observe samples of glass-ceramic materials at higher magnification than possible with SEM. Samples were crushed to a powder using an agate pestle and mortar and cold embedded in epoxy resin. The sample was crushed to protect the cutting blade of the microtome

instrument (RMC, Boeckeler Instruments, Arizona, USA) due to the relatively high hardness of the materials and to increase the likelihood of capturing many small samples within each thin section. The resin was then sectioned using a diamond knife on a Power Tome XL microtome to obtain samples of 1 mm^2 with a thickness of ~ 50 nm. Samples were supported on copper grids. The samples were carbon coated (Emitech K450 equipment, Quorum Technologies Ltd, East Sussex, United Kingdom) and stored in a desicator for further TEM investigation.

3.2.5 Thermo-gravimetric differential thermal analysis (TG/DTA)

Thermo-gravimetric differential thermal analysis was used to identify physical and chemical changes in the untreated, pre-treated wastes, glasses and glass-ceramics upon heating. A Stanton Redcroft STA 780 series simultaneous thermal analyser was used. The technique records the changes in temperature associated with physical and chemical processes as a function of temperature and associated changes in mass. Changes in state and/or composition are generally accompanied by endothermic or exothermic energy exchanges [111] and these effects can be used to understand changes in physical or chemical state of materials upon heating. TG/DTA analysis allows the measurement of the changes in temperature of a sample in comparison to an inert reference material heated at the same rate with a constant record of the mass.

Powdered samples were prepared (<75μm) by crushing samples in a mortar and pestle. Glass and samples were analysed in powder and bulk form. Bulk samples were prepared by crushing larger sample blocks to obtain pieces of approximately 2mm x 2mm x 2mm. All samples were heated in air in platinum crucibles using an alumina

reference. Samples exhibiting possible oxidation reactions were analysed in an inert argon atmosphere to confirm the presence of the reaction. Heating rates varied according to the sample and information required from each experiment and they are described in the relevant section.

3.3 Glass-Ceramics from Non-Vitrified Wastes

3.3.1 Processing routes

Three possible routes for producing glass-ceramics from APC residues were investigated; these are conventional melting followed by bulk crystallisation and two different powder-based methods using different combinations of waste residues and additives. The powder methods involve the compaction of powders that are subsequently sintered however; one route uses powdered, vitrified glass from a suitable waste composition, whilst the other involves powder compositions that are compacted and sintered without a previous vitrification stage. Figure 3-1 shows a summary of the glass-ceramic processing routes investigated.

3.3.2 Formation and sintering of powder compacts

Sintered samples were prepared from WAPC, glass cullet and EP dust according to the compositions shown in Table 3-1. The proportion of WAPC residue was kept constant at 50 weight percent and the EP dust and cullet proportions were systematically varied. The resulting powder mixes were milled using an automatic

agate pestle and mortar. The milled powders were sieved to a particle size of <45µm determined from the literature and preliminary trials.

Approximately 0.5g of each powder mix were pressed using a steel die at 124 MPa to form 9.6mm diameter, 3-4mm high disc samples. It should be noted that 9.6mm die was used as a standard for producing all powder compacts (raw powder and glass powder compacts) apart from samples produced specifically for mechanical tests which required a rectangular die. No binder was used as the compacts were easily handled without damage. The green samples were sintered at a range of temperatures between 850°C and 1150ºC using a 2 hour dwell time and a ramp rate of 10°C/minute, in an electric furnace (Lenton) (refer to appendix 1). Samples were slowly cooled to room temperature within the furnace.

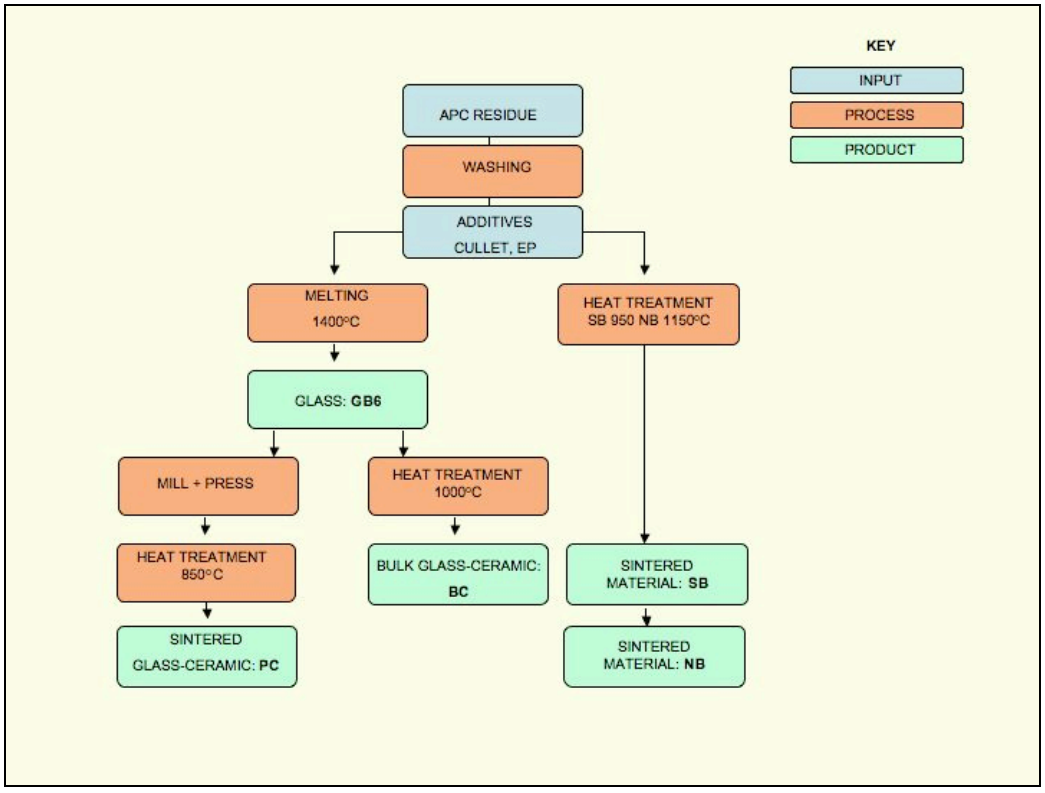


Figure 3-1: Overview of glass-ceramic processing routes developed and investigated in this project.

3.3.3 Use of sodium borate as EP dust replacement

Preliminary trials were carried out to determine whether an inexpensive commercially available source of borate could be used in place of EP dust. It is possible that the availability or composition of EP dust may change in the future due to changes in the production methods of fibreglass (of which EP dust is a waste by-product). Therefore, it is important that consideration is given to an alternative source of borate for the present technological approach of producing glass-ceramics from APC residues at low processing temperatures.

For these experiments, sodium tetraborate pentahydrate ($Na_2B_4O_7 \cdot 5H_2O$), commercially available as Neobor® was used in combination with WAPC residues, glass cullet and quartz sand. The Neobor® was supplied by Rio Tinto Minerals. Neobor® is used as a flux and network former in the production of a range of glass and ceramic products. It increases the strength, scratch resistance, and chemical resistance of ceramic wall and floor tiles, porcelain, and enamelled appliances. Batch mixes were based on the optimised sintered material, SB2 from earlier experimental work outlined in section 3.3.2 and Appendix 1. The ratio of WAPC residues to cullet remained constant (5:4 respectively) whilst the amount of sodium borate and quartz sand was varied. Quartz sand was used as an additive based on previous (unpublished) work carried out by Rio Tinto Minerals, which demonstrated that sodium borate and quartz sand are capable of forming a eutectic at low temperatures (starting at 600^{o}C) in certain ratios, according to the batch ingredients. Table 3-2

shows the batch compositions in weight percent. The prefix NB was used for those samples containing Neobor®.

Table 3-1. Batch mixes for powder sintering.

Sample number	WAPC wt%	Cullet wt%	EP dust wt%
S1	90	10	0
S2	80	20	0
S3	70	30	0
S4	60	40	0
S5	50	50	0
S6	50	0	50
SB1	50	45	5
SB2	50	40	10
SB3	50	35	15
SB4	50	30	20

Table 3-2 Batch mix compositions for trials using Neobor® as an additive.

Sample number	WAPC wt%	Cullet wt%	Neobor wt%	Quartz wt%
NB1	54	44	1	1
NB2	44	35	1	20
NB3	54	43	3	1
NB4	43	34	3	20

3.4 Vitrification of wastes

3.4.1 Production of melts

A number of batch compositions were formulated based on initial experimental mixes as shown in Table 3-3. The experimental mixes were heated in a gradient tube furnace to assess their glass-forming ability and approximate melting temperatures. The batch

powders for resulting glass-forming compositions were weighed out and mixed in a rotary mixer for fifteen minutes. The mixed powder was then put into a platinum crucible and heated in an electric (Lenton) furnace at a temperature and duration adequate to produce a homogenous melt. The melts were poured onto a graphite plate and allowed to cool to room temperature. Casting the melts in this way allowed the viscosity, colour and behaviour (did it shatter, crack or remain as cast) on cooling to be observed for each composition.

From the initial experimental batch mixes those containing untreated APC residue and calcined APC residue were disregarded due to their production of chloride containing gaseous emissions the production of which is potentially hazardous to health. Further experimental melts were produced based on WAPC residues and cullet to determine the maximum amount of WAPC residue that could be used to form an amorphous glass melt. The batch mixes are listed in Table 3-4. Having determined the optimum amount of WAPC addition, further experimental melts were made based on this mix, with the addition of EP dust. The ratio of WAPC residue to cullet remained constant for each batch mix while the weight% of EP dust was gradually increased (see Table 3-5).

Individual bars were cast from the optimised glass composition for the purposes of mechanical tests and bulk crystallisation investigations. Melts were cast directly into a steel mould heated on a hotplate to 350^{o}C. The cast bars were allowed to cool to room temperature then removed from the mould. Bars were annealed by heating at 5^{o}C/min from room temperature to 600^{o}C then cooling to room temperature at 5^{o}C/min.

Bar-shaped samples were also produced for mechanical tests on sintered glass-ceramics produced from glass powder. Approximately 5g of milled powder (45-75μm determined from optical heating microscope investigation) of the parent glass was mixed with two drops of distilled water as a binder and then pressed using a steel die at 124 MPa. Powder compacts had dimensions of 4x3x40mm.

Table 3-3: Batch compositions for experimental glass melts

Sample	APC wt%	WAPC wt%	CAPC wt%	Cullet wt%	EP wt%	Temp. °C	Time min
1	50	0	0	50	0	1400	40
2	0	50	0	50	0	1400	30
3	0	0	50	50	0	1350	30
4	50	0	0	40	10	1350	60
5	0	50	0	40	10	1390	60
6	0	0	50	40	10	1350	30

Table 3-4: Batch compositions for optimisation of WAPC content in melts

Sample	WAPC wt%	Cullet wt	EP wt%	Temp. °C	Time min.
G1	30	70	0	1400	30
G2	40	60	0	1400	30
G3	50	50	0	1400	30
G4	60	40	0	1400	30
G5	70	30	0	1400	30

Table 3-5: Batch compositions for optimisation of EP dust in melts

Sample	WAPC wt%	Cullet wt	EP wt%	Temp. °C	Time min.
GB1	57	38	5	1400	30
GB2	54	36	10	1400	30
GB3	51	34	15	1400	30
GB4	48	32	20	1400	30
GB5	45	30	25	1400	30
GB6	42	28	30	1400	30

3.5 Glass-Ceramics from Vitrified Wastes

Glass-Ceramics were produced from the waste derived glass samples by two methods; powder sintering and bulk devitrification using conventional thermal treatment methods.

3.5.1 Differential thermal analysis

Amorphous melts were primarily analysed to determine their ability to crystallise. Powdered and bulk samples were analysed using TG/DTA. Samples weighing 20mg were heated at 10^{o}C/minute in air to 1200^{o}C using a platinum crucible and alumina reference. The resulting DTA traces were analysed to identify glass transition temperature, exothermic crystallisation peaks as well as compare the overall thermal behaviour of each glass sample.

3.5.2 Optical heating microscopy

Optical heating microscopy provides a convenient way to study the effect that variables such as heating rate and particle size may have on the sintering of powder compacts. This part of the investigation was carried out in collaboration with the Department of Materials, Politecnico di Torino, Italy.

Two glass compositions were studied: GB6 and G4. The powders were obtained by crushing the glass with an agate mortar and pestle then sieved to produce particle sizes of <45µm and 45µm-75µm.

The sintering was carried out using an optical heating microscope (Leica Wetzler, Germany) with a digital webcam attached to the optical eyepiece to allow images of the compact to be captured during heating. The heating microscope consisted of a tube furnace with optically clear covers at either end. The samples were introduced into the furnace on a flat-ended probe with a thermocouple. The compacts were produced by manual, uniaxial compaction of powders, with distilled water as a binder, in a steel die. The samples were cubic in shape with dimensions of 3x3x3mm. Compacts were placed on an alumina support on which they could be introduced in to the furnace of the optical heating microscope. Compacts were sintered in air at a constant heating rate. Three heating rates were used. Heating rates for the smaller particle size were 5^{o}C/minute, 10^{o}C/minute and 20^{o}C/minute and studies were carried out in triplicate. Heating rates of 5^{o}C/minute and 20^{o}C/minute were used for the larger particle size and repeated twice.

Digital images were taken every 10^{o}C during heating from 500^{o}C, past the crystallisation temperature, previously determined by DTA, to 850^{o}C. The diameter and width of samples were measured from images using an image analysis software package. Figure 3-2 shows an image of a typical powder compact at room temperature, indicating the position of measurements. The glass-ceramics produced from parent glasses G4 and GB6 are referred to as GC4 and GCB6 respectively. The

radial and axial measurements were used to calculate possible anisotropic sintering behaviour.

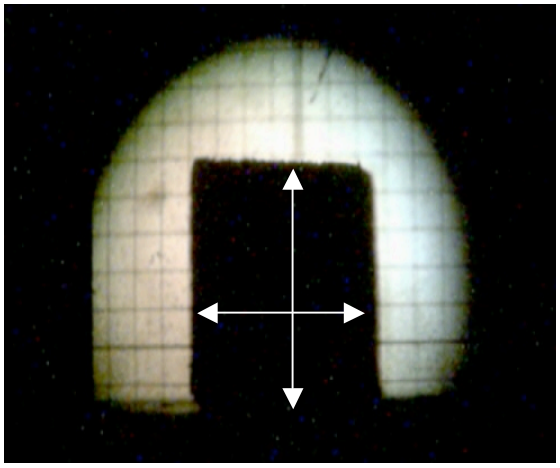


Figure 3-2: Image of a glass powder compact showing position of height and diameter measurements.

3.5.3 Determination of nucleation temperature and time

DTA analysis was used to determine the optimum nucleation temperature of the waste-derived glass chosen for further characterisation. The reasons for selection of a single glass composition for further analysis are explained in Chapter 4. A sample of crushed glass was powdered using an agate pestle and mortar and sieved to <75μm (based on particle size used for optical heating microscopy that produced isotropic shrinkage). To determine the optimum nucleation temperature for powder sintering of the parent glass, 20mg samples were heated from 20^{o}C to a specified nucleation temperature at 10^{o}C/minute, held for 30 minutes then heated to 1000^{o}C. Samples were heated in a platinum crucible with calcined alumina reference material. The hold temperatures were based around the glass transformation temperature of the glass, previously determined as approximately 600^{o}C from a DTA trace of an identical

sample as explained earlier. The hold temperatures were increased by 50°C increments from 400°C to 700°C inclusive. Each analysis was repeated three times. The crystallisation peak height was measured for each sample and the average height plotted against nucleation temperature. The hold temperature from which the highest crystallisation peak was derived was considered to be the optimum nucleation temperature.

The period of time for which the sample should be held at the optimum nucleation temperature was also determined using DTA analysis. Samples, prepared as for determining the nucleation temperature, were heated to the nucleation temperature at 10°C/minute and held for dwell times of 0, 30 and 60 minutes before heating resumed to 1000°C. The heights of the crystallisation peaks were measured. The highest peak was considered to be the optimum dwell time for nucleation to enhance crystallisation.

3.6 Determination of physical and mechanical properties

A range of measurements were carried out on samples fabricated by the sintering method and by bulk crystallisation. These measurements are described below.

3.6.1 Linear Shrinkage

The linear shrinkage of disc-shaped specimens during sintering was determined by measuring diameter before and after sintering. An average of at least four sample measurements were taken.

3.6.2 Water Absorption

The weights of oven dried, sintered samples were noted. The sintered samples were submerged in distilled water for 24 hours at room temperature. Samples were then rapidly surface dried and weighed. The change in weight was used to calculate the percentage water absorption.

3.6.3 Density and Porosity

The bulk density of sintered samples was determined using the Archimedes principle. The true density of the sintered material was determined using a 5ml glass density bottle of known volume. The density bottle was filled with distilled water, dried, and then weighed. Samples were crushed using an agate pestle and mortar and sieved to a particle size smaller than the pore size (appropriate to the specific glass-ceramic sample) determined my SEM analysis. The density bottle was then emptied and a sample of powder of known weight added. Distilled water was then added to the bottle and then outside dried before weighing. The volume of the powder is equal to that of the water displaced. This value can then be used to calculate the particle, or true density of the powder.

3.6.4 Wear resistance

The resistance of sintered glass ceramic samples was determined using a ball on disk wear resistance test. An alumina ball was rubbed linearly on the surface of the sample at a velocity/rate of 0.27 m/s with a load of 10N. The sample was rubbed continuously 250 times. This was repeated 4 times in order to get a total of 2000 revolutions. After each cycle the loss of mass was recorded.

3.6.5 Microhardness

Average Vickers microhardness values were determined on polished surfaces of samples using a Zwick/Roell Indentec ZHV micro indenter with integrated computer software, making at least ten indentations per specimen, with a hold of 10 seconds. Different indentation weights were used (ranging from 20g to 500g) as the samples had a wide variation in their hardness and porosity, which affected the ability to produce a clear, well-defined indentation.

3.6.6 Bending strength

Bending strength was determined using a three-point bend test. A Hounsfield H5KS tensile/compression equipment was used with a loading of 0.5mm min^{-1} and a support span of 20mm. Samples were polished to a 1μm finish with upper most edges bevelled at an angle of 45^{o} with 1μm diamond spray.

The average size of the specimens was 56x7x7mm. Specimen bars were fabricated individually. Glass bars and sintered glass-ceramic bars were fabricated as described in section 3.5.1 and 3.4.2 respectively.

3.6.7 Modulus of Elasticity

The modulus of elasticity (Young's modulus) was measured by a non-destructive resonance frequency technique (Mk5 Grindosonic, J.W. Lemmens Ltd, Belgium). Bar-shaped samples of dimensions as stated in section 3.3.5 were used for the measurements. A special tool was used to tap the supported sample to induce vibrations within the sample. The frequency, at which the sample naturally resonated, was detected by the equipment. At least ten bars of each glass and glass-ceramic composition were analysed and the results averaged. Frequency readings, sample dimensions and mass were used to determine Young's modulus values.

3.6.8 Coefficient of Thermal Expansion

Samples of glasses GB6 and G4, of approximate dimension 5x4x4mm (in accordance with ASTM E1545), were ground from larger glass pieces using 320μm silicon carbide paper. The upper and lower surfaces of the sample were parallel. The sample was then heated at 5°C/min from 50°C to 500°C in helium at a static pressure of 5 mN using a Perkin Elmer Dynamic Mechanical Analyser DMA7. This part of the

investigation was carried out at the Department of Materials Science at Politecnico di Torino, Italy.

3.6.9 Granular Leach Test

A distilled water leach test was used to determine the chemical durability of sintered samples. The British standard test procedure BS EN 12457-4:2002 "Characterisation of Waste – Leaching – Compliance" test for leaching of granular waste materials and sludges was followed [112]. The material to be tested was crushed using a pestle and mortar to give a particle size of less than 10mm. A sub sample of 10g was placed in a polypropylene bottle and 100ml of distilled water added (a liquid to solid ratio of 10). This procedure was carried out in quadruplicate. A fifth control sample, containing 100ml of distilled water was prepared. All samples were placed in a mechanical rotator for twenty-four hours. After twenty-four hours the samples were left to stand for fifteen minutes. The elute was filtered using a 542 Whatman filter paper and vacuum filter. Inductively coupled plasma atomic emission spectroscopy (ICP-AES) was used to determine the concentration of selected ions present in the leachate. The presence of chloride ions was determined using a standard silver nitrate titration of chloride [113]. The results of the leachate test were compared with the leachate limits set for disposal of hazardous and non-hazardous wastes in the UK [114].

These methods and analysis techniques were used to investigate the problem area and address the aims and objectives of the research identified in Chapter 2. The next chapter presents the results of waste characterisation and powder processing to produce sintered materials.

4 SINTERED MATERIALS FROM RAW MATERIAL POWDERS

4.1 Introduction

Following characterisation of raw materials, a simple method of powder sintering, without a prior vitrification stage was used to produce sintered materials from selected combinations of WAPC residues, glass cullet, EP dust and sodium borate (Neobor®).

4.2 Characterisation of Material

4.2.1 APC Residues

Table 4-1 shows the chemical composition of APC residues determined by ICP-AES and XRF analysis. The major components are calcium oxide and chloride. The total chloride content is high compared to values reported for APC residues in other studies including values reported for UK APC residues of the order of ~16wt% [37, 46, 115, 116]. The XRD data shown in Figure 4-1 indicates that the major crystalline phases present in APC residues are $Ca(OH)_2$, CaClOH, $CaCO_3$, KCl, NaCl and $CaSO_4$. The data also indicates that a low percentage of SiO_2 is present. This silica content primarily originates from entrained fly ash particles, and the low SiO_2 value indicated that it would probably not be possible to produce a glass from APC residues by melting without the addition of glass-forming additives. Figure 4-2 shows the typical appearance of as-received APC residues. The particles are spherical with a mean particle size of 35μm, which was determined by light scattering particle size analysis.

Table 4-1 Elemental composition of APC residues, WAPC residues and EP dust.

Element	Composition wt% (determined by XRF)		
	APC	WAPC	EP
Aluminium oxide	2.80	5.23	0.80
Calcium oxide	42	50.75	34
Carbon	2.13	N/A	0.47
Chloride (ion-chromatography)	21	2.52	0.10
Chromium oxide	0.03	0.05	0.08
Copper oxide	0.40	0.90	0.03
Fluorine	0.13	N/A	2.20
Iron oxide	0.47	0.70	0.11
Potassium oxide	1.87	0.22	11.31
Magnesium oxide	0.05	0.09	0.32
Sodium oxide	2.68	0.60	4.14
Phosphorus pentoxide	0.78	1.09	0.05
Lead oxide	0.10	0.24	0.89
Silicon dioxide	7.14	10.15	2.96
Sulphur trioxide	5.66	5.51	10.88
Titanium dioxide	0.56	0.90	0.02
Boric oxide (by ICP-AES)	0.70	N/A	29.60
Zinc oxide	0.87	1.64	0.02
Loss on ignition (1025^{o}C)	16.12	19.86	7.11

Low totals due to light elements, such as fluoride, not detected by analysis method.

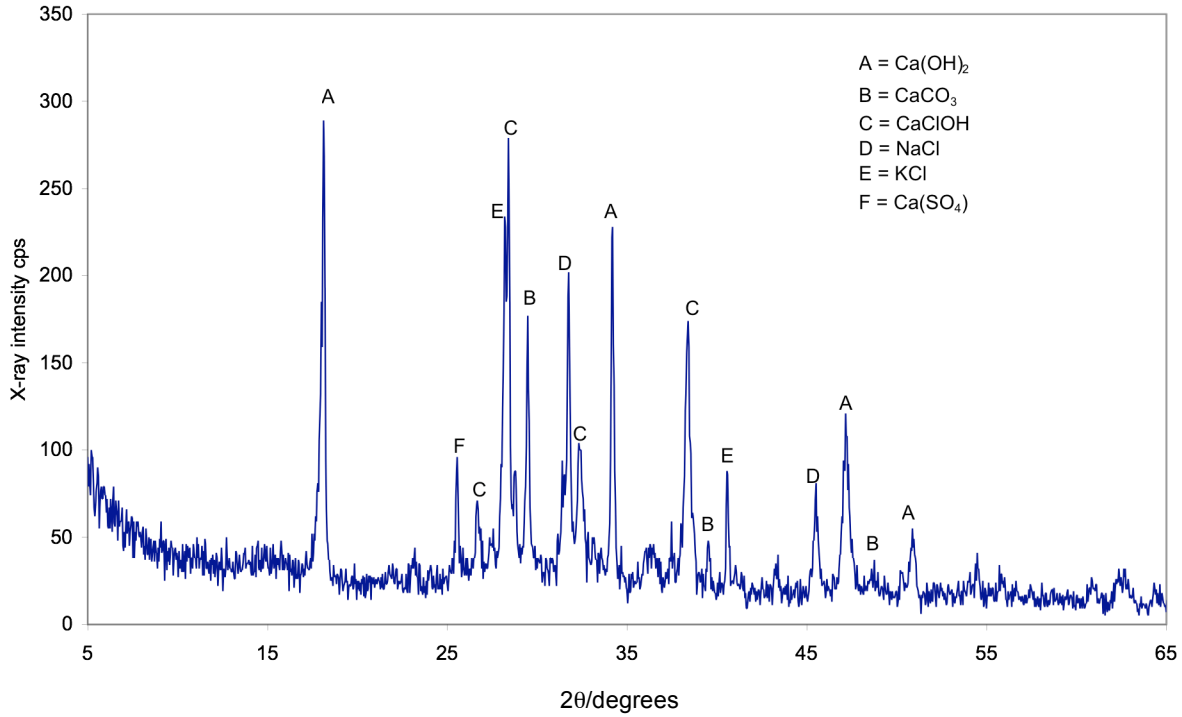


Figure 4-1: XRD trace of crystalline phases in as-received APC residues.

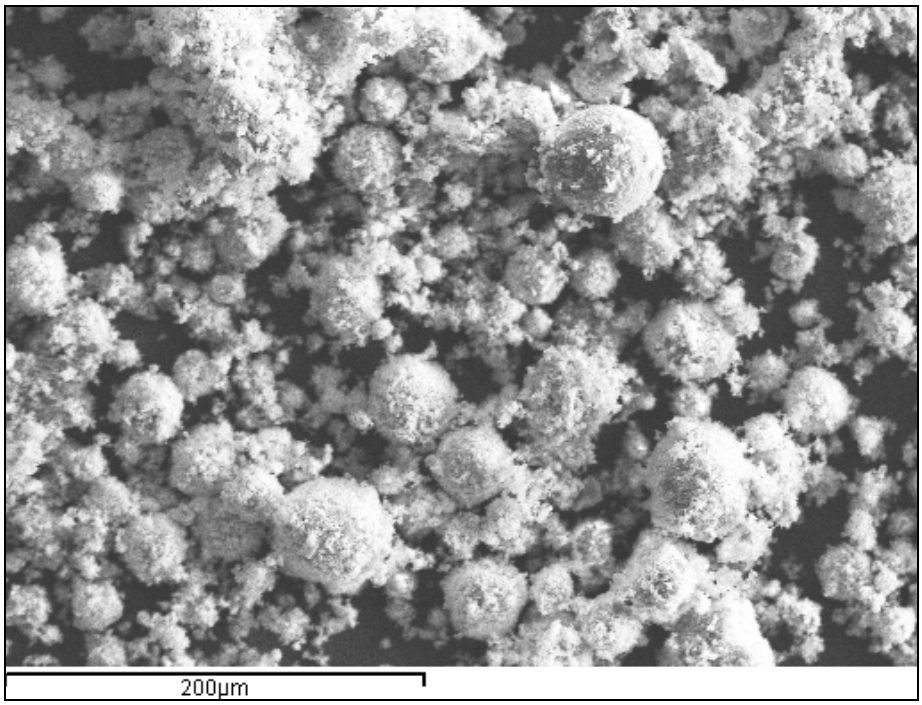


Figure 4-2: Secondary electron SEM micrograph of as-received APC residue

4.2.2 WAPC residues

It was necessary to pre-treat the as received APC residues to remove or lower the chloride content to prevent the evolution of potentially harmful chloride gases during planned thermal treatments. Washing of APC residues is a simple, low cost and effective method for removing chlorides from incineration residues as discussed in section Chapter 3 [51].

Table 4-1 also shows chemical composition data for the WAPC residues. Washing removed 97% of the soluble chloride content. This compares favourably with other results, which concluded that the majority of chloride compounds could be readily removed [11,12]. It can be seen in Figure 4-3, that the appearance of APC residues is unchanged by the washing procedure. Particle size analysis showed that the mean particle size had increased slightly to 51μm which may have been due to the dissolution of some of the finer particles during the washing process.

The XRD traces shown in Figure 4-4 of APC residues washed at different liquid to solid ratios, indicate that the major crystalline phases present in APC residues after washing are $Ca(OH)_2$, $CaCO_3$, and $CaSO_4$. It can also be seen that all liquid to solid ratios used for washing APC residues, for a time period of 2 hours, have successfully removed chloride phases to below detection limits. This result was expected and supports the chloride analysis of the same WAPC residues by ion chromatography as shown in Table 4-2. Effective removal of chloride phases at low L/S ratios is important, as reducing the amount of water used would also reduce the cost of the washing treatment. Furthermore, the lower washing ratios result in a reduction of the

filtered wash water, which is a secondary waste stream. The analysis of the wash water from a L/S ratio of 20 is shown in Table 4-3. The levels of metals tested are very low. Elements calcium, potassium and sodium are likely to be combined with the chlorine as salts. The treatment and use of the wash water as a secondary waste stream is discussed in Chapter 7. A reduction in mass of 40wt% occurred by washing of APC residues.

The production of the secondary waste stream is undesirable but unavoidable to allow safe thermal treatment on a laboratory scale. It is preferable to handle chlorides as a salt solution rather than a hazardous gaseous form. Further work, which is outside of the scope of this project is required to optimise the washing procedure. However, for the purposes of this project washing of APC residues was conducted using L/S of 20 due to optimisation studies that were carried out after initial vitrification and sintering studies had begun.

Table 4-2: Chloride content of WAPC residues washed at different L/S ratios determined by ion chromatography (original chloride content of APC residues 21wt%).

L/S Ratio	WAPC Cl content wt%
5	4
10	3
20	3
40	2

Table 4-3: ICP elemental analysis of APC residues washed at L/S ratio 20.

Element	Concentration ppm
Calcium	5470
Potassium	1360
Sodium	1380
Lead	39
Copper	0.17
Chromium	0.33
Aluminium	0.03
Iron	<0.01
Manganese	0.02
Zinc	6.7

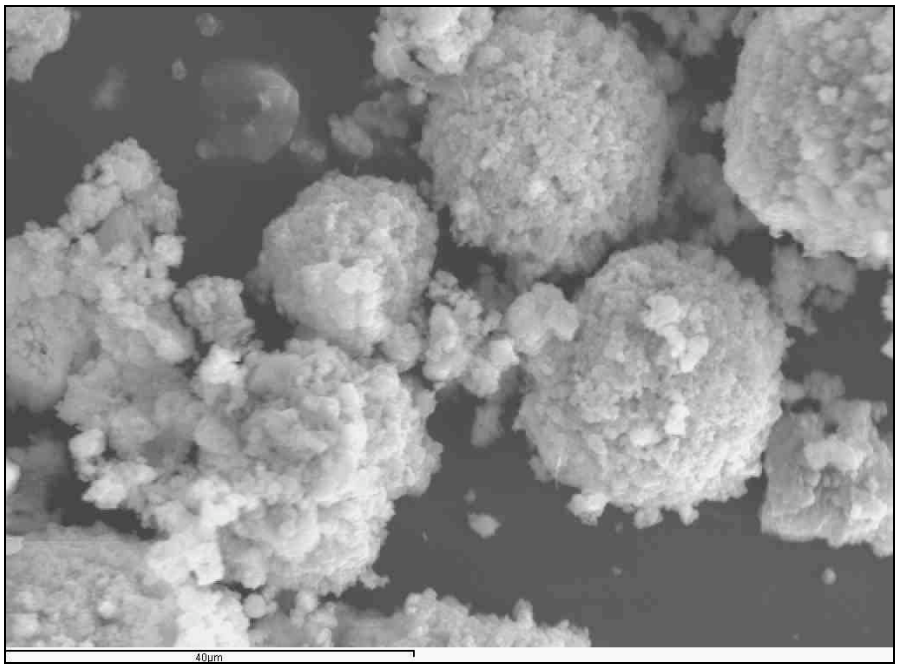


Figure 4-3: Secondary electron SEM micrograph of soft agglomerates of washed APC residues

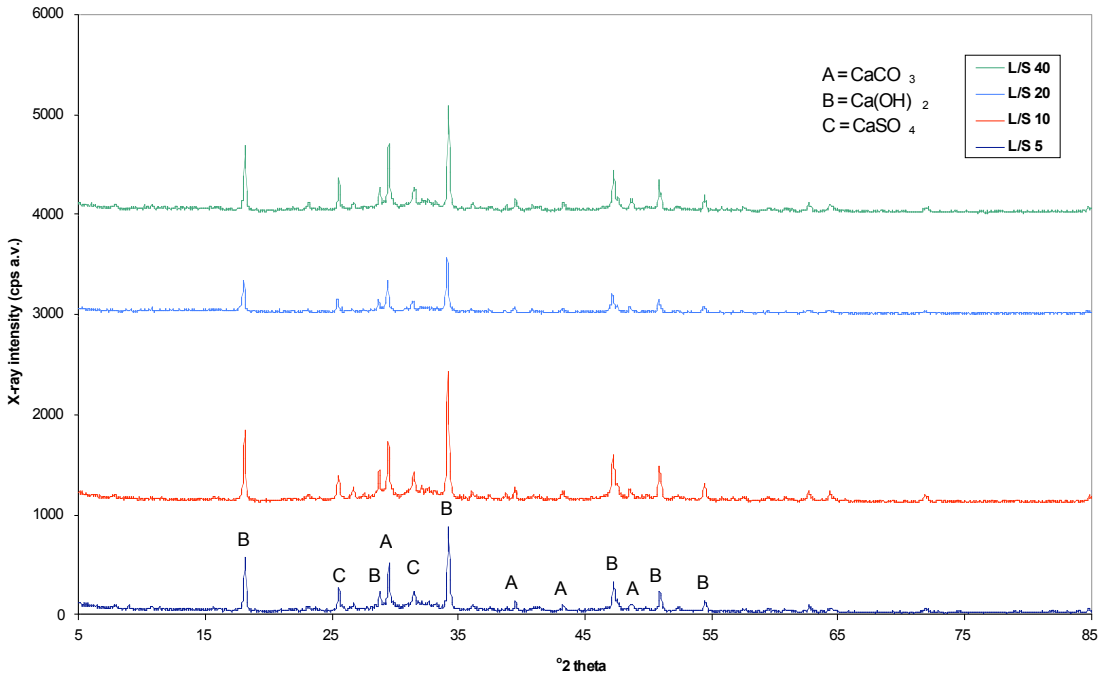


Figure 4-4: XRD trace showing crystalline phases in APC residues washed at different liquid to solid ratios.

The TG-DTA curve (Figure 4-5) for as-received APC residues showed a number of strong endothermic troughs during heating. The decomposition of $Ca(OH)_2$ occurred between 400°C and 450°C. This was followed by the decomposition of CaOHCl, NaCl and $CaCl_2$ at approximately 500°C and the decomposition of $CaCO_3$ and $CaSO_4$ at around 680°C. The comparatively less well-defined endotherm at around 1050°C is attributed to the decomposition of further, minor amounts of chloride containing compounds. When compared to the DTA trace for WAPC residues (Figure 4-6) it can be seen that the endotherms associated with chloride containing compounds are no longer present. The small endotherm at around 1150°C may be due to the insoluble chloride compounds not removed by washing as discussed previously. This supports the results from analysis of WAPC residue by ion chromatography confirming the process of washing APC residues removes the majority of chloride containing compounds.

The TG trace for as received APC residues shows that upon heating there is an associated weight loss. Up to a temperature of 1200^{o}C there was a total weight loss of 30%. The most significant period of weight loss occurred during the decomposition of $CaCO_3$ at 680^{o}C and chloride compounds at around 1050^{o}C. The total weight loss for WAPC residues was found to be 21%. However, with a reduced weight percentage of chloride compounds, the most significant periods of weight loss occurred at 400^{o}C to 450^{o}C due to $Ca(OH)_2$ decomposition (to CaO and H_2O) and between 600^{o}C and 700^{o}C due to $CaCO_3$ and $CaSO_4$ decomposition (to give CaO and CO_2 and SO_3).

4.2.3 APC residues from other UK EfW facilities

APC residues from Marchwood, Portsmouth UK EfW facilities, as well as those produced at SELCHP during a different time of the year (winter 2005) were subjected to the same L/S 20 washing procedure. Figure 4-7 shows the crystalline phases present in the as-received APC residues. After washing the WAPC residues were analysed by XRD to compare their crystalline phase composition (Figure 4-8).

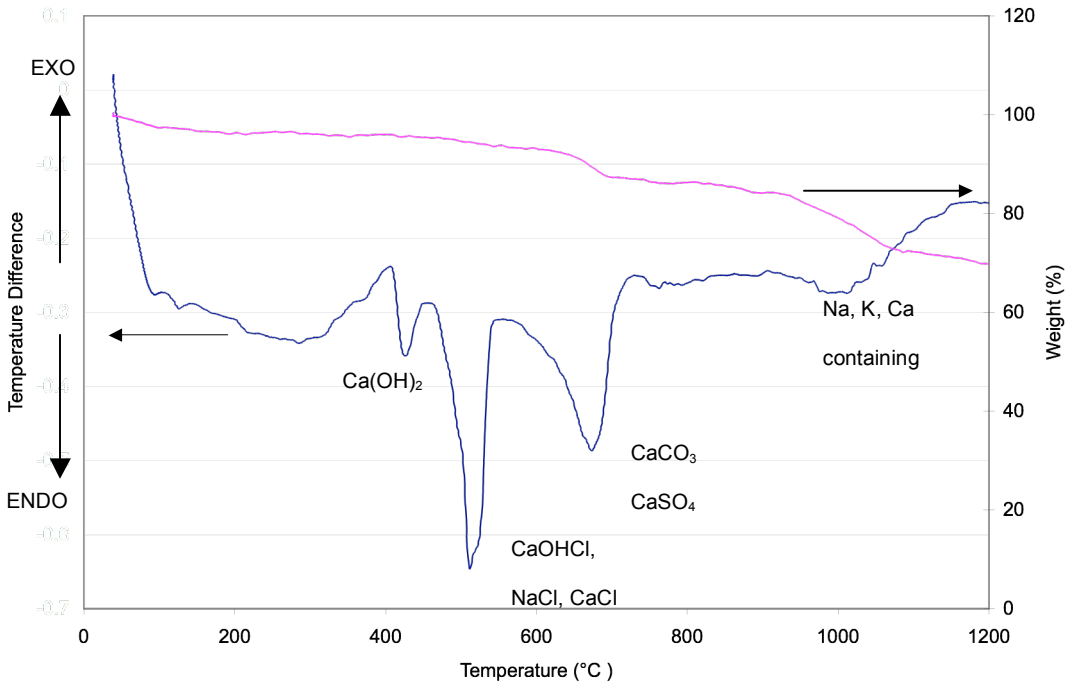


Figure 4-5: TG-DTA results for as-received APC residues heated at 10°C/min to 1200°C showing associated weight loss, endothermic and exothermic changes.

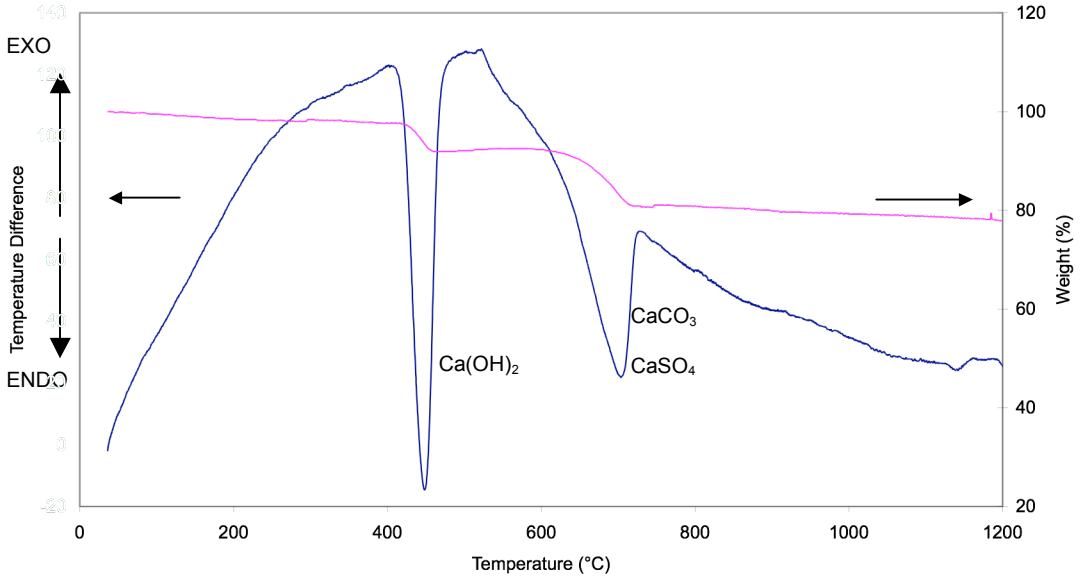


Figure 4-6: TG-DTA results for washed APC residues heated at 10°C/min to 1200°C showing associated weight loss, endothermic and exothermic changes.

The phases present were the same for each WAPC residue with slight variations in concentrations. The samples from SELCHP November 2005 and Marchwood also contained SiO_2. This is due to the variation in waste input into the incinerator. The variation in waste input is unavoidable and a characteristic of this type of waste material. The XRD analysis showed that the variation between sources is minor. However, the application of thermal treatments needs to be applicable for as many sources of APC residues as possible throughout the UK. For this reason the WAPC residues from these sites were also used to produce glasses by the process developed in this research and discussed in greater detail in chapter 5.

4.2.4 Electrostatic precipitator (EP) dust

EP dust, which was sourced as a waste by-product from flue gas cleanup during the manufacture of fibreglass was characterised to determine its composition and thermal behaviour. EP dust contains approximately 30wt% boric oxide. Figure 4-9 shows the XRD trace of EP dust. It can be seen that the boric oxide is present as calcium borate ($Ca_2B_2O_5$). Fluorine is also combined with calcium as calcium fluoride (CaF_2). The other crystalline phases present were calcium sulphate ($CaSO_4$) and calcium hydroxide ($Ca(OH)_2$). The high level of boric oxide is beneficial as it reduces the effective amount of EP dust that must be added to the batch mixes in order to achieve the possible flux and physical effects the borate may impart to the resulting glass-ceramic materials.

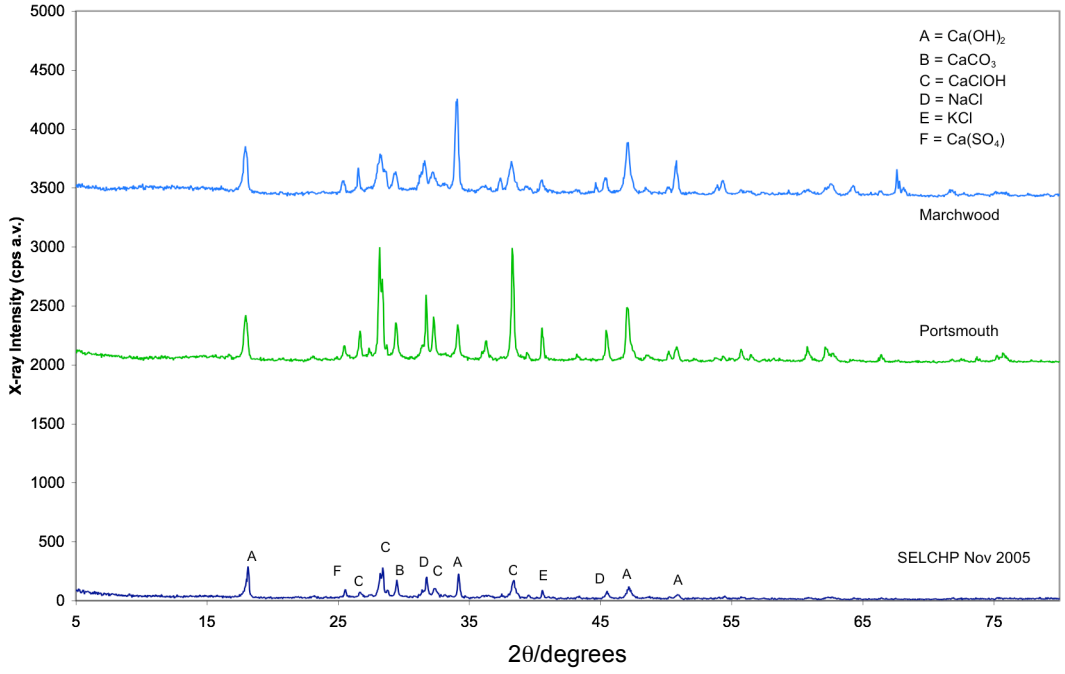


Figure 4-7: XRD patterns of as-received APC residues from different UK EfW facilities ('noise' past 55 2θdegrees are not significant features).

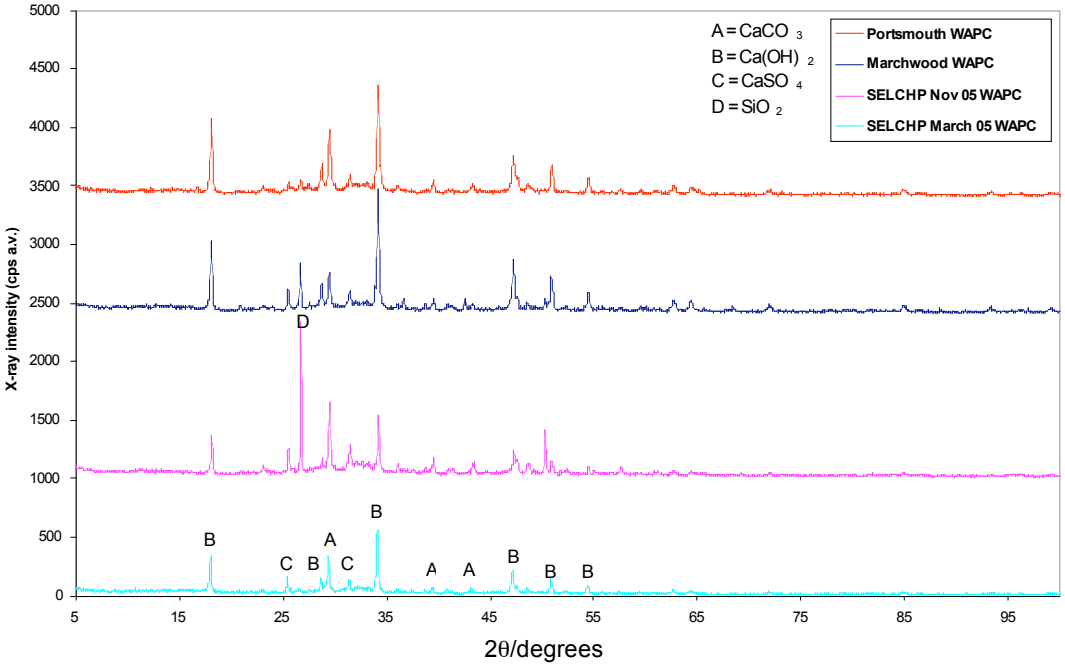


Figure 4-8: XRD patterns of WAPC residues from different EfW facilities washed at a L/S ratio of 20.

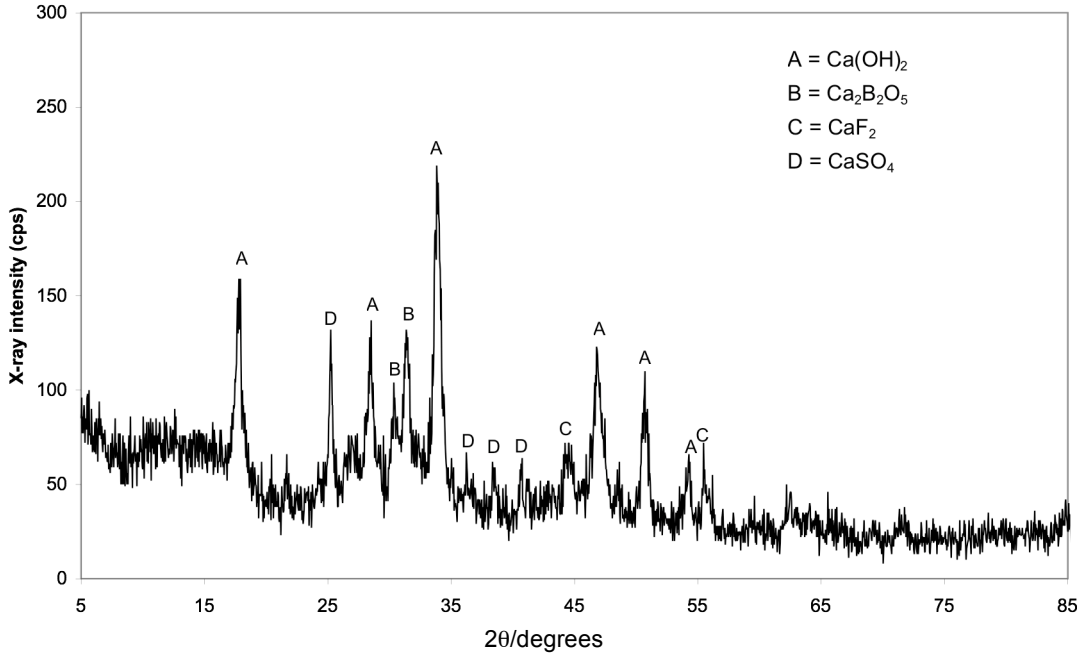


Figure 4-9: XRD pattern of EP dust showing main crystalline phases.

4.3 Characterisation of sintered materials

The sintered materials, labelled S1-S6 and SB1 to SB4, were produced from pressed compacts containing WAPC residues, EP dust and glass cullet as outlined in section 3.3. The effects of batch composition and thermal treatment on the sintered samples were investigated. Samples S1 to S4 did not produce an acceptable sintered product within the operating temperature of the furnace (1100^{o}C). In this context 'acceptable' meant a material of sufficient structural integrity that could be handled easily without damage or leaving a 'chalky' residue. A temperature of 1000^{o}C was required to sinter sample S5, which contained equal amounts of WAPC and glass cullet. In contrast, it was possible to produce fully sintered samples at 950^{o}C with the addition of EP dust. For this reason samples produced from batch mixes S6 and SB1-SB4, which sintered well, were used for further investigation.

4.3.1 Sintering linear expansion and shrinkage

Figure 4-10 shows the variation in linear shrinkage and expansion with sintering temperature. It can be seen that the addition of EP dust causes a significant increase in shrinkage. The values for sample SB1 (5wt% EP) did not exhibit such a strong trend as samples SB2-4, following a similar behaviour to that of S5 (0wt% EP dust), although with greater linear shrinkage.

As observed in Figure 4-11 the general trend for all sintered samples containing EP dust was an increase in density with increasing temperature, up to an optimum temperature where maximum density was achieved. This was followed by a decrease in density as the optimum sintering temperature was exceeded. Sample SB1 (5wt% EP) exhibited a minor increase in density at the optimum sintering temperature.

The samples that contained EP dust showed a greater degree of linear shrinkage over the full range of sintering temperatures when compared to sample S5, which contained no EP dust. The low melting temperature (~970^{o}C) of EP dust promotes viscous flow sintering and enhances densification of samples. Sample S5, which does not contain EP dust, exhibited a fairly constant linear dimension during firing but developed surface cracking at the edges and circumference.

Table 4-4 shows the Vickers microhardness values for each sample sintered at optimum temperatures. It can be seen that the addition of EP dust improved the microhardness of sintered samples for samples SB2-4. The lack of full crystal formation and higher porosity may explain the low microhardness of sample S1 and

the high variation in values (standard deviation of 1.5GPa) compared to samples SB2-4. Samples containing EP dust exhibit microhardness values up to 4.5GPa which is similar to or greater than values obtained for sintered products from municipal waste incineration residues reported from other studies which ranged from 3.8GPa to 6.7 GPa [27, 30, 37, 117]. It was observed that sample SB2 possessed a fine microstructure with nano-sized crystallites, determined by TEM (section 4.3.3.1), which when combined with the randomly orientated structure (Figure 4-14) would lead to a high microhardness value. In comparison, the microhardness of a typical commercially available porcelain stoneware tile is reported as 5.9GPa [118]. This indicates that these waste derived glass-ceramics could be used as tiles for the construction sector. A high hardness leads to materials with improved wear and abrasion resistance. However other properties of the glass-ceramics need to be considered for possible technical applications such as fracture toughness, thermal shock resistance and chemical durability (leaching resistance).

Table 4-4: Vickers microhardness values for sintered samples S5, SB1-4
(Standard deviations in square parentheses).

Sample	EP dust wt%	Microhardness GPa
S5	0	2.2 [1.5]
SB1	5	1.3 [0.5]
SB2	10	4.5 [0.7]
SB3	15	4.0 [1.0]
SB4	20	4.1 [0.8]

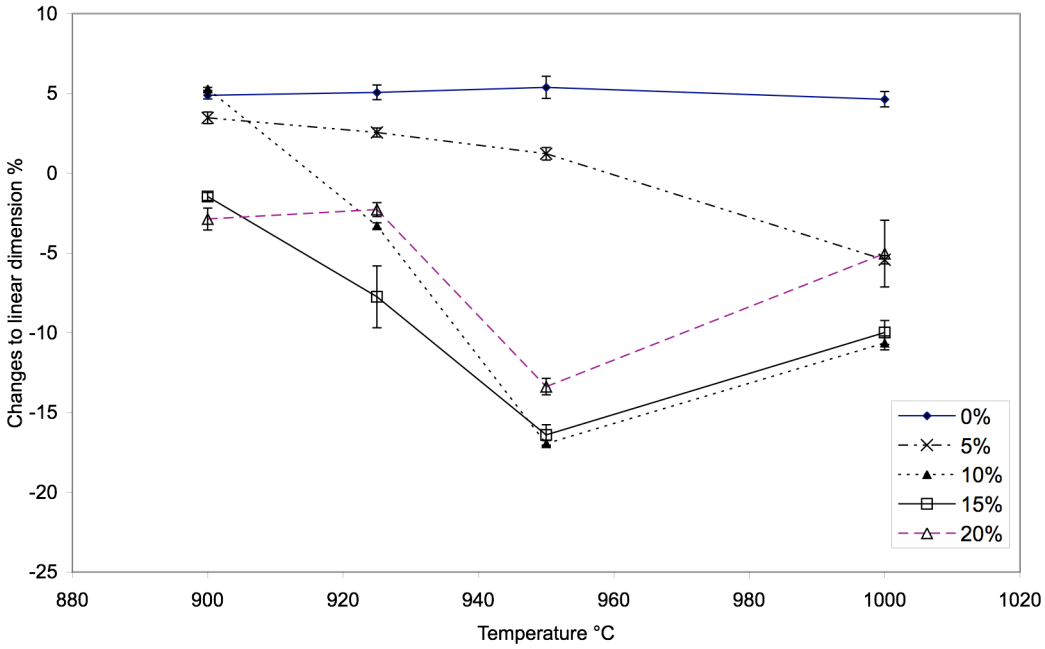


Figure 4-10: Sintering temperature versus change in linear dimension for samples containing different concentrations of EP dust.

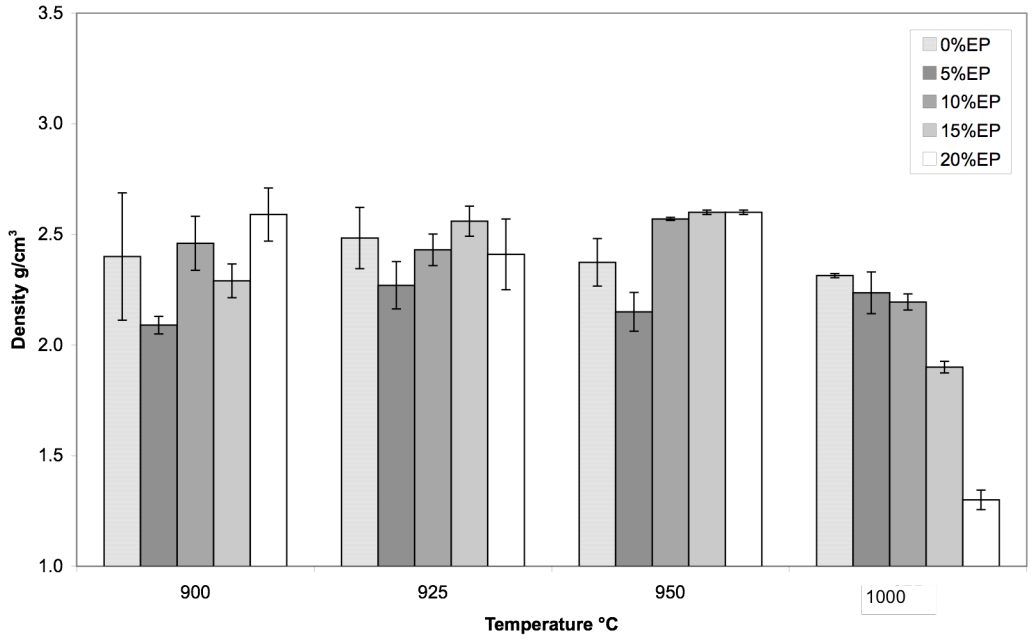


Figure 4-11: Sintering temperature versus bulk density for samples containing different concentrations of EP dust.

4.3.2 Densification of sintered samples containing EP dust

As observed in Figure 4-11, the general trend for all sintered samples containing EP dust was an increase in density with increasing temperature up to an optimum temperature where maximum density was achieved. This behaviour was followed by a decrease in density as the optimum sintering temperature was exceeded. As mentioned previously the presence of EP dust promotes viscous flow during sintering leading to increased densities of samples up to the optimum sintering temperatures. It can be seen that sintering and associated densification occur over a relatively narrow temperature "window" of 100^{o}C with 950^{o}C being the optimum temperature and bloating due to evolution of gases occurring at 1000^{o}C.

4.3.3 Microstructure analysis

Figure 4-13 shows an SEM micrograph of the fracture surface of sintered sample SB2 after sintering at 900^{o}C for 2 hours. The sintering temperature was 50^{o}C below the optimum temperature. However, early stages of crystal formation are visible. A number of long, thin, blade-like crystal formations can be seen, as can some agglomeration or 'necking' of powder particles. When sintered at 950^{o}C (Figure 4-14) the microstructure of the SB2 is markedly different. Large bladed crystals of up to 60μm in length had developed throughout the sample. The surrounding matrix appeared to be formed of densely packed irregularly shaped and cubic crystals with the powder particles no longer visible. A sintering temperature of 950^{o}C was determined as the optimum sintering temperature due to the high density achieved, leading to high microhardness and aesthetic qualities, as discussed previously. Figure

4-15 shows a higher magnification SEM micrograph of a sintered SB4 sample where the smaller, crystalline phase can be seen.

As mentioned previously, samples bloated when the firing temperature was too high for a particular batch mix, which caused pores to form within the sample. Such a process is visible in Figure 4-16, which shows a higher magnification micrograph of the fracture surface of sample SB2 when sintered above optimum temperature, at 1000^{o}C. The porosity is clearly visible at approximately 50μm up to 100μm and rounded in shape, which supports the theory that they are caused by the evolution of a gas within the sample due to the decomposition of compounds.

As discussed, EP dust was a beneficial choice of additive in the present investigation involving APC residues as shrinkage and densification were enhanced during sintering. Comparison of only those samples containing EP dust showed that porosity was reduced up to an EP dust addition of 15wt%. Above this value the porosity started to increase due to "over-fluxing" of the powder mix and associated bloating. The addition of 15wt% EP dust or greater led to undesirable shape change of the sample, apart from sintering shrinkage.

The fully sintered samples SB3 (15wt% EP) and SB4 (20wt% EP) exhibited concave upper surfaces and sides. For this reason sinter batch mix SB2 is aesthetically superior compared to all other mixes. Indeed, if these materials were to find applications as building elements and construction blocks (e.g. floor tiles), minimal shape distortion of the material during sintering is required.

The crystal phases were found to be wollastonite and a lesser amount of gehlenite (Figure 4-12). The variation in crystal morphology is due to substitutions of elements within the typical wollastonite and gehlenite structures as seen in studies of other materials produced during this research (see chapter 5).

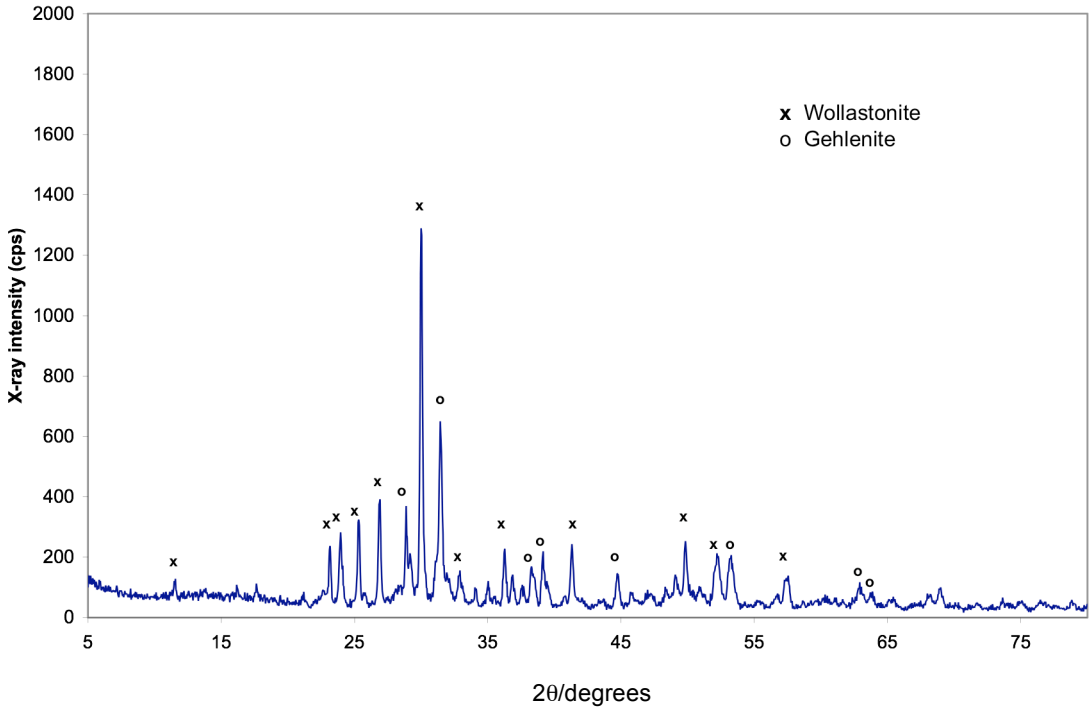


Figure 4-12: XRD pattern of sample SB2 sintered at 950°C for 2 hours.

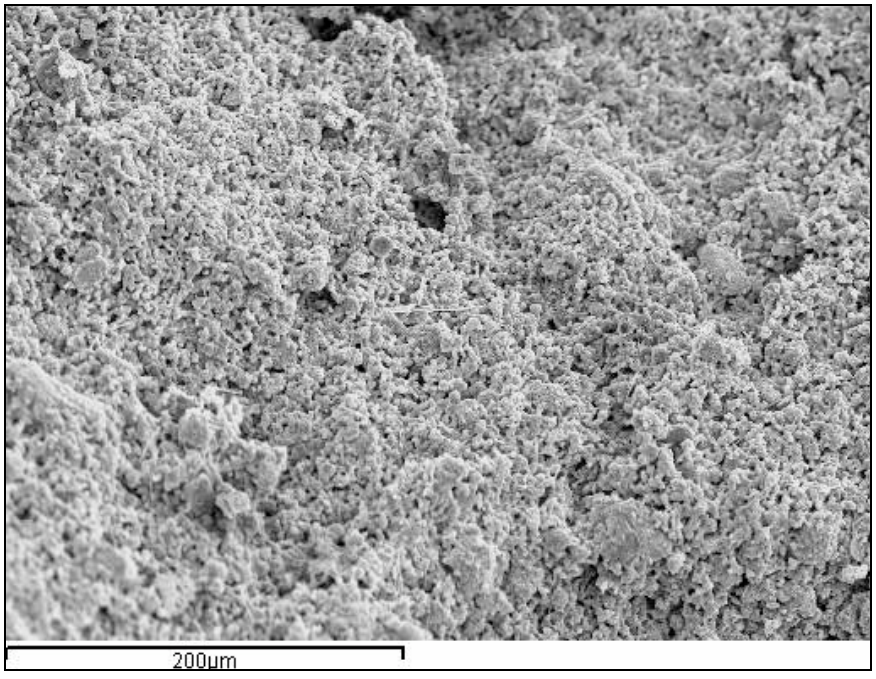


Figure 4-13: Material SB2 sintered at 900°C for 2 hours showing early stages of bladed crystal formation.

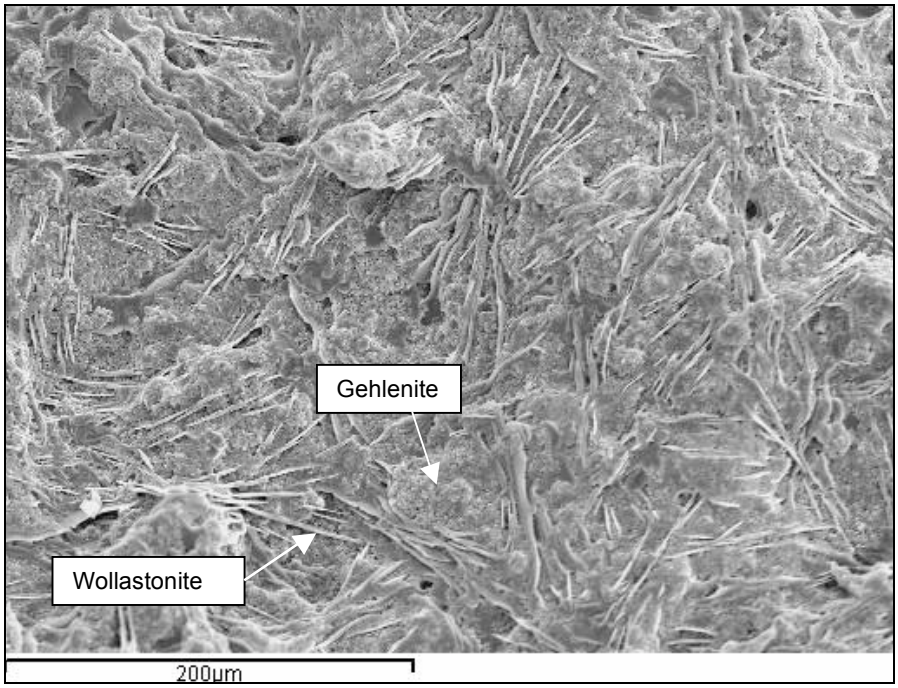


Figure 4-14: Material SB2 sintered at 950^{o}C for 2 hours showing bladed crystals and cubic crystalline matrix.

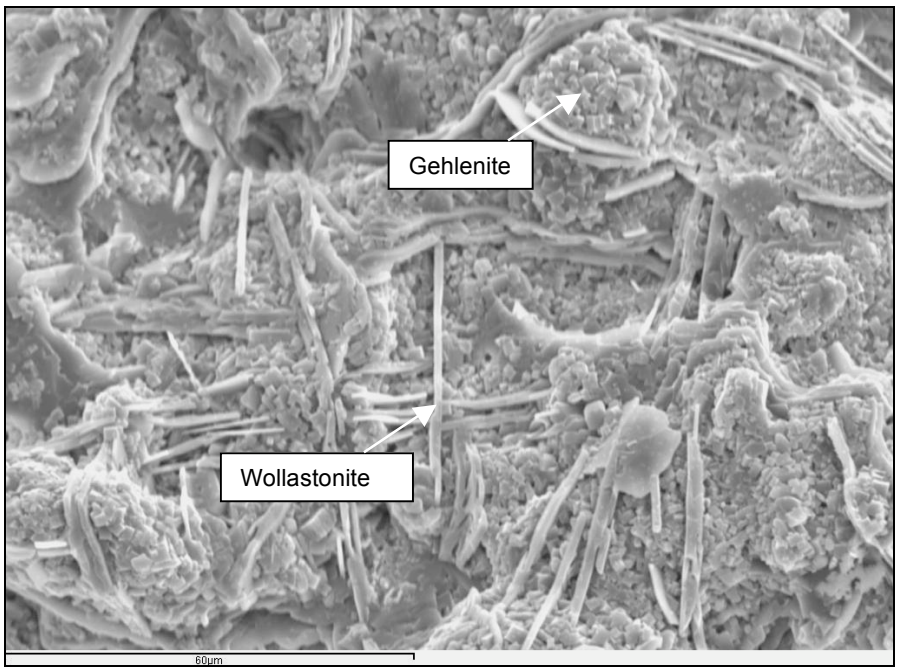


Figure 4-15: Material SB4 sintered at 950^{o}C for 2 hours showing well-developed crystalline structure composed of a high percentage of cubic crystal phase (x1000).

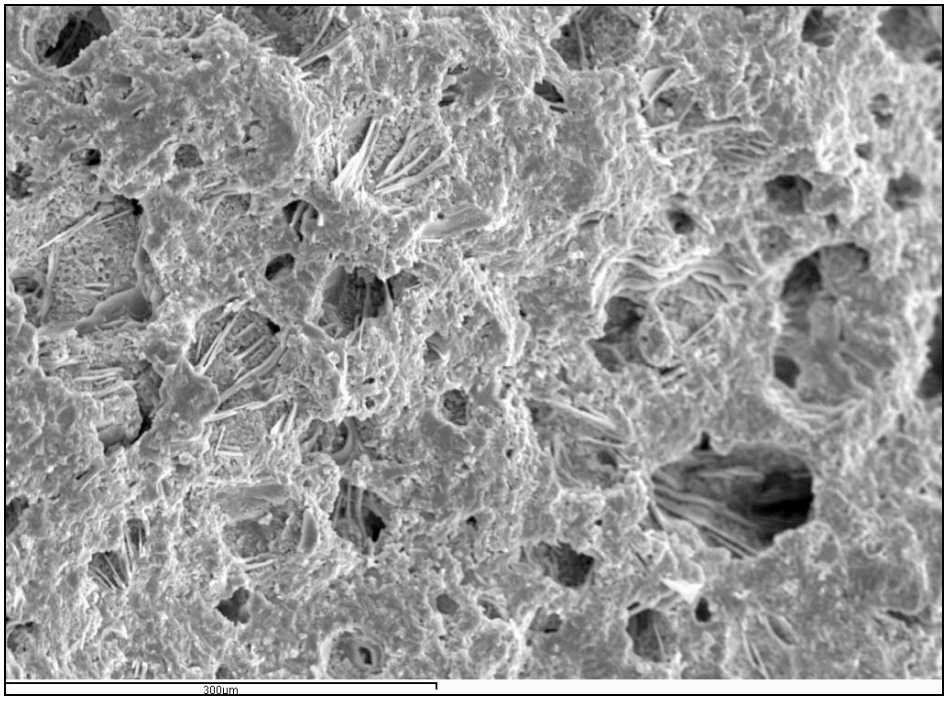


Figure 4-16: Material SB2 sintered at 1000^{o}C for 2 hours showing bladed crystals and pore voids.

4.3.3.1 TEM analysis of sintered material SB2

Thin section samples of sintered sample SB2 were prepared for TEM analysis by microtomography as outlined in chapter 4. It can be seen in Figure 4-17 that two distinct structures were identified. The dark area dissecting the image is a large bladed crystal corresponding to those observed by SEM (Figure 4-14 and Figure 4-15). The diffraction pattern (Figure 4-17, area 1) indicates that this is a single crystalline phase and is also an individual crystal as determined by SEM analysis. The remaining structure, either side of the bladed crystal, has a much finer and less distinct structure. When compared with the SEM micrographs this corresponds to the much smaller crystals (Figure 4-15). The diffraction pattern from Figure 4-17, area 2 is multi-ringed showing that it is polycrystalline in structure. XRD analysis (Figure 4-12) showed that SB2 as a whole is composed of wollastonite and gehlenite. It is clear from the many

elements in the starting waste materials that these phases are not 'pure' but have many element substitutions. The crystal phases in area 2 may be formed by variations of just one or both of wollastonite and gehlenite. However, similar large elongated crystal structures were observed in a glass-ceramic derived by bulk vitrification of a glass produced from a mix of the same three waste materials, but with a slightly different wt% combination (refer to chapter 6). EDX analysis of these crystals determined that they were composed of Ca, Si and O, the three elements that make up wollastonite whilst the surrounding matrix (crystal phases and residual glass) contained these plus the remaining elements.

Figure 4-18 shows a TEM micrograph the polycrystalline area 2 of sintered sample SB2 containing homogenously distributed crystallites. EDX analysis (Figure 4-20) of the area containing the crystallites (Figure 4-18) showed the area to be rich in titanium. Analysis of an area not containing a crystalline phase did not detect titanium as a constituent. Therefore, the submicron crystals (Figure 4-19) may be TiO_2 crystals. This was interesting, as titanium had not been detected by other analytical techniques, possibly due to the submicron size of the crystallites.

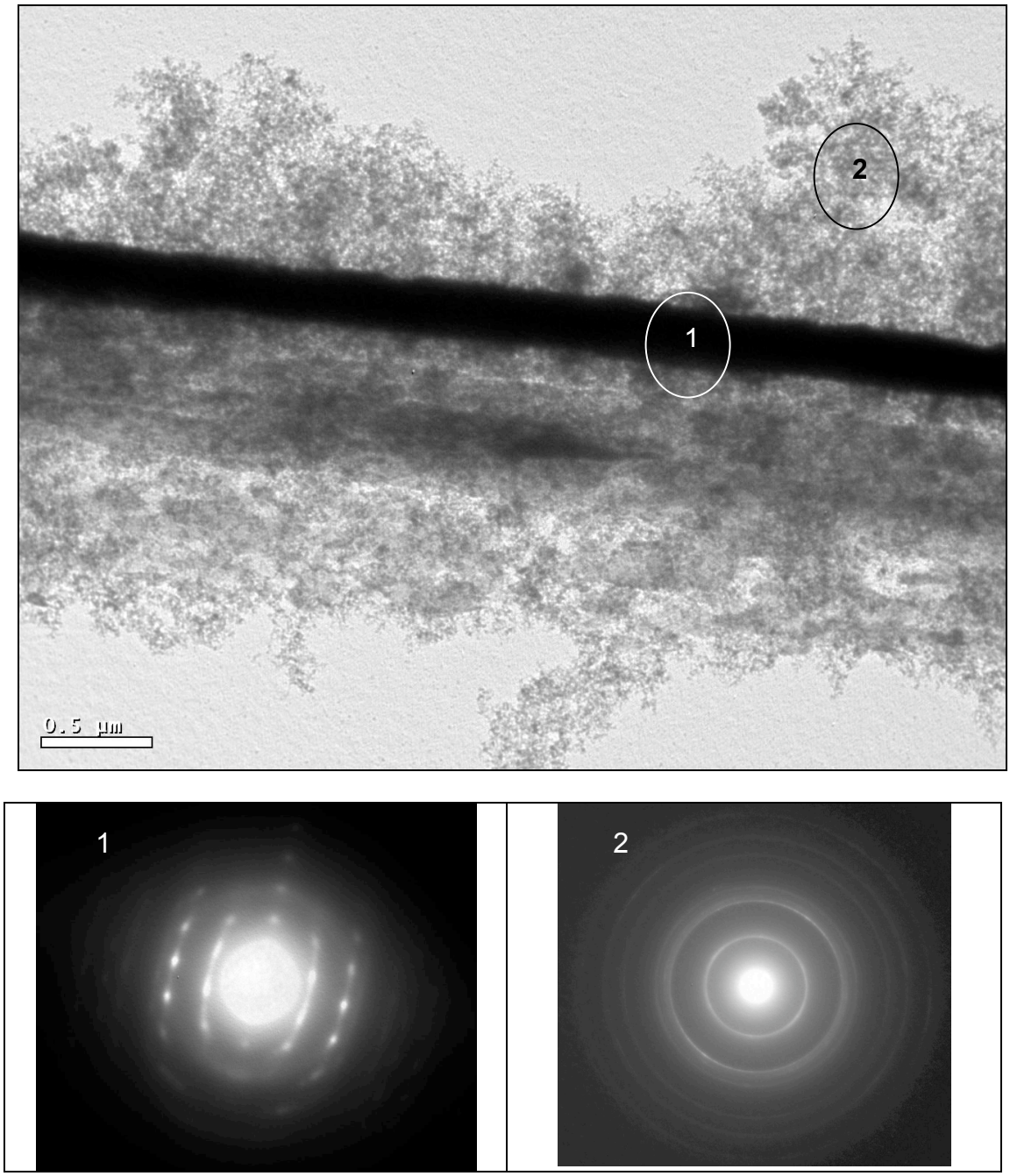


Figure 4-17: TEM bright field image of sample SB2 sintered at 950^{o}C for 2 hours (x30,000) and X-ray diffraction patterns. Area 1 is a single crystalline phase whilst area 2 corresponds to a polycrystalline area.

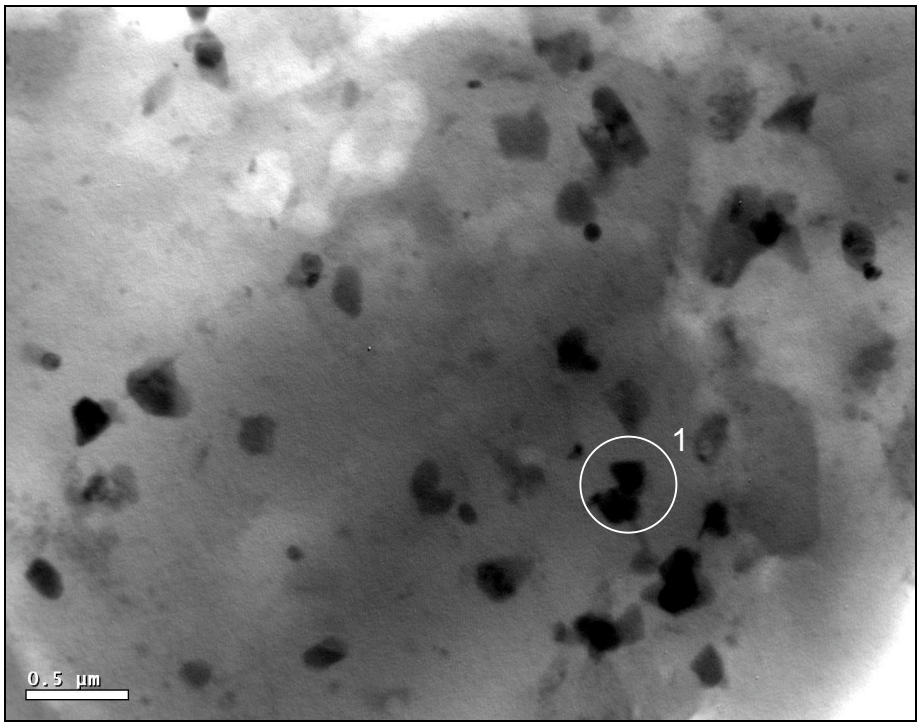


Figure 4-18: TEM bright field image of sintered sample SB2, area 2, polycrystalline matrix (x30,000) showing homogenously distributed crystals of < 0.5µm.

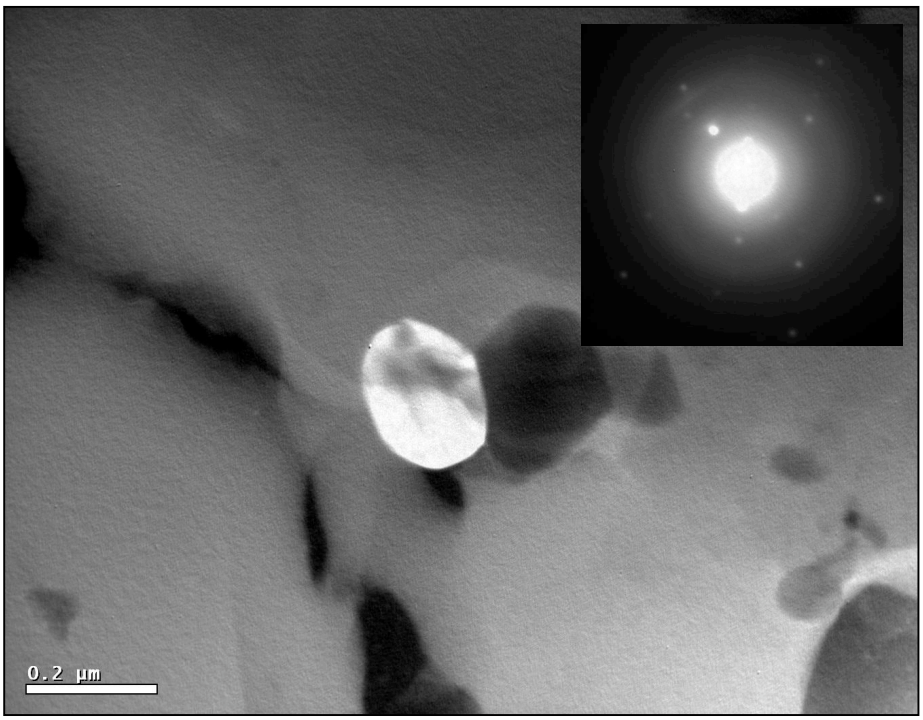


Figure 4-19: Centre dark field (-g) diffraction pattern from polycrystalline area 2 in Figure 4-17. Inset image shows crystalline diffraction pattern. 1000mm camera lens.

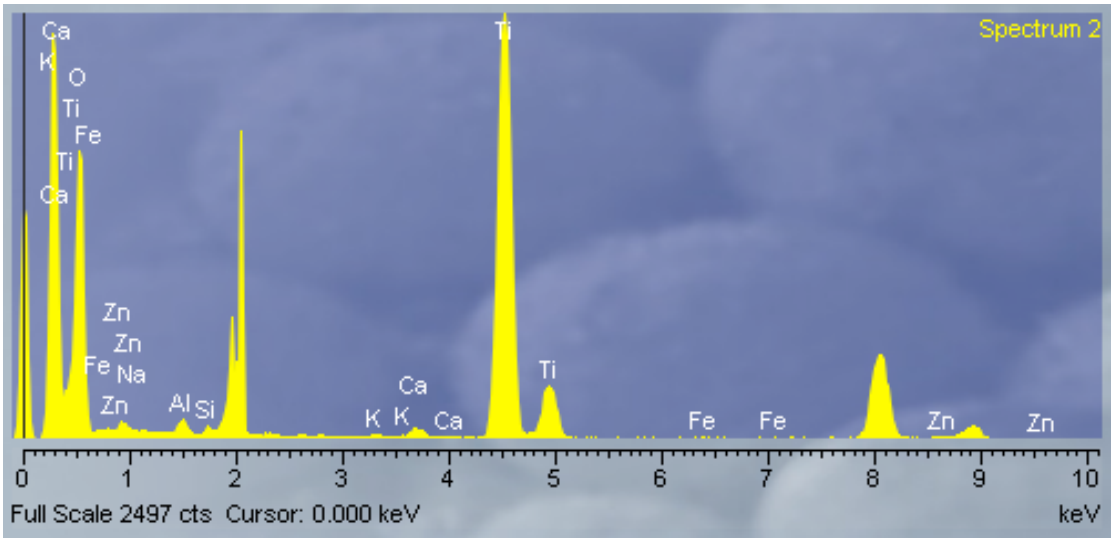


Figure 4-20: EDX spectrum of crystalline area rich in titanium (area 1 in Figure 4-18).

4.4 Characterisation of sintered materials containing Neobor®

The results of experimental work carried out to investigate the use of sodium borate as a substitute for EP dust in the production of WAPC containing sintered materials are presented below. The investigation of a substitute source of borates was necessary to address possible changes to availability or composition of EP dust in the future.

4.4.1 Linear expansion and density

As explained in Chapter 4 four experimental batch mixes were tested based on sintered material SB2 but with variation in the sodium borate and quartz sand content. Table 4-5 summarises the composition of each batch mix.

Table 4-5: Batch mix compositions for sodium borate trials

Sample number	WAPC wt%	Cullet wt%	Neobor wt%	Quartz wt%
NB1	54	44	1	1
NB2	44	35	1	20
NB3	53	43	3	1
NB4	43	34	3	20

Figure 4-20 shows the linear expansion of samples NB1-4. It can be seen that in all cases there was an increase in diameter at a sintering temperature of 950^{o}C. With increasing temperature above 950^{o}C there was a decrease in the linear expansion. The samples containing higher levels (3wt%) of sodium borate exhibited negative linear expansion (shrinkage) at a temperature of 1050^{o}C and higher. It can also be seen that samples with higher levels (3wt%) of quartz sand had lower, or negative, linear expansion compared to those containing 1wt%.

Bulk density of sintered pellets increased with increasing sintering temperature (Figure 4-21). It is also clear from the plot of density versus sintering temperature that density increased with increasing temperature. Samples containing 3wt% sodium borate exhibited greater densification at all sintering temperatures compared to those containing 1wt% sodium borate. While samples containing 20wt% quartz were denser than those containing 1wt% quartz (with identical sodium borate content).

The true density of sample NB4 was determined using a density bottle as described in Chapter 3. NB4 had a true density of 2800 kg.m^{-3} and a calculated porosity of 18%.

4.4.2 Water absorption

Figure 4-22 shows the plot of water absorption for sintered samples NB1-4. As sintering temperature increases water absorption decreases for all samples. After 24 hours submerged in distilled water it was observed that some of the samples had released a yellow leachate as can be seen. Samples NB2 and NB4 did not release any observable leachate for samples sintered at temperatures of 1100^{o}C and 1150^{o}C suggesting that higher levels of sand were beneficial in the sintering and immobilisation of leachable elements or phases. The leaching exhibited by some samples makes them unsuitable for further investigation, as this is an undesirable characteristic. Further investigation, which was beyond the scope of the present study, should be carried out to characterise the composition of the leachate from the water absorption procedure.

Sintered samples NB2 and NB4, sintered at 1150^{o}C, were selected for further investigation, as time did not permit all samples to be investigated and these two compositions did not produce any visible leachate. Sample NB4 was of particular interest due to its high density and 0% water absorption. It also possessed good aesthetic properties with an even colour and flat surfaces. A comparison of the physical appearance of samples NB1-4 sintered at different temperatures can be seen in Figure 4-21. Aesthetic properties may change when the process is scaled up with larger powder compacts and so further investigation would be required to evaluate surface appearance (e.g. colour, roughness, pitting).



Figure 4-21: Macrograph of sintered samples NB1-4 heat treated at different temperatures a)950^{o}C b)1050^{o}C c)1100^{o}C d)1150^{o}C.

The XRD patterns of samples NB2 and NB4 are show in Figure 4-23. The only crystalline phase detected was wollastonite. Gehlenite was not detected unlike the related sintered material SB2 (which contained EP dust rather than sodium borate). It is possible that gehlenite was present, although in levels that may have been below detectable limits of approximately 2wt%. The source of aluminium in the ceramic materials, produced in the research, were WAPC residues, glass cullet and the EP dust. By excluding EP dust from this batch mix and introducing quartz and sodium borate lower levels of aluminium were available to form a gehlenite phase.

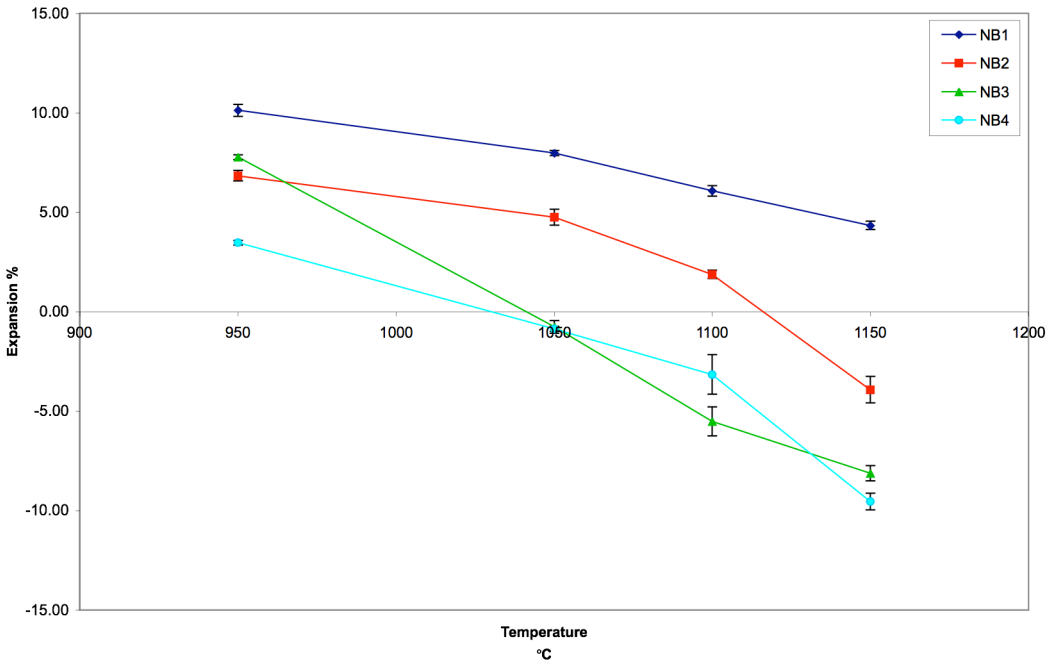


Figure 4-22: Plot of linear expansion versus sintering temperature of samples containing different concentrations of sodium borate.

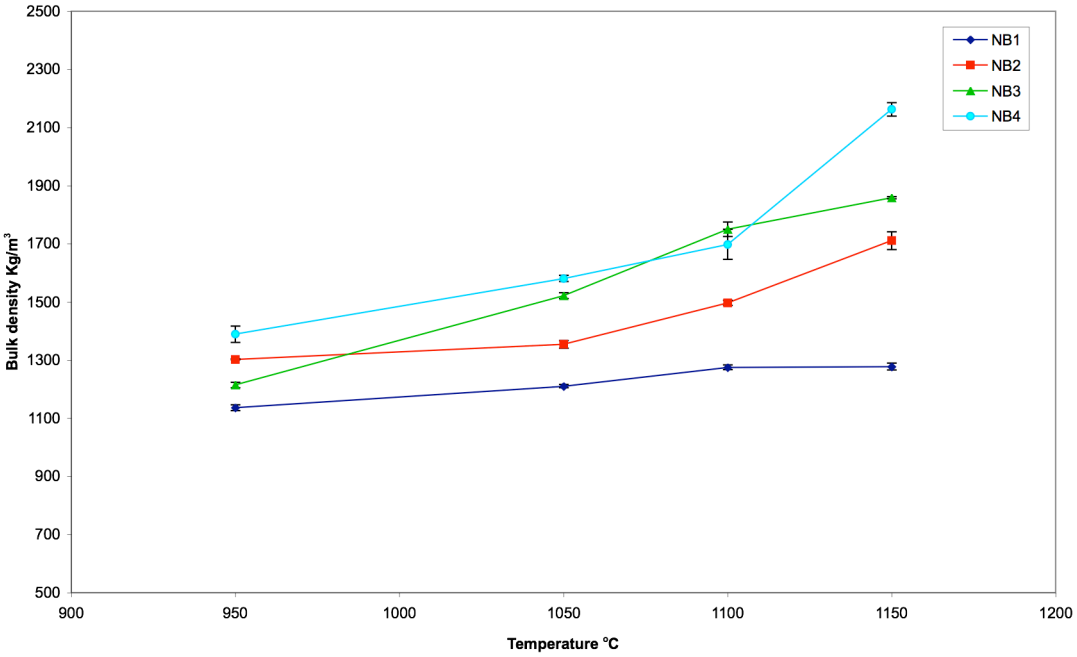


Figure 4-23: Plot of density versus sintering temperature of samples containing different concentrations of sodium borate.

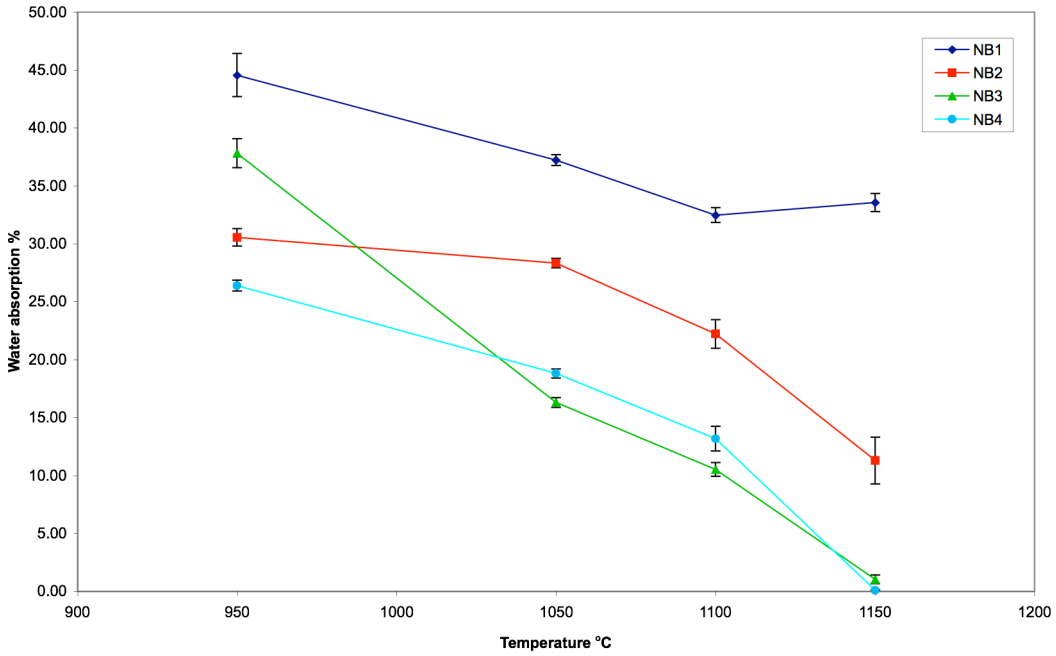


Figure 4-24: Plot of water absorption versus sintering temperature for samples containing different concentrations of sodium borate.

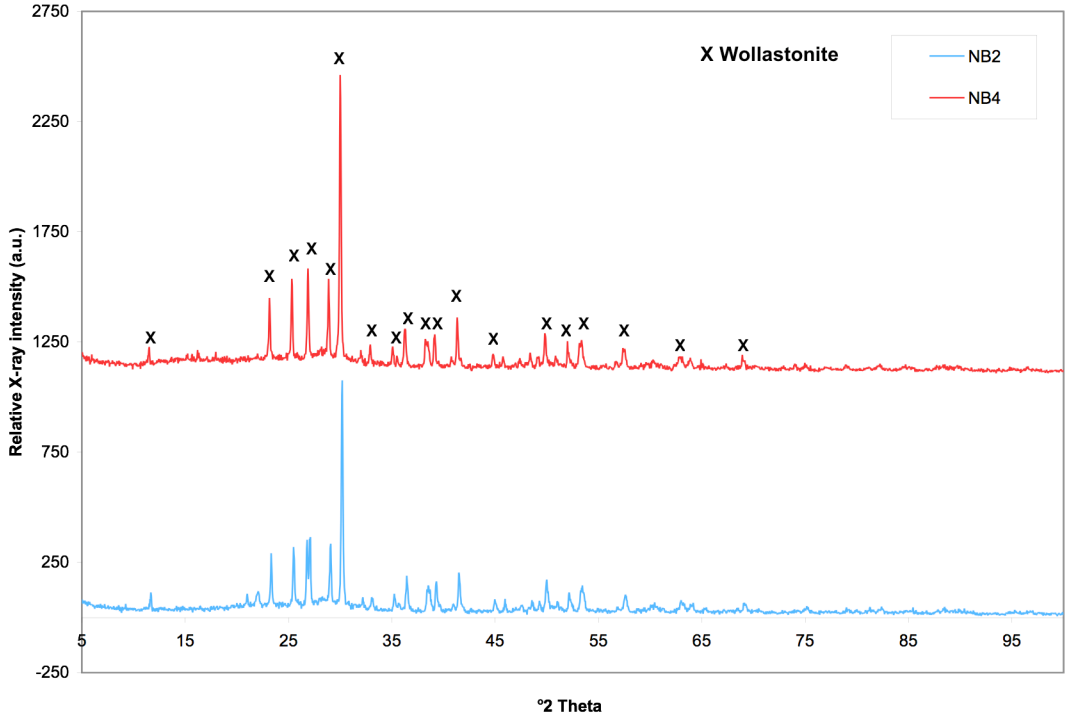


Figure 4-25: XRD patterns of samples NB2 and NB4 sintered for 2 hours at1150^{o}C.

4.4.3 Microhardness

A Vickers microhardness value of 5.4GPa was determined for sintered samples NB2 and NB4. This is a relatively high microhardness value when compared to the sintered samples that contained EP dust, as discussed in section (4.3.1). This value is close to that of porcelain stoneware tiles [118], which suggests that these materials could potentially (with further investigation) be suitable for construction materials. The high microhardness is possibly due to the fine and randomly orientated crystalline microstructure determined by SEM analysis (discussed in section 4.4.5).

4.4.4 Distilled water leach test

Sample NB4 was subjected to a distilled water leach test. The results shown in Table 4-6 are from ICP-AES analysis of leachate liquors. The concentration of the elements tested for are below those specified in the waste acceptance criteria for disposal in non-hazardous landfill [114, 119]. This indicates that these potentially harmful elements have been immobilised in the sintered material.

Table 4-6: ICP-AES analysis of leach test leachate liquors for sample NB4.

Element	Concentration ppm
Aluminium	3.6 [0.05]
Barium	<0.01
Chromium	0.1 [0.01]
Copper	<0.01
Lead	0.3 [0.01]
Manganese	0.1 [0.01]
Zinc	0.1 [0.01]
Chlorine	1.35

4.4.5 Microstructure analysis

Figure 4-26 and Figure 4-27 show SEM micrographs of fracture surfaces of sintered samples NB2 and NB4. It can be seen that sample NB4 has a lower porosity than sample NB2 and the porosity is closed, especially at the surface, as confirmed by 0% water absorption (Figure 4-24). The pore shape in sample NB4 is almost spherical, suggesting that they are due to evolved gases or air trapped within the sample during sintering. The shape, lack of connectivity and lower percentage of porosity in sample NB4 is linked to the higher levels of sodium borate within the batch mix (3wt% compared to 1wt% in NB1 and NB2, respectively) which, due to its low melting point, promotes viscous flow during sintering. This leads to increased densification of the material and associated decrease in the number and size of pores. It can be seen that sample NB2 has a degree of connectivity between pores, which accounts for its higher water absorption when compared to sample NB4. The lower levels of sodium borate in sample NB2 mean that viscous flow during sintering is hindered compared to that of sample NB4 and so densification and closing of the pores is lessened.

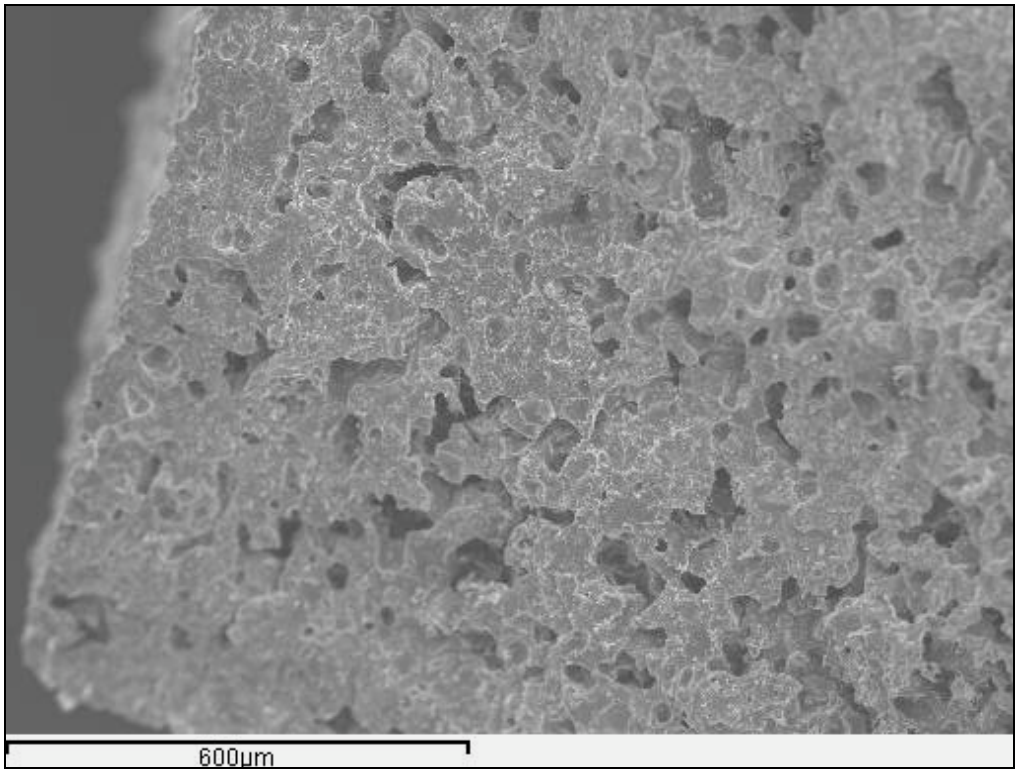


Figure 4-26: Secondary electron SEM micrograph of sintered sample NB2 fracture surface showing interconnected pores.

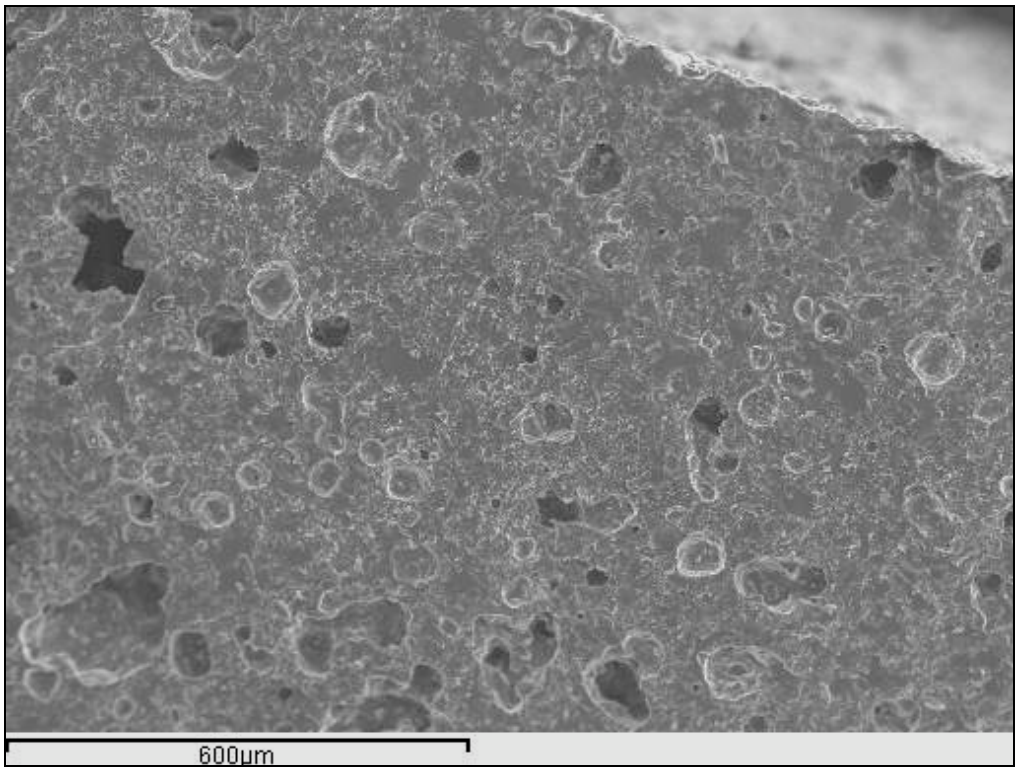


Figure 4-27: Secondary electron SEM micrograph of sintered sample NB4 fracture surface showing closed porosity.

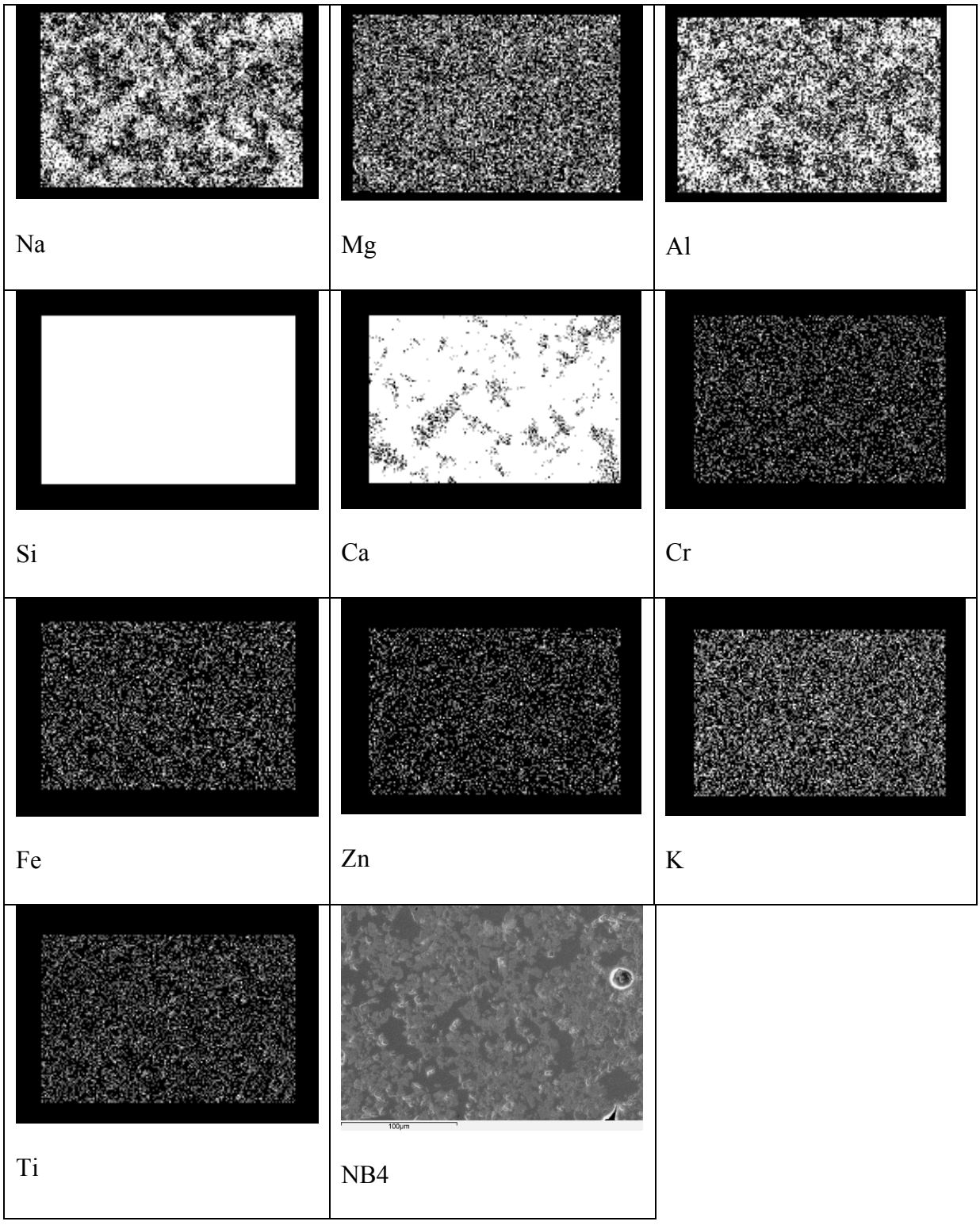


Figure 4-28: SEM secondary electron image of polished surface of sample NB4 and individual EDX element maps for Na, Al, Si, Ca, Mg, K, Zn, Cr, Fe, Ti (x500) light areas show presence of element, dark areas show absence.

It can be seen from the element maps in Figure 4-28 that Si, Ca, Na, Mg, Al, Cr, Fe, Zn, K and Ti were detected by EDX in the selected area of the polished surface of samples NB4. There was a high Si and Ca content as expected due to these elements being in the WAPC residue in high concentration. Elements Si, Mg, K, Cr, Fe, Ti and Zn appeared to be evenly distributed throughout the sintered material, in both observed crystalline phases and the residual glassy matrix. Ca is most concentrated in the crystalline phases, visible as lighter grey areas in the image, with a relatively lower amount in the darker, glassy matrix. Na and Al are detected throughout the sample area but are more concentrated in the glassy phase. The same elements were detected in the area of sample NB2 selected for elemental mapping (Figure 4-29) with the addition of Cl and Ti, which were not detected in the selected area of analysis for sample NB4 shown in (Figure 4-28). Ti was more concentrated in the crystalline phase. Ti is a nucleating agent and so it was expected that it would be concentrated in the crystalline areas.

Figure 4-31 shows a high magnification (x2500) secondary electron SEM micrograph of the fracture surface of sintered sample NB4. The higher magnification analysis was used to investigate the fine microstructure of the fracture surface of sample NB4. The matrix and crystalline areas are clearly distinguishable. These areas were analysed using EDX point analysis. The samples were gold coated rather than carbon coated to achieve a clearer image at the high level of magnification. Due to this, peaks for the presence of gold can be seen in the EDX spectrum (Figure 4-32). The crystalline area, labelled '1', was rich in Ca and Si with no trace elements detected in the area. This agrees with the XRD analysis (Figure 4-25) where the crystalline phase, wollastonite was the only phase detected.

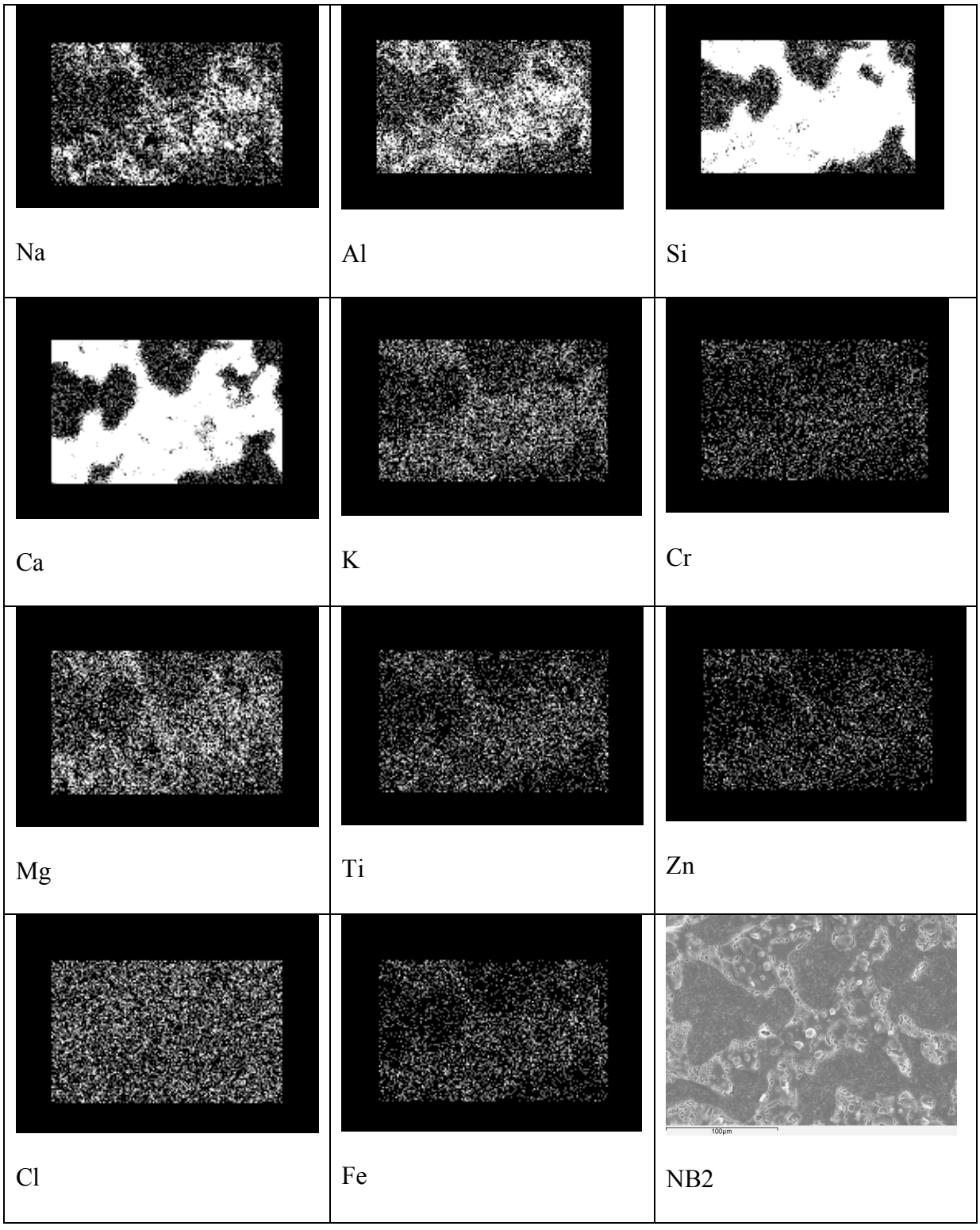


Figure 4-29: SEM secondary electron image of polished surface of NB2 and individual EDX element maps for Na, Al, Si, Ca, K, Cr, Cl (x500) light areas show presence of element, dark areas show absence.

Area ‘2’ appeared to be glassy matrix as no crystalline structures were visible. EDX point analysis (Figure 4-33) showed that the glassy phase was rich in Ca and Si, but the concentration of Ca was less so in comparison to area ‘1’. In contrast to area ‘1’, the elements Zn, Na, Ti, Fe were also detected in area ‘2’. Elements K, Al and Mg were also detected, in a different area of glassy phase, within the same sample. The XRD and EDX analysis suggested that not all of the elements are substituted into the crystalline structure but remain in the glassy phase.

The element mapping in Figure 4-29 detected a number of elements distributed throughout the crystalline and glassy phases of sample NB2 without the distinct separation indicated by the XRD and EDX point analyses. This may be due to the higher magnification, rough surface and point analysis producing a less representative picture of the crystalline phase and low concentrations of a number of elements being substituted into the crystalline phase not being detected by XRD. Alternatively, it may be that the low magnification used for the elemental mapping (x500) caused overlap of the EDX signals.

The glassy phase of sintered sample NB4 (Figure 4-31, area ‘2’) has a lot of what appear to be small pores or areas of phase separation. An SEM image of the same area was produced using backscattered electrons (Figure 4-34). The porosity/phase separation was not visible in the backscattered image, which suggests that the features are pores rather than phase separation, which would be visible as areas of contrast due to variation in atomic number of the different elements.

The fracture surface of sample NB4 has a very irregular surface with unaligned wollastonite crystal surfaces. The progression of the fracture surface through the glass phase, in contrast, was uninterrupted and produced a smooth surface. The rough surface of the crystalline phase could be an indication of increased fracture toughness of this material by a mechanism of crack deflection. Such a surface is produced when a crack is forced to follow a torturous path as it is deflected by a high number of small crystallites producing a rough fracture surface. Figure 4-30 (adapted from Boccaccini and Winkler, and Rawlings and Mathews [120, 121]) shows the mechanism of deflection of a crack as its path is interrupted by crystallites. It was not possible to test the fracture toughness of sample NB4 due to limited material. However, the relationship between fracture surface roughness and fracture toughness would suggest that this material might possess high fracture toughness. The correlation between fracture surface roughness and fracture toughness was observed by Boccaccini and Winkler [121] in a platelet reinforced borosilicate glass. They determined that a glass composite could be toughened by increasing the volume of platelets in the glass matrix and that surface roughness and fracture toughness can be correlated by a linear function.

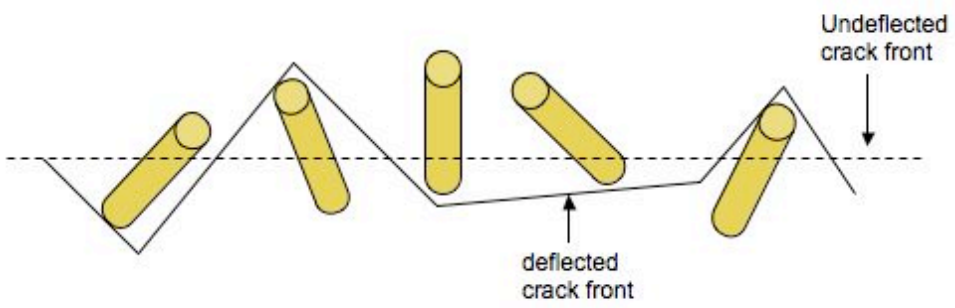


Figure 4-30: Schematic showing fracture path with crack deflection in a glass-ceramic.

Fracture toughness of a material is related to its brittleness. Brittleness is the susceptibility of a material to deformation and fracture. Boccaccini proposed that a brittleness index can be determined by the ratio of hardness (which quantifies resistance to deformation) to the fracture toughness (which quantifies the resistance to fracture) of a glass-ceramic ($B=H/K_{1c}$) and gives an estimation of machinability [122]. Combining the response of a glass-ceramic to both fracture toughness and hardness will give a better quantification than a single parameter [122]. This relationship was confirmed using experimental data and data from literature for a range of glass-ceramics. Sintered materials NB2 and NB4 had microhardness values of 5.4GPa (section 4.4.3) and, as discussed, the observed fracture surface roughness suggests that the samples could possess high fracture toughness. This could indicate that the sintered samples may have a relatively low brittleness index. A value below $4.3\mu m^{-1/2}$ was determined to be a material with good machinability and values for glass and ceramics being in the range of $3\mu m^{-1/2}$ to $9\mu m^{-1/2}$ [122].

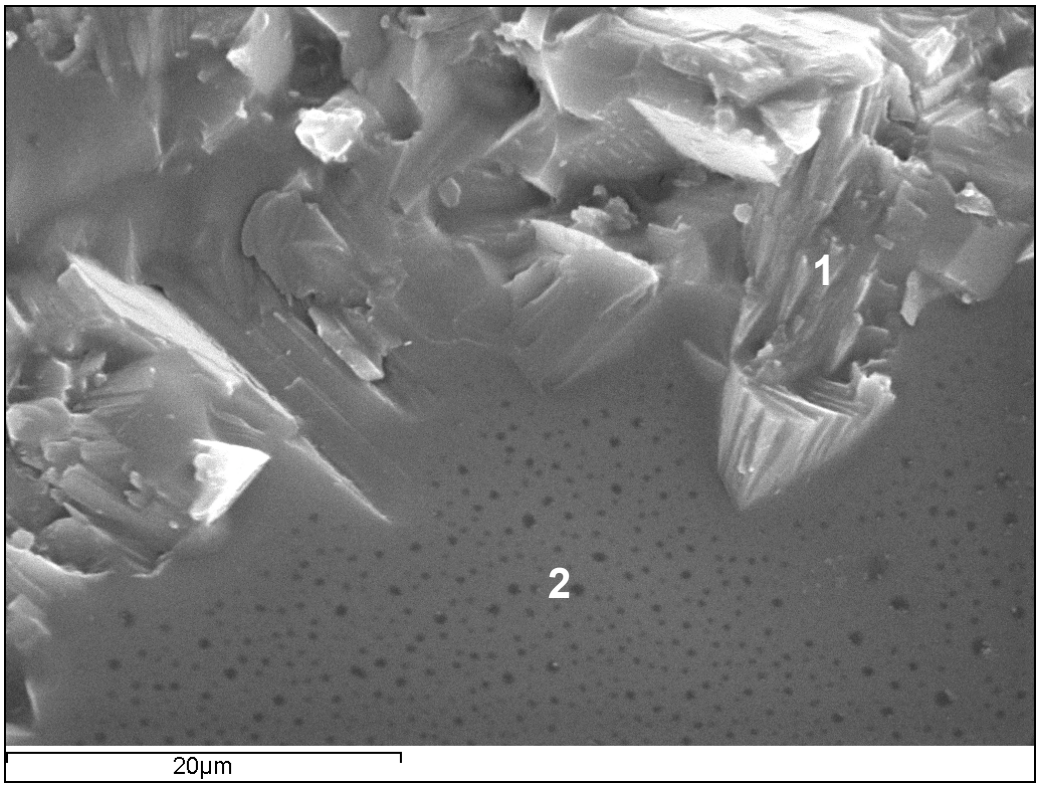


Figure 4-31: SEM micrograph of a fracture surface of sample NB4 sintered at 1150°C for 2 hours (gold coated x2500).

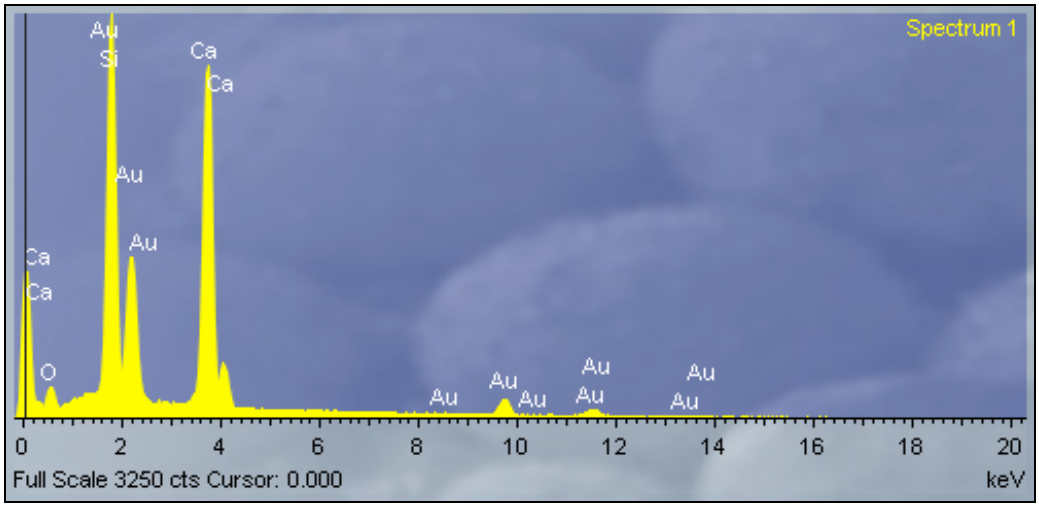


Figure 4-32: EDX element spectrum for sample NB4 point 1, sintered at 1150°C for 2 hours (gold coated).

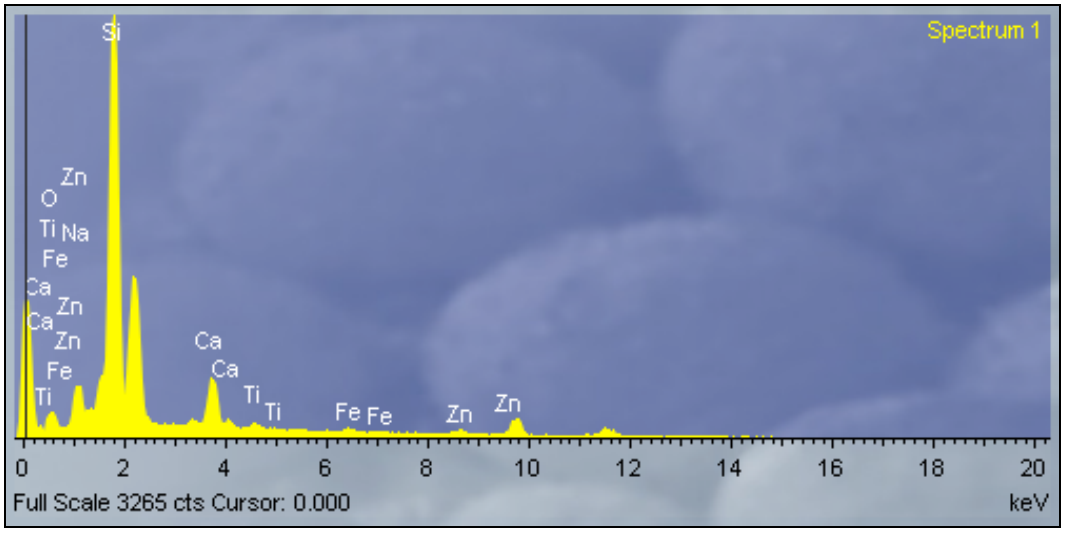


Figure 4-33: EDX element spectrum for sample NB4 point 2, sintered at 1150°C for 2 hours (gold coated). Peaks without labels are gold.

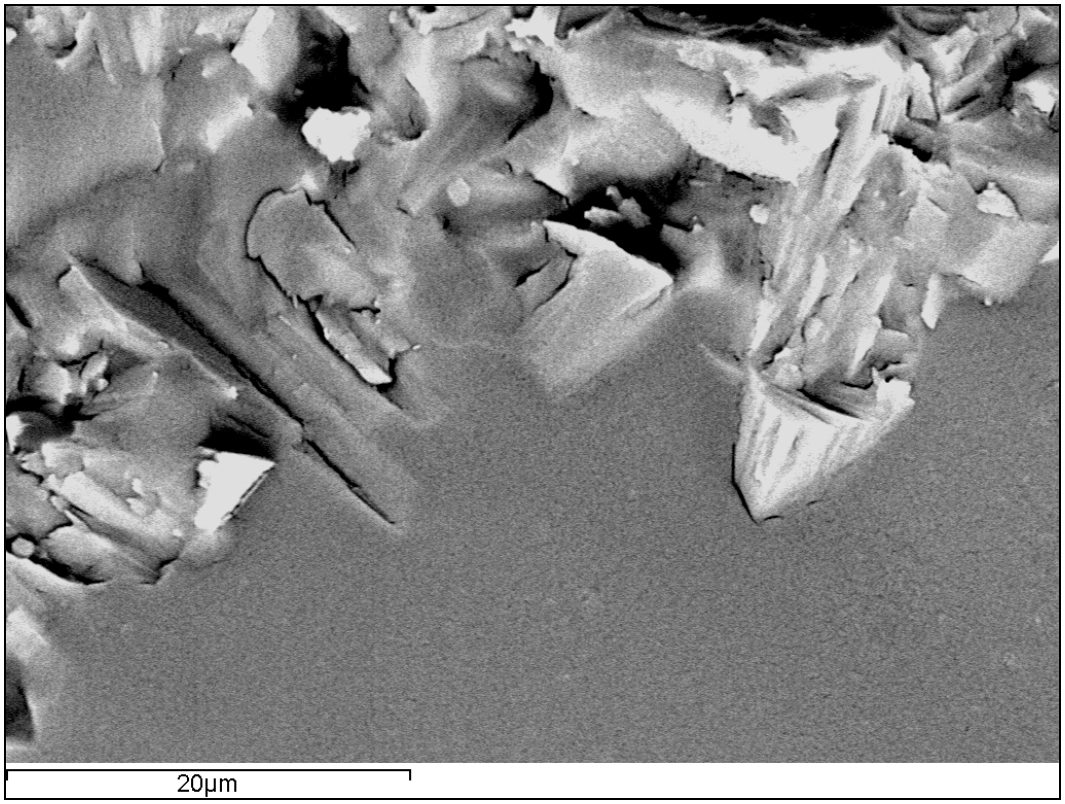


Figure 4-34: Backscattered SEM macrograph of fracture surface of sample NB4 sintered at 1150°C for 2 hours (gold coated x2500).

4.5 Chapter Summary

The APC residues required pre-treatment in the form of washing in order to remove the high levels of chlorides. It was determined that up to 93% of soluble chlorides were removed by the simple washing procedure at a liquid to solid ratio of 20. The washing procedure permitted thermal treatment of the WAPC residues.

The WAPC residues contained more than 50wt% CaO, which meant that additives would be required to produce a glass or a ceramic material, able to be sintered at a low temperature by exploiting viscous flow sintering. A combination of glass cullet and EP dust were used as additives to provide a source of SiO_2 and B_2O_3, respectively. WAPC from other EfW facilities was shown to be of similar crystalline phase composition. This meant that thermal processes developed during this investigation could potentially be applied to APC residues from across the UK or from a single incinerator at different times of the year.

Sintered materials containing wollastonite and gehlenite phases were produced by a powder processing route combining WAPC, cullet and EP dust. TEM analysis showed the presence of nanocrystalline TiO_2. It was found that the addition of EP dust lead to enhanced densification and a reduction in sintering temperature.

It was determined that Neobor® could be used as an alternative source of borate, to produce a sintered material with high density and hardness, low waster absorption, and resistance to leaching. The sintered material was composed of a wollastonite crystalline phase in a glass matrix. A crack deflection mechanism, detected by

investigating fracture surfaces should indicate the material has a high fracture toughness and low brittleness.

This chapter has discussed the successful production of sintered materials from problematic wastes with beneficial properties via a simple production route. Alternative methods, though more energy intensive, for producing glass-ceramics from the wastes via vitrification were also investigated. The results of these investigations are discussed in the following chapter.

5 Glass and Glass-Ceramics from Vitrified APC Residues

5.1 Introduction

A range of glass melts were formed from combinations of WAPC residues, glass cullet and EP dust as described in section 4.4. A systematic approach was used to determine which wastes or combinations of wastes would produce glass melts possessing favourable characteristics, such as a relatively low melting temperature, ability to crystallise to a uniform glass-ceramic structure and low leachability whilst incorporating optimum amounts of WAPC residues. From the selected glasses, glass-ceramics were developed via the two methods; powder sintering and bulk crystallisation as outlined in section 3.4.

5.2 Glass melts

The experimental melts of batches containing solely APC, WAPC and CAPC residues did not produce amorphous melts. In each case a sintered, brittle material formed in the crucible. It was not possible to produce a melt or a glass from APC residues alone below 1500^{o}C. The inability of APC residues to form a glassy melt without additives is due to its chemical composition. XRF analysis of both as-received and pre-treated APC residues showed it to be low in the glass network former SiO_2 (7wt% and 10wt%, respectively). Addition of one or more additives to increase the amount of glass forming oxides was therefore necessary. This is not uncommon in the recycling of wastes and previous research has found it necessary to add other silicate materials to the waste, such as glass-cullet, sand or pure chemicals to aid glass formation [55, 61]. It was found that is was possible to produce glass melts from APC residues, treated and untreated in combination with EP dust and/or glass cullet. Table 5-1 shows a list of the compositions investigated including the results of the preliminary melts at 1400^{o}C.

Table 5-1: Results of preliminary glass melt investigation

Sample	Composition (wt%)	Melt description	Comments/ observations
1	APC (50) cullet (50)	Opaque, dark green melt	Porous, chlorine gas produced
2	WAPC (50) cullet (50)	Amorphous, dark green	Shattered easily
3	CAPC (50) cullet (50)	Opaque, light green melt	Porous, chlorine gas produced
4	APC (50) cullet (40) EP (10)	Amorphous, mid-green	Chlorine gas produced
5	WAPC (50) cullet (40) EP (10)	Amorphous, dark green	No gas, broke into large pieces
6	CAPC (50) cullet (40) EP (10)	Amorphous, light green	Chlorine gas produced

It was determined that as-received APC residues would not be used in batch mixes due to the evolution of chloride containing gas during melting. Subsequently all APC-residues used in this project were pre-washed before use to minimise chloride levels. Calcined APC residues did not produce a melt without the addition of EP dust. Moreover, the calcined APC residues in the batch mix caused problematic gaseous emissions as well as being energy intensive due to the extra heat treatment stage so CAPC was not chosen for further investigation. Batches 2 and 5 containing WAPC residues produced amorphous melts. It was observed that the addition of EP dust to the batch mix prevented shattering of the glass upon rapid cooling to room temperature (i.e. due to thermal shock) although the cast glass broke into a few pieces on handling.

5.2.1 Optimisation of the addition of WAPC residues

By gradually increasing the amount of cullet in the batch mix, the maximum amount of WAPC residue content that could be combined to produce a glass melt was determined (Table 5-2). It was important to maximise the amount of WAPC residue in the batch mix, whilst still producing an amorphous material, to provide a viable recycling route for APC residues. The maximum WAPC residues content that formed a glass melt when combined with cullet was 60wt%. Above this percentage it was not possible to form a glass, only a sintered, fragile material was obtained. Thus, the optimised glass batch mix was referred to as G4 and contained 60wt% WAPC residues and 40wt% glass cullet.

Table 5-2: Results of increasing WAPC residue addition to glass batch mixes melted at 1400^{o}C

Sample	Composition (wt%) WAPC wt%/cullet wt%	Melt Description
G1	90/10	No melt. Powdery
G2	80/20	No melt
G3	70/30	No melt
G4	60/40	Amorphous melt
G5	50/50	Amorphous melt

5.2.2 Effect of borate addition

It was noted previously that the addition of EP dust to the batch mix improved the thermal shock resistance of the resulting melt. Gradual addition of EP dust to the glass melt batch mix (based on the optimised G4 WAPC/cullet glass batch mix) was carried out to observe any associated changes to the physical properties of the melt such as viscosity, melting temperature and ability to crystallise. The results of increasing the EP dust content to the batch mix are summarised in Table 5-3. All batch mixes produced amorphous melts. The most obvious difference was a gradual colour change from dark brown to light green and a decrease in viscosity with increasing EP dust content. Again, increased levels of EP dust appeared to reduce the shattering of samples upon rapid cooling.

Table 5-3: Result of increasing EP dust addition to glass batch mix.

Sample	Composition wt% WAPC/cullet/EP	Melt description of glass	Observations/Comments
GB1	57/38/5	Brown	Viscous
GB2	54/36/10	Lighter brown	-
GB3	51/34/15	Streaked green and brown	-
GB4	48/32/20	Amorphous, light green	Noticeably less viscous
GB5	45/30/25	Amorphous, green	Quenched at room temperature without cracking
GB6	42/28/30	Amorphous, green	Lowest viscosity.

Based on the observations made on the meting behaviour, two glasses were selected for further investigation for their conversion into glass-ceramics. These were glasses G4 and GB6. The amorphous XRD patterns for these two melts are shown in Figure 5-1. G4 was selected as it contained the maximum amount of WAPC residues possible without the addition of any borate in the form of EP dust, whilst still achieving an amorphous product. GB6 was selected as it exhibited a simple and predictable thermal behaviour which was the least complicated evolution of crystallisation of the EP dust containing glasses with a clearly defined crystallisation peak when analysed by DTA (Figure 5-2). A further benefit of GB6 over the other glasses was the ability to work with the hot melt relatively easily. GB6 could be cast in moulds heated to 300^{o}C on a hotplate then allowed to cool slowly to room temperature without cracking prior to the annealing stage. It was also possible to cast small freeform discs from the melt onto a steel plate at room temperature, however, this was less reliable as cracks occasionally occurred.

Figure 5-2 shows the DTA traces for G4 and GB6 powdered glass samples. The small endothermic troughs at 600°C and 700°C correspond to the glass transformation temperature of each glass. Both glasses produce a distinct, single exothermic crystallisation peak. It can be seen that the addition of 30wt% EP dust to the batch mix reduces the glass transition temperature by 100°C and the peak crystallisation temperature by 40°C. Glass compositions containing less than 30wt% EP dust addition (GB1-5) exhibited more complex crystallisation behaviours, with less distinct crystallisation peaks than those visible in Figure 5-2.

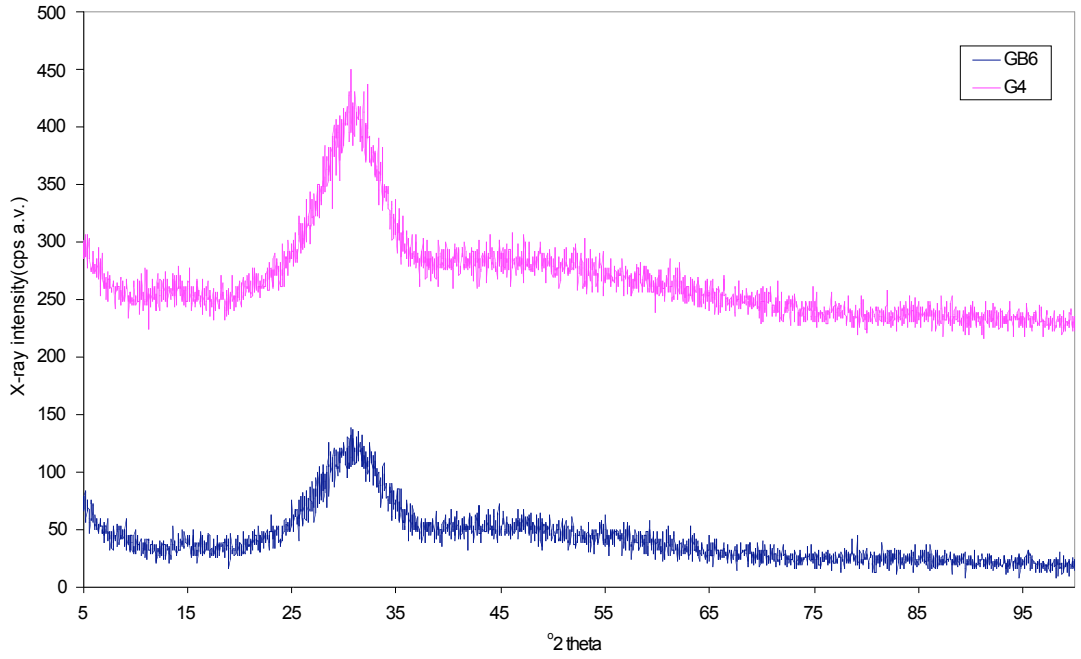


Figure 5-1: XRD patterns of glasses G4 and GB6 showing halos from short range period order.

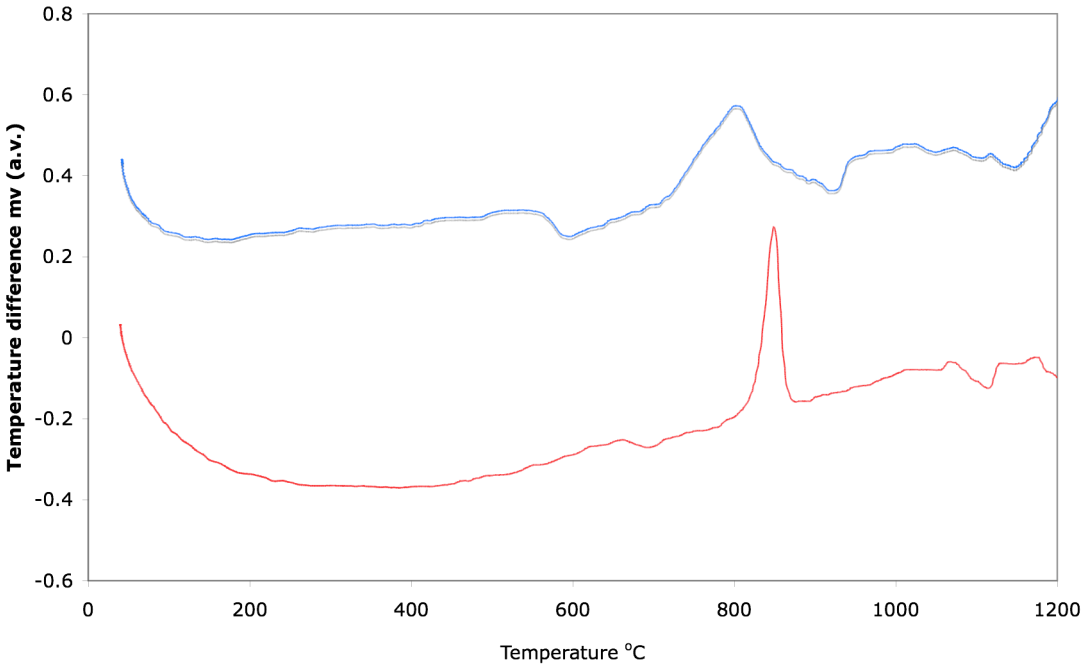


Figure 5-2: DTA traces of powdered glasses G4 and GB6 heated to 1200°C.

5.3 WAPC residues from other UK EfW facilities

Figure 4-8 (Chapter 4) shows the XRD patterns of the as-received APC residues from Portsmouth, Marchwood and SELCHP (November sample) EfW facilities. The XRD analysis shows that the same crystalline phases are present in all four samples. This was expected due to the EfW facilities using the same technology and similar waste input. However, there is some variation in the amount of each phase present shown by the changes in X-ray intensity and resultant peak height. WAPC residues sampled in November 2005 from SELCHP EfW facility contain a strong SiO_2 peak, also present in the Marchwood sample but not visible in the remaining samples. The cause for the higher SiO_2 content is unknown, however, the higher level of glass forming oxide was not detrimental to glass formation.

Glass melts based on the GB6 batch mix composition were made by the same methodology to determine whether a similar glass could be formed with WAPC residues of other EfW facilities and seasons. Typical specimens are shown in Figure 5-3. Each WAPC residue successfully produced an amorphous melt of a light green colour as seen with the original glass GB6. An approach that can accommodate a number of WAPC residue sources and possible seasonal fluctuations in APC residue composition is important for possible future application of such methodologies in an industrial setting.

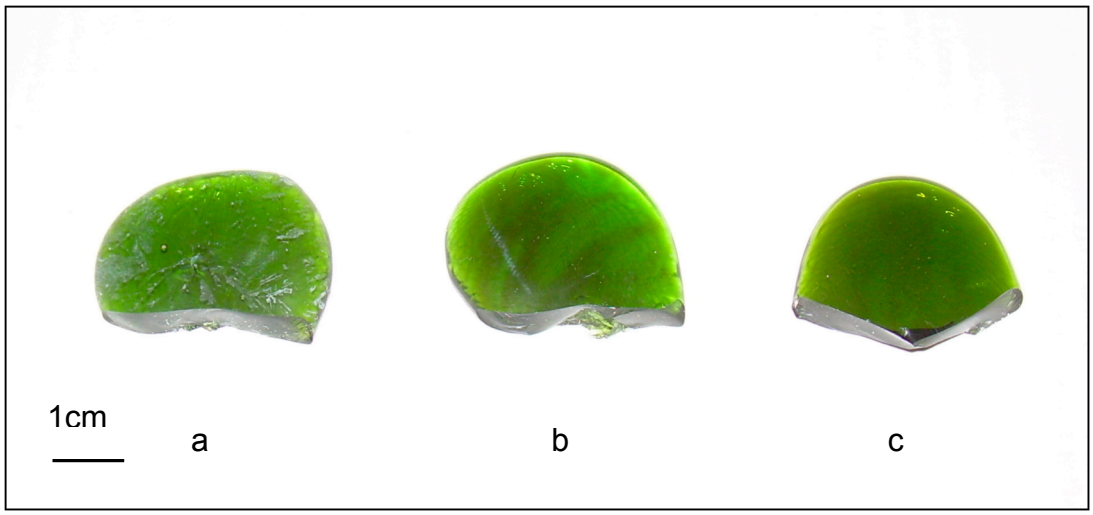


Figure 5-3: Macrograph of vitrified WAPC residues from other UK EfW facilities: a) Portsmouth b) Marchwood c) SELCHP (November)

5.4 Mechanical and physical properties of Glasses

Various mechanical tests were carried out on glass composition GB6. The mechanical properties of glass G4 were not investigated as this glass was not used for the production of glass-ceramics (see section 5.5). Thermal studies for powder sintering of glasses G4 and GB6 determined that GB6 possessed the most favourable densification and crystallisation characteristics and lower treatment temperatures than glass G4.

5.4.1 Vickers microhardness

The Vickers microhardness for glass GB6 was 6.0 ± 0.2GPa. This compares favourably with glasses made from waste residues by similar methods, such as,

4.6GPa achieved for a glass made by vitrification of sewage sludge fly ash with 10wt% CaO at 1500^{o}C for 1 hour [123]. Romero *et al* [97] produced a glass from domiciliary waste incineration fly ash without additives with a Vickers hardness of 5.1GPa for. A glass produced by melting of bottom ash from Italian municipal waste incineration at 1400^{o}C for 1 hour, without additives, possessed a hardness value of 6GPa [26]. Oxide glasses range in Vickers hardness from 2 to 8GPa [80] putting glass GB6 towards the upper end of the range and would be expected to improve when converted, via thermal treatment, to a glass-ceramic due to crystallisation.

5.4.2 Bending strength

A three-point bending test was conducted to determine the flexural strength of GB6 parent glass. The average modulus of rupture of glass GB6 was 65 ± 8MPa producing a linear stress v strain plot exhibiting brittle fracture. This is comparable to typical values for soda-lime glass and Pyrex glass at 69MPa [83] as even with careful sample preparation it is impossible in practise to remove all surface flaws from the glass bars so some variation is inevitable. The modulus of rupture for glass GB6 compares favourably to those of other glasses formed from wastes; 70MPa, 50MPa, 59MPa [26, 101, 123].

5.4.3 Modulus of elasticity

The modulus of elasticity (E) of glass GB6 was measured by an impulse excitation technique as described in chapter 4. The value of E was 83 ± 6GPa. This value

compared well to that of similar glasses produced from wastes, including fly ash from municipal waste incineration 45GPa [101]. Elastic modulus is related to the bond strength within the glass structure and the more interrupted the network is, due to non-bridging oxygens, the lower the value of E. Similarly, layered, or planar glass structures tend to have lower elastic moduli than those with a well connected 3-dimensional structure an example of which is vitreous boric oxide [80]. In a borosilicate glass the degree of connectivity of the structure is affected by the alkali oxide (e.g. NaO_2) concentration with increasing concentrations gradually changing the structure from planar boroxol rings, through to tetrahedral coordination, with high concentrations leading to increased occurrence of non-bridging oxygens until glass can not form [80]. The concentration of NaO_2 is relatively low in glass GB6 at 6wt%, determined by XRF (Table 6-4), and should indicate a fairly well connected structure possibly containing both boroxol rings and tetrahedral accounting for the favourable modulus of elasticity.

5.4.4 Distilled water leach test

Distilled water leach tests on glasses G4 and GB6 were carried out to determine whether the glasses would meet WAC leachate limit values for inert and hazardous waste landfill as specified in the Landfill Regulations 2004 [124]. Table 5-5 shows the levels of those elements present in the leachate solution and specified in the Landfill Regulations 2004. The analysis data shows that the leachate limits for hazardous and inert wastes were not exceeded for any element. Therefore, if the glass was not to be used as, or to produce a useful material of value, it could be safely disposed of according to current landfill regulations with the benefit of a reduction in volume

compared to disposing of as-received APC residues without treatment or those treated by a method such as cementitious stabilisation or carbonation as discussed in chapter 2. Table 5-4 shows the result of XRF analysis of glass GB6. It can be seen that due to the short hold time at temperature the batch mix has retained 10wt% boric oxide. It is important that the boron is retained within the glass and not lost to the atmosphere during vitrification as its presence in the glass structure is required to achieve improved thermal shock, low thermal expansion coefficient, enhanced chemical durability and lower processing temperatures compared to a silicate glass with no boron content [80].

Table 5-4: XRF analysis of glass GB6 (1400^{o}C, 25 minutes).

Determinands	Proportion wt%
Silicon dioxide	32.09
Titanium dioxide	0.53
Aluminium oxide	3.88
Iron (III) oxide	0.53
Calcium oxide	38.96
Magnesium oxide	1.34
Potassium oxide	2.64
Sodium oxide	5.89
Phosphorus pentoxide	0.63
Chromium (III) oxide	0.07
Manganese (II, III) oxide	0.06
Zirconium oxide	0.02
Hafnium (IV) oxide	<0.01
Lead oxide	0.21
Zinc oxide	0.7
Barium oxide	0.04
Strontium (II) oxide	0.04
Tin (IV) oxide	014
Copper oxide	0.06
Boric oxide (by ICP)	10.6
Total	98.43

Table 5-5: ICP-AES analysis of glass leach test samples.

Glass sample	G4	G4 control	Standard deviation	GB6	GB6 control	Standard deviation
Determinants	ppm	ppm	ppm	ppm	ppm	ppm
Lead	0.03	0.03	0.01	0.02	0.02	0.01
Copper	0.01	0.01	0	0.01	0.01	0
Chromium	0.01	0.01	0	0.03	0.01	0.01
Aluminium	0.88	0.05	0.03	0.55	0.05	0.05
Manganese	0.01	0.01	0	0.01	0.01	0
Zinc	0.01	0.01	0	0.01	0.01	0.01
Barium	0.01	0.01	0	0.03	0.01	0
Chloride (titration)	0.32		n/a	0.42		n/a

5.5 Powder sintering of glass

Selected glasses were thermally treated to induce crystallisation *i.e.* devitrification to form glass-ceramics. Two routes for producing a glass-ceramic were investigated; powder sintering and bulk crystallisation. Powder sintering is a well-established method of producing glass-ceramics for practical applications such as wall tiles. The following results are the result of investigating the suitability of glasses G4 and GB6 for use to produce glass-ceramics via this method.

5.5.1 Densification of powder compacts during sintering

Optical heating microscopy was used to observe the densification behaviour of GB6 and G4 glass powders during sintering. The optical microscopy technique has been described in full in chapter 3. Powder compacts for each glass powder were sintered at different heating rates to observe the effect on densification. The effect of powder

particle size was also studied using grain sizes of <45µm and 45-75µm. Figure 5-4 shows the morphology of the glass GB6 powder used for sintering experiments which was crushed using a pestle and mortar then sieved to a particle size the required particle size. The particles are angular with many faces and finer particulates adhered to the surface. Such irregular morphology provides a large surface area for the promotion of crystallisation.

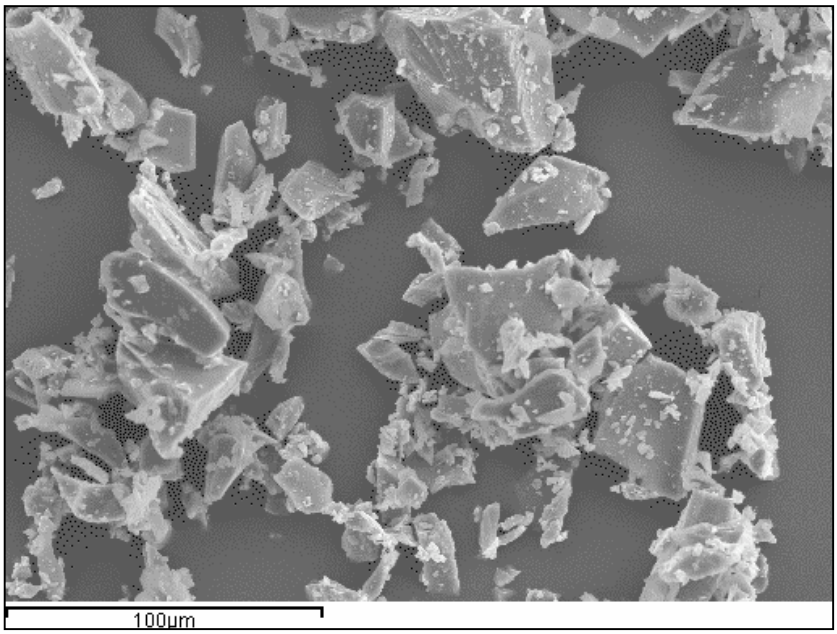


Figure 5-4: SEM micrograph of typical GB6 glass powder morphology <75µm.

To calculate anisotropic behaviour that may have occurred during sintering an anisotropy factor, k was determined using equation (1) where H*o* is the original height of the sample and R*o* is the original radius of the sample. k values greater or less than 1 represent anisotropic shrinkage. When k≈1 isotropic shrinkage has occurred [125].

$$k = \frac{\Delta H / Ho}{\Delta R / Ro} \qquad \text{(Equation 6.1)}$$

Values less than 1 show anisotropic shrinkage with radial shrinkage being greater than axial shrinkage. Values greater than one also represent anisotropic shrinkage however, axial shrinkage exceeds radial shrinkage. It can be seen in Table 5-6 that glass GB6 exhibits anisotropic shrinkage behaviour with radial shrinkage exceeding axial shrinkage. G4 undergoes anisotropic shrinkage however; axial shrinkage is slightly greater than radial shrinkage. Anisotropic behaviour is expected for samples made by isostatic pressing with axial (height) shrinkage being less than radial shrinkage, [126] as exhibited by glass GB6. Figures 5-5 and 5-6 Show the change in sample morphology after sintering for glasses G4 and GB6 sintered at heating rates of 5^{o}C, 10^{o}C and 20^{o}C to a temperature 850^{o}C and 810^{o}C, respectively. The samples were cooled upon reaching the maximum temperature.

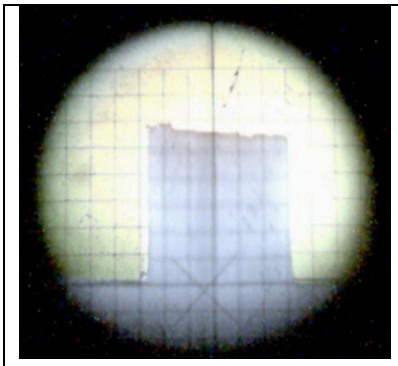
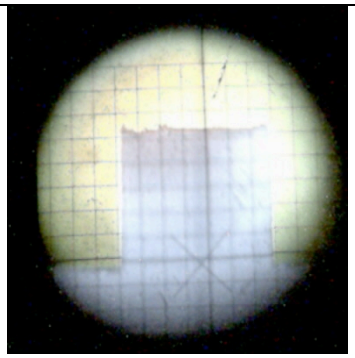
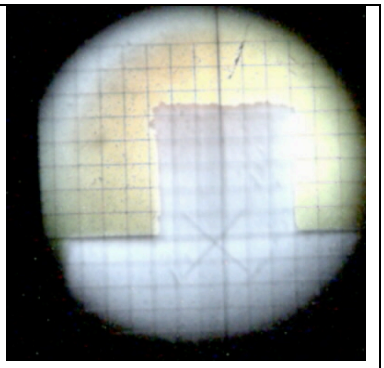
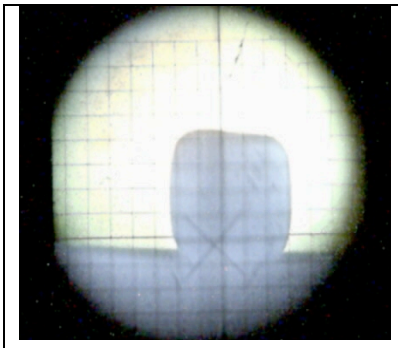
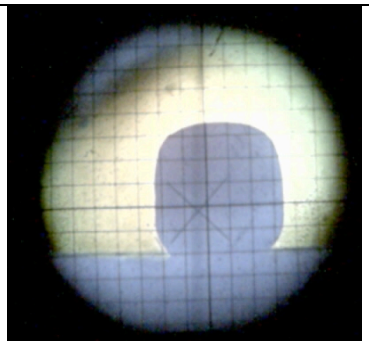
		
G4 5^{o}C/min 850^{o}C	G4 10^{o}C/min 850^{o}C	G4 20^{o}C/min 850^{o}C

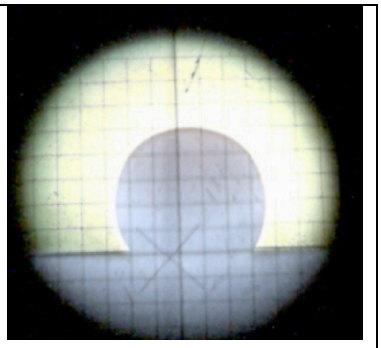
Figure 5-5: OHM images showing effect of heating rate on sample G4 morphology after sintering at 850^{o}C.



GB6 5°C/min 810°C



GB6 10°C/min 810°C



GB6 20°C/min 810°C

Figure 5-6: OHM images showing effect of heating rate on sample GB6 morphology after sintering at 810°C.

5.5.1.1 Effect of heating rate

The densification of powder compacts (<45 μm grain size) G4 and GB6 are markedly different. Compacts composed of GB6 glass undergo far greater densification in both height and width compared to G4. This is due to the lower viscosity of the borate-containing glass GB6 which has a lower SiO_2 content than the more viscous glass G4 [126]. GB6 compacts exhibit a wider temperature range during which the densification occurs, 600-750°C, compared to that of G4, 650-750°C (Figures 5-7 and Figure 5-8).

It can be seen that shrinkage or densification of G4 compacts is not strongly influenced by heating rate with final width and height measurements being very similar with low standard deviations (refer to Table 5-6). However, during the most rapid period of densification (650-750°C) a heating rate of 5°C/min can be seen to have lead to the greatest amount of shrinkage at any temperature point for both radius and height. A heating rate of 20°C/min produces the least shrinkage at any point during the same temperature period. This would suggest that time has a greater

influence than heating rate on G4 glass sintering. SEM analysis of polished GC4 samples showed consistent microstructure for each of the three heating rates. The secondary electron micrographs of GC4 (heated at 5°C/min and 20°C/min) in Figure 5-9 illustrate the crystalline phases with darker, discontinuous areas of residual glassy phase. It can also be seen that there was no obvious effect of heating rate on compact microstructure during sintering, moreover, there was no observable change in macroscopic shape of the powder compact pre and post sintering.

The shrinkage in height of GB6 compacts during the rapid period of densification (600-750°C) follows a similar behaviour to that of G4 samples, with lower heating rates producing the greatest rate of shrinkage. However, the opposite trend is seen for changes in specimen width, where the lowest heating rate leads to the lowest rate of shrinkage and increasing heating rates lead to higher degrees of shrinkage. Even with these conflicting behaviours during the most rapid period of densification it can be seen in Table 6-6 that the heating rate did not affect the final shrinkage values.

Table 5-6: Shrinkage measurements during sintering of GB6 and G4 powder compacts for a particle size <45µm at different heating rates.

Sample	Shrinkage measurement %	5°C/min	10°C/min	20°C/min
GB6	Height	21 (1)	20 (N/A)	19 (3)
	Diameter	25 (2)	25 (10)	26 (2)
	k factor	0.82	0.81	0.73
G4	Height	10.4 (0.5)	10.8 (0.8)	12.3 (2)
	Diameter	9 (N/A)	9.8 (0.8)	9.9 (0.5)
	k factor	1.21	1.05	1.25

Standard deviations stated in brackets.

Analysis of the microstructure and the observed change of shape during sintering suggest that heating rate may have an influence on the sintering process of GB6. It can be seen in Figure 5-6 that the shape of the samples at the peak crystallisation temperature is different. The profiles became more rounded with increasing heating rate. This suggests that the glass powder becomes less viscous with increasing heating rate which should facilitate viscous flow within the compact during sintering [127]. By the completion of densification at 750^{o}C, at a heating rate of 20^{o}C/min the compact has become spherical due to the aforementioned reduction in viscosity. This change in shape suggests that the higher heating rate leads to improved densification. The internal microstructures of fully sintered GB6 specimens at heating rates of 5^{o}C/min and 20^{o}C/min are shown in Figure 5-9 a) and b). It can be seen that the crystalline microstructures produced are similar. However, at the higher heating rate the structure is marginally denser compared to that produced at the lower heating rate.

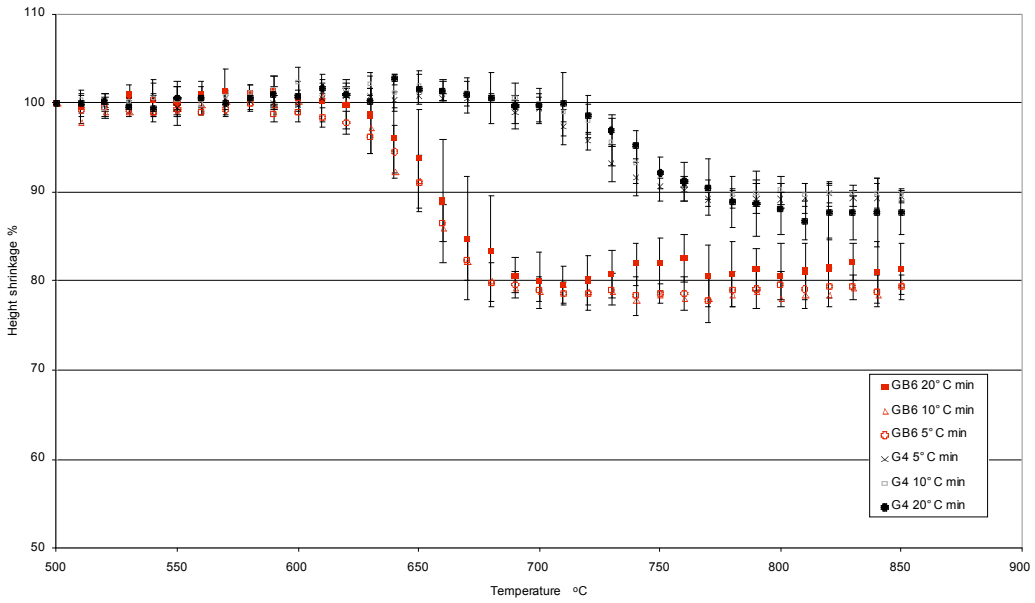


Figure 5-7: Plot of relative change in height (ΔH/Ho) during sintering of G4 and GB6 glass powder compacts at different heating rates (small particle size <45µm).

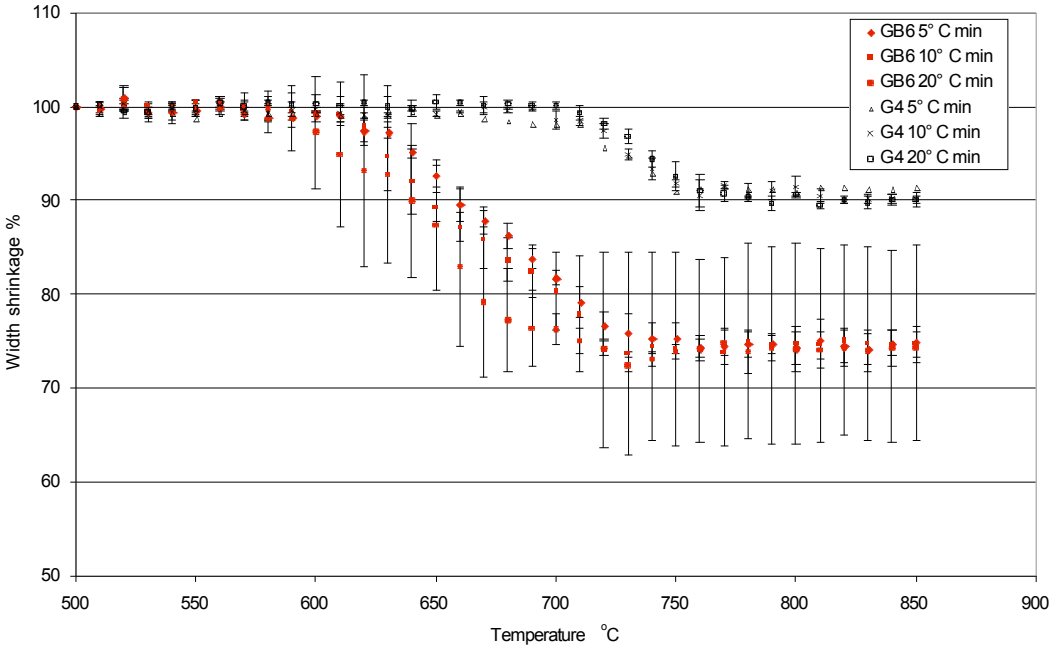


Figure 5-8: Plot of relative change in diameter (ΔR/Ro) during sintering of G4 and GB6 glass powder compacts (small particle size <45µm).

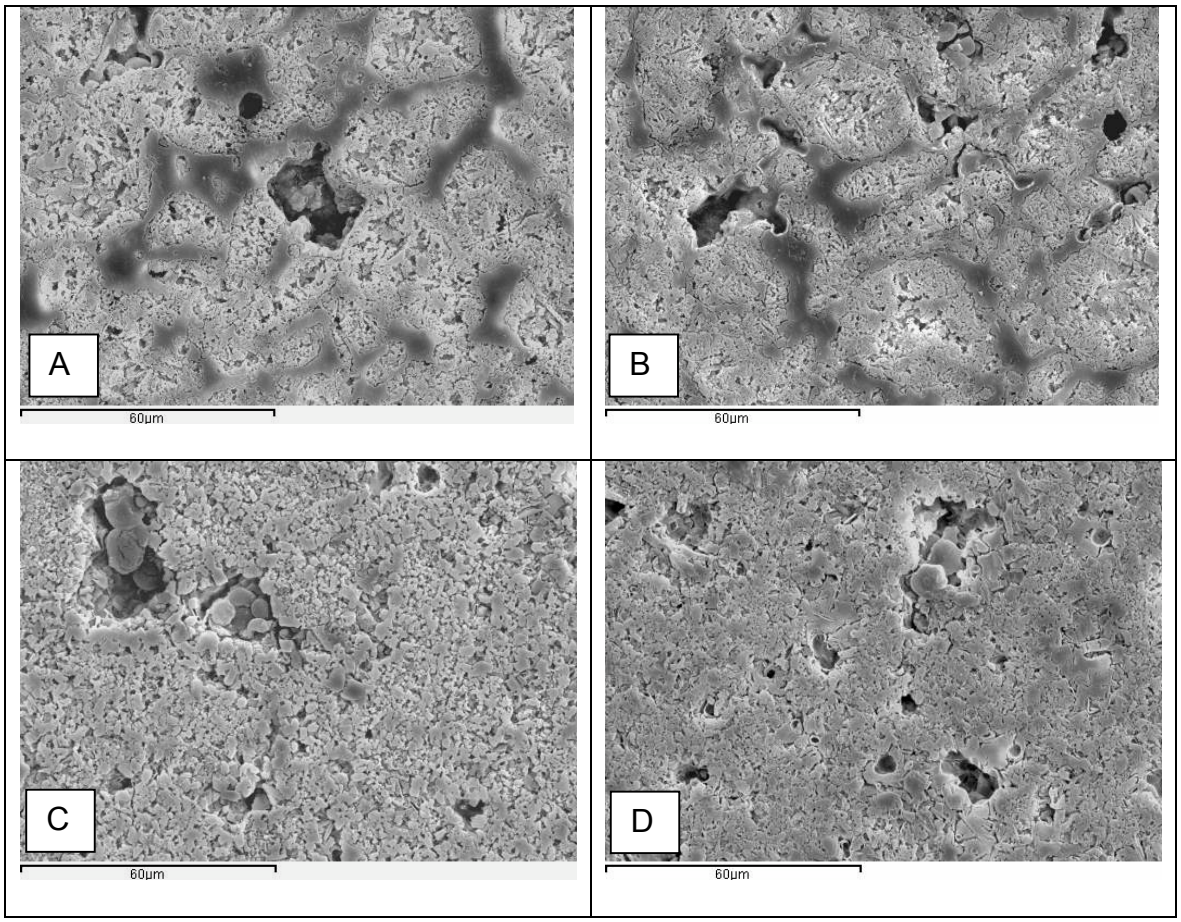


Figure 5-9: SEM micrographs of polished cross sections of: A) G4 glass sintered at 5°C/min, B) G4 glass sintered at 20°C/min, C) GB6 glass sintered at 5°C/min, GB6 glass sintered at 20°C/min to a final temperature of 850°C.

5.5.1.2 Effect of powder particle size

The sintering behaviour of G4 and GB6 glass powder compacts with a larger particle size of 45-75µm showed similar patterns to those samples with a smaller particle size, with densification occurring within the same temperature ranges. However, the actual measured shrinkage in both height and width differed greatly for both G4 and GB6 sintered powder compacts compared to the smaller particle size of <45µm.

When comparing the data in Table 5-7 it is apparent that G4 glass powder compacts underwent less overall shrinkage with a larger particle size. There was a difference in height shrinkage of approximately 6% and 8% and in width they differed by approximately 5% and 9% for heating rates of 20^{o}C/min and 5^{o}C/min, respectively. It should be noted however, that the radial measurement for G4 glass compacts at a heating rate of 20^{o}C/min is the mean of two data points with wide variation so these values are of questionable validity. Moreover, GB6 glass did not show the same degree of variation in height and width measurements when produced with the larger glass powder particle size in comparison to G4 glass samples. GB6 glass specimens exhibited isotropic shrinkage for the large particle size. Isotropic shrinkage can be a beneficial property in order to accurately predict the size and shape changes of manufactured glass-ceramic products during heat treatment. The plots of relative changes in height and width for GB6 and G4 compacts (large particle size) during sintering at 50C and 20^{o}C heating rates are shown in Figures 5-10 and 5-11, respectively.

Table 5-7: Shrinkage measurements during sintering of GB6 and G4 glass powder compacts for particle size 45µm-75µm.

Sample	Shrinkage measurement %	5^{o}C/min	20^{o}C/min
GB6	Height	24	20
	Diameter	23	21
	k factor	1.05	0.95
G4	Height	4	5
	Diameter	4	1
	k factor	1.13	3.66

No standard deviations as values are mean of two data points.

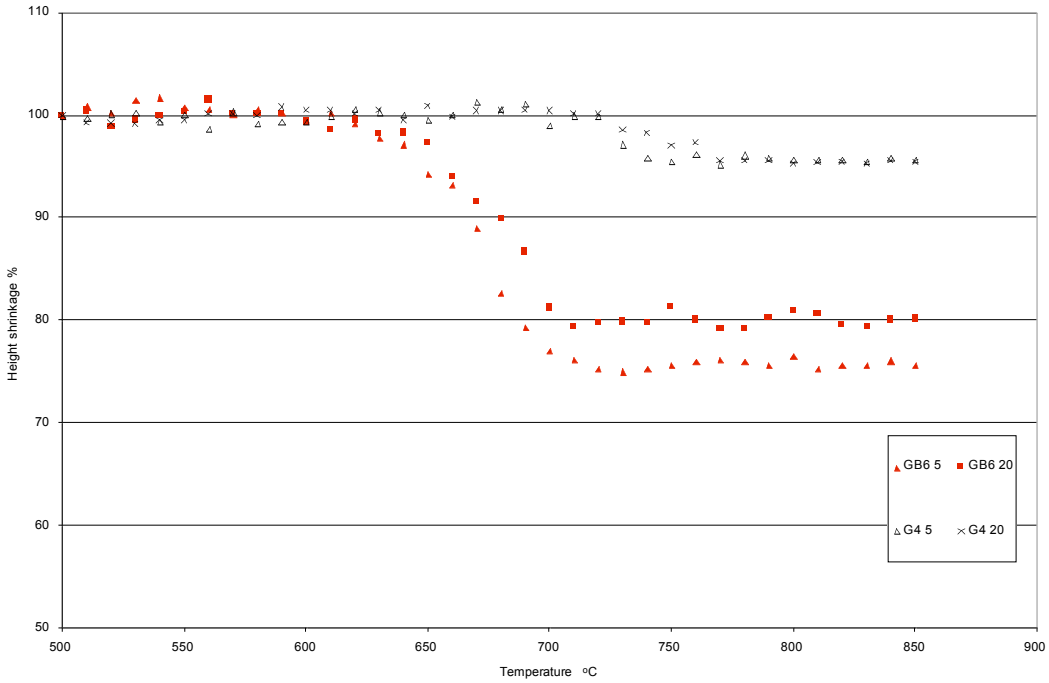


Figure 5-10: Plot of relative change in height (ΔH/Ho) during sintering of G4 and GB6 glass powder compacts (45-75µm).

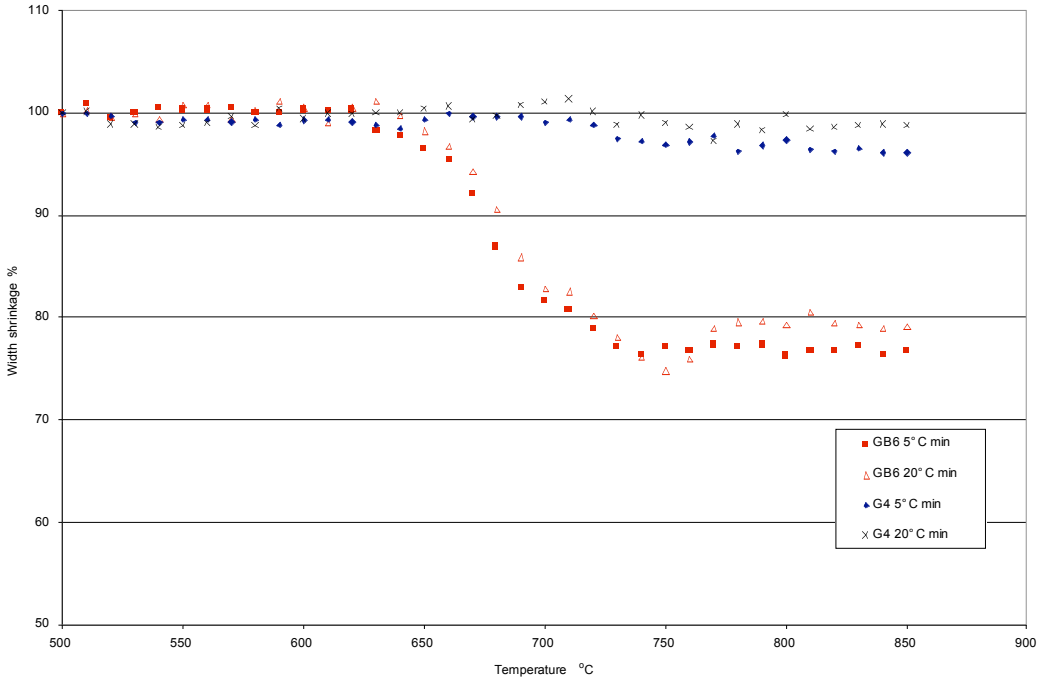


Figure 5-11: Plot of relative change in width (ΔR/Ro) during sintering of G4 and GB6 glass powder compacts (45-75µm).

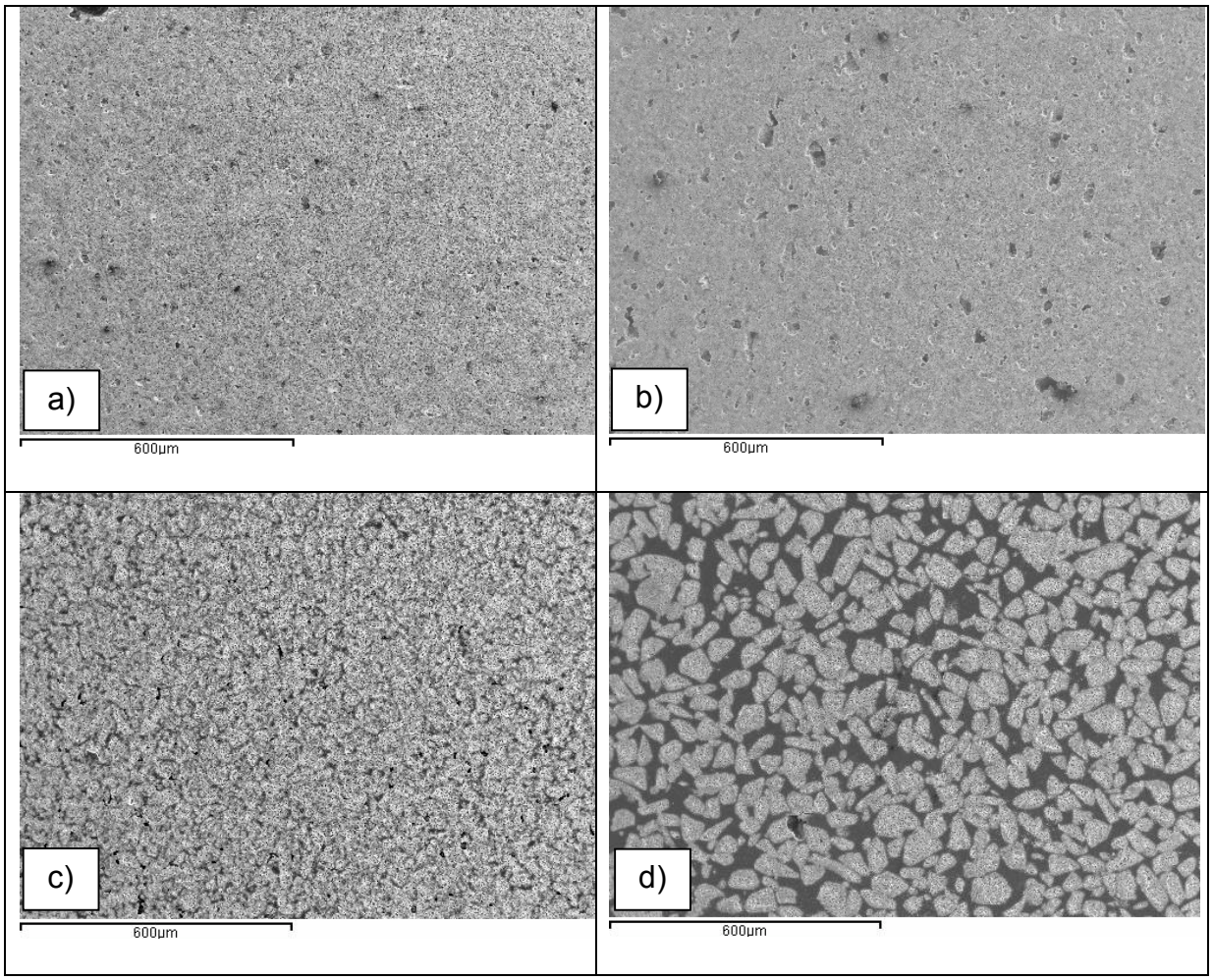


Figure 5-12: Secondary electron SEM micrographs of polished sections of sintered GB6 specimens, heating rate: 5^{o}C/min a) <45µm grain size b) 45-75µm grain size and sintered G4specimens heating rate: 5^{o}C/min c) <45µm grain size d) 45-75µm grain size.

The secondary electron SEM micrographs of polished sections of sintered glass-ceramics formed from G4 and GB6 glass powders show the effect on microstructure due to using different particle sizes (Figure 5-12). For sintered G4 powder compacts the outlines of glass particles are visible but far more so for the larger particle size. It can clearly be seen that there is a higher proportion of glassy matrix relative to the sample formed from the smaller particle size. This is due to glass G4 having greater

surface crystallisation than bulk crystallisation ability. Therefore, the higher surface area to volume of the smaller particle size leads to a higher proportion of crystallinity compared to that produced by the large particle size sample. Both samples derived from glass G4 had low porosity. There was little observable difference between the sintered glass-ceramics produced from glass GB6. Samples produced from both particle size ranges appeared to be fully crystallised possibly due to a more rapid crystallisation and the lower crystallisation temperature of glass GB6 compared to glass G4 which would produce a higher degree of crystallinity compared to glass G4 compacts under the same heat treatment. Bulk crystallisation may also have played a part as at around 850^{o}C this process is beginning as seen in the DTA trace in Figure 5-13. However, the larger particle size appeared to lead to a higher level of porosity possibly due the larger particle size not packing so well during pressing, e.g. due to the absence of small particles filling gaps between large particles to produce a denser green body. This could result in the irregular shape and larger size of the pores.

The results of the optical heating microscopy study determined that glass GB6 would be further investigated for production of a sintered glass-ceramic. Glass GB6 demonstrated greater densification with isotropic shrinkage for a particle size range of 45-75μm. The sintered GB6 compacts had a higher proportion of crystallinity compared to G4 glass that may enhance mechanical properties. Indeed, sintered G4 samples had a Vickers microhardness value of 2.0 ± 0.1GPa and were easily damaged during handling. GB6 sintered compacts had a Vickers microhardness value of 5.0 ± 0.3GPa. A heating rate of 5^{o}C/min was used with the larger powder particle size for subsequent production of sintered glass-ceramics from glass GB6. The heating

microscopy results showed that this heating rate and particle size minimised deformation of the compact shape.

5.5.2 Nucleation and crystallisation studies of glasses

The ability of glasses G4 and GB6 to nucleate and crystallise was studied in order to determine the superior glass composition for glass-ceramic production and the optimisation of thermal processes required for glass-ceramic fabrication. Figure 5-3 shows the DTA traces for powdered glasses G4 and GB6. Both glasses exhibited an exothermic peak characteristic of crystallisation. The crystallisation temperature of glass G4 peaks at approximately 850^{o}C whilst GB6 peaks at 810^{o}C. However, as discussed previously, glass GB6 was chosen for use as a parent glass to produce a sintered glass-ceramic due to its superior densification and thermal behaviour.

DTA analysis of glass GB6 was carried out for both powdered and bulk samples (Figure 5-13). Clearly defined crystallisation peaks were observed for both powdered and bulk samples at temperatures of approximately 800^{o}C and 975^{o}C, respectively.

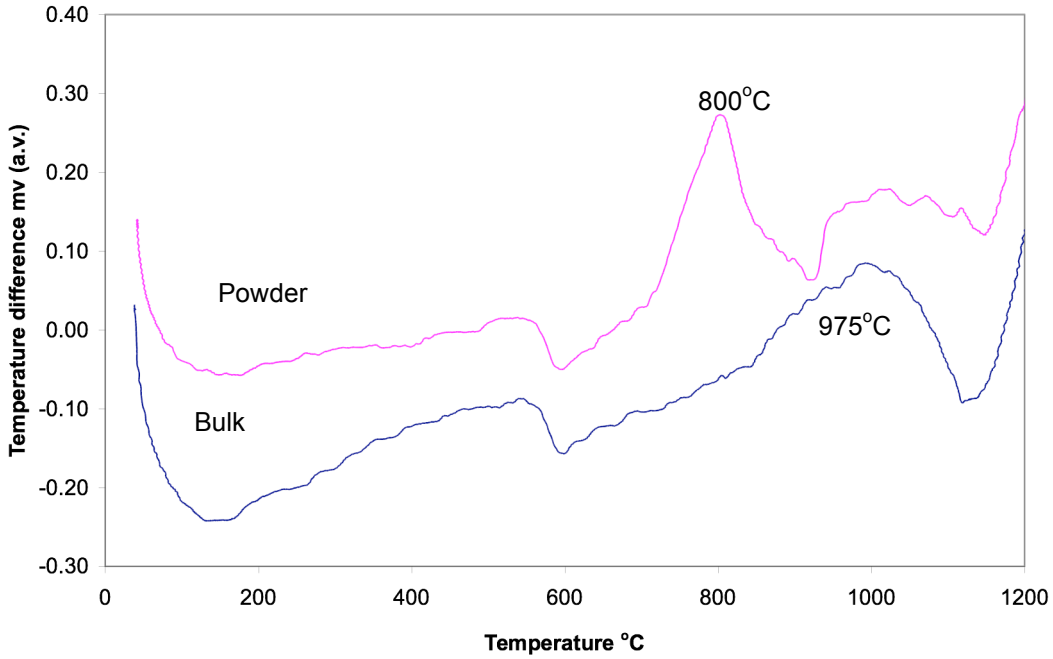


Figure 5-13: DTA traces of GB6 glass powdered and bulk, heated to 1200°C.

Further DTA analysis as described in Chapter 3 was used to determine the optimum nucleation temperature and nucleation dwell time, prior to crystallisation. The height of the crystallisation exothermic peak varied according to the nucleation temperature that the samples were subjected to during a 30 minute dwell time, prior to crystallisation at a higher temperature (Figure 5-14). The largest crystallisation peak occurred following nucleation at 600°C, which is therefore the optimum nucleation temperature. It was found that holding the glass powder compacts at the nucleation temperature for a set dwell time was not necessary as doing so did not result in an increase in crystallisation exothermic peak height (Figure 5-15).

The optimum time that powder compacts should be held at the crystallisation temperature of 850^{o}C was determined by comparing the bulk densities (measured using an Archimedes technique) and SEM analysis of the microstructures (see section 6.6.1).

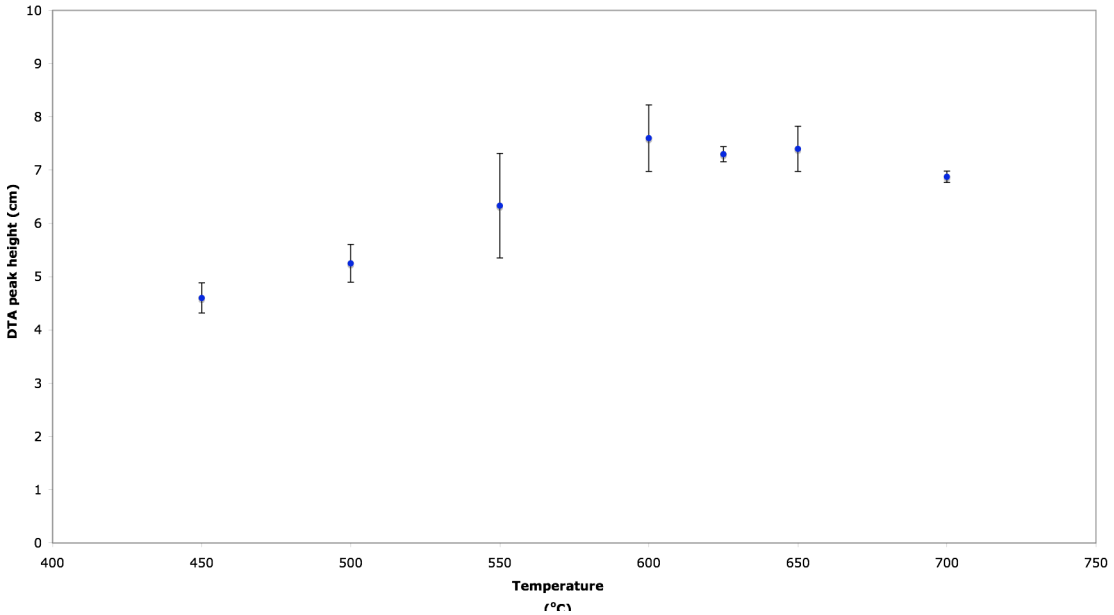


Figure 5-14: Plot showing crystallisation peak heights versus nucleation temperature for sintered glass-ceramic from glass GB6.

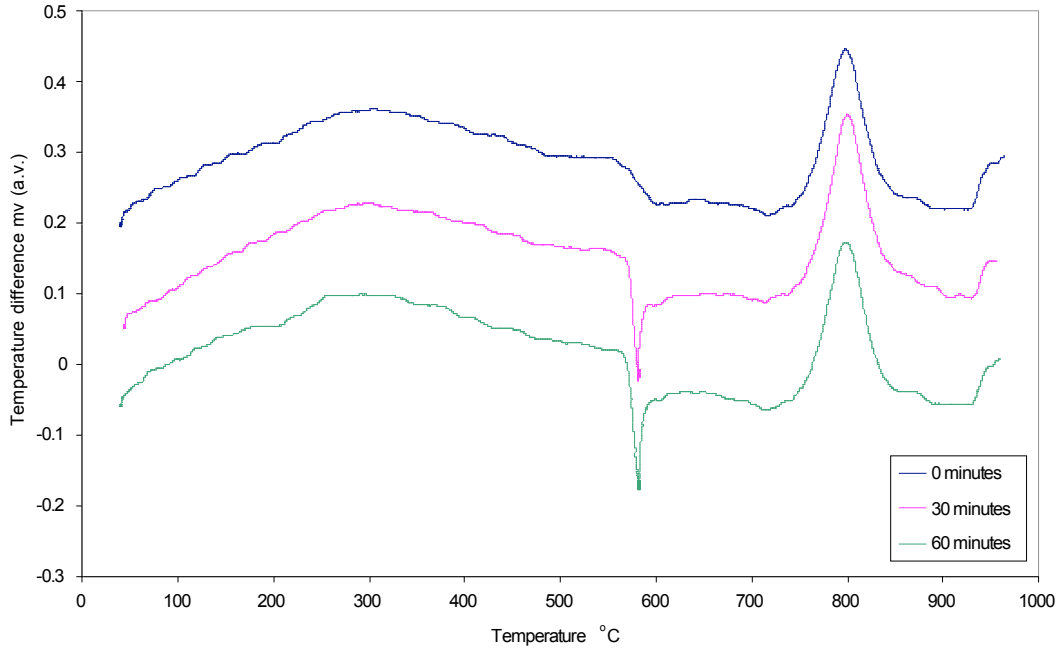


Figure 5-15: DTA traces showing crystallisation peaks of sintered glass-ceramic from glass GB6, following different nucleation temperature hold times.

5.6 Microstructure of sintered glass-ceramics

5.6.1 SEM analysis of sintered glass-ceramic

Figure 5-16 shows an SEM micrographs of the fracture surface of a sample of sintered glass-ceramic produced from parent glass GB6. It can be seen that the glass-ceramic has a porous microstructure. The percentage porosity is approximately 14% as determined by use of a density bottle. The porosity is 'closed' with no interconnection between pores that accounts for the 0% water absorption of the material. The higher magnification SEM micrograph in Figure 5-16 (B) illustrates the morphology of the bladed crystals visible within pores.

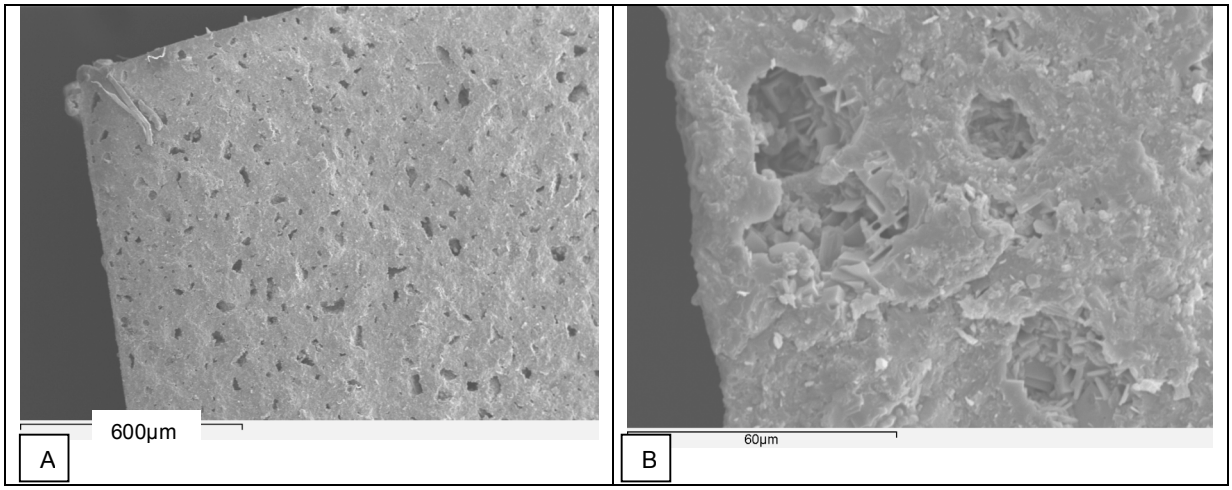


Figure 5-16: A) Secondary electron SEM micrograph of sintered glass-ceramic PC fracture surface showing porosity size and distribution (x100). B) Secondary electron SEM micrograph of sintered glass-ceramic PC fracture surface showing typical bladed crystal formations (x1000).

Figure 5-17 shows SEM micrographs of polished samples of sintered glass-ceramics held at crystallisation temperatures of 1 hour and 3 hours. The microstructures of the two samples show an observable difference in grain size. The sample held at temperature for 1 hour has a finer grain structure with individual grains as small as

2µm compared to the sample held for 3 hours. At a hold time of 3 hours the grains are courser with the majority of grains being larger than 5µm. A sample held at 850^{o}C for 2 hours was also analysed showing crystal morphology as observed for the sample held for 3 hours. Samples held at temperature for 0 hours exhibited a microstructure as observed for a 1 hour hold. However, a minor amount of unreacted glass phase was observable in the sample. A small grain size is considered to be beneficial in terms of mechanical properties such as wear resistance and microhardness [1, 78]. The optimum hold time was therefore, determined to be 1 hour.

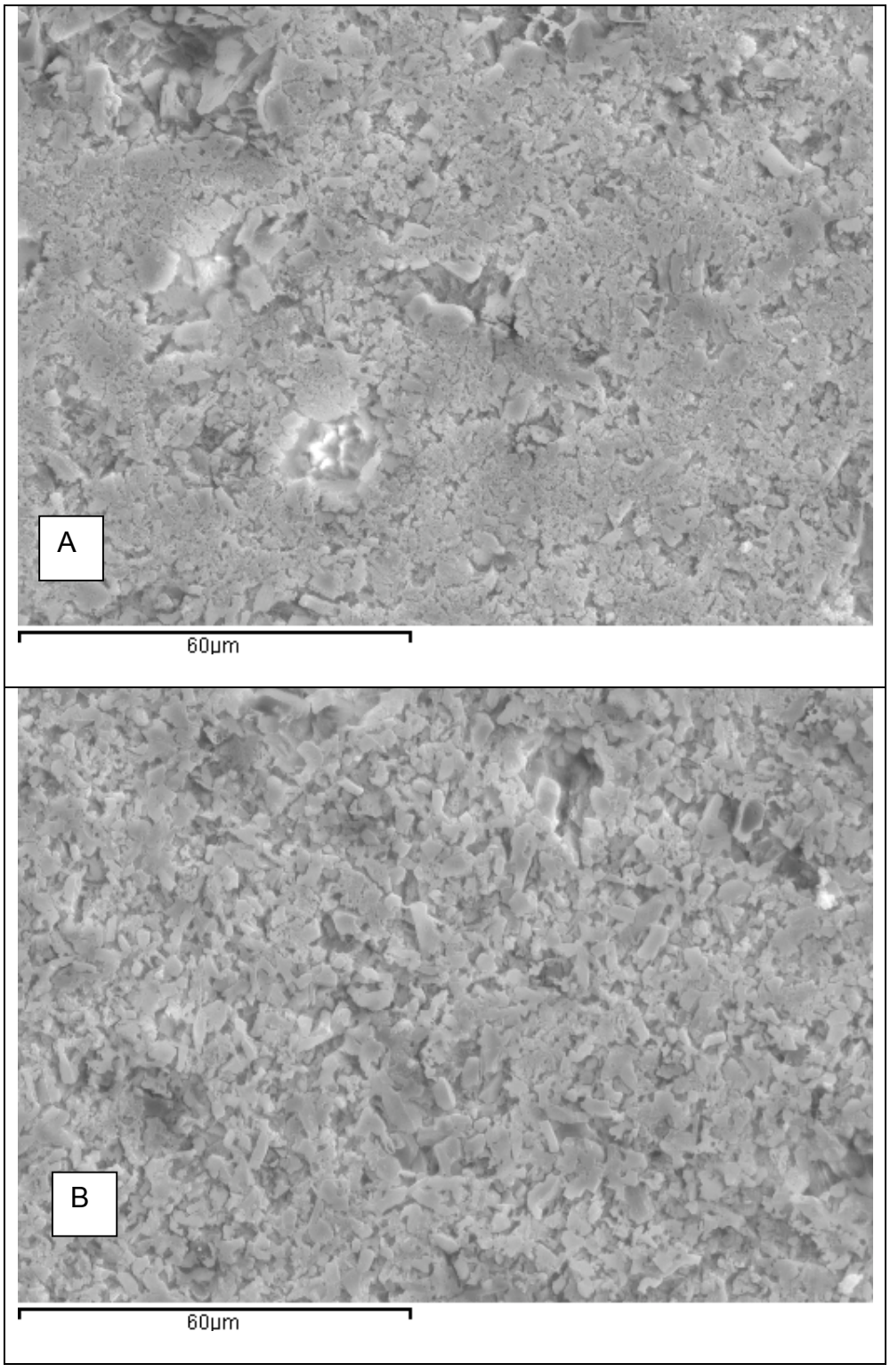


Figure 5-17: SEM micrographs of sintered glass-ceramic polished samples sintered at 850^{o}C for A) 1hr B) 3hr (x1000).

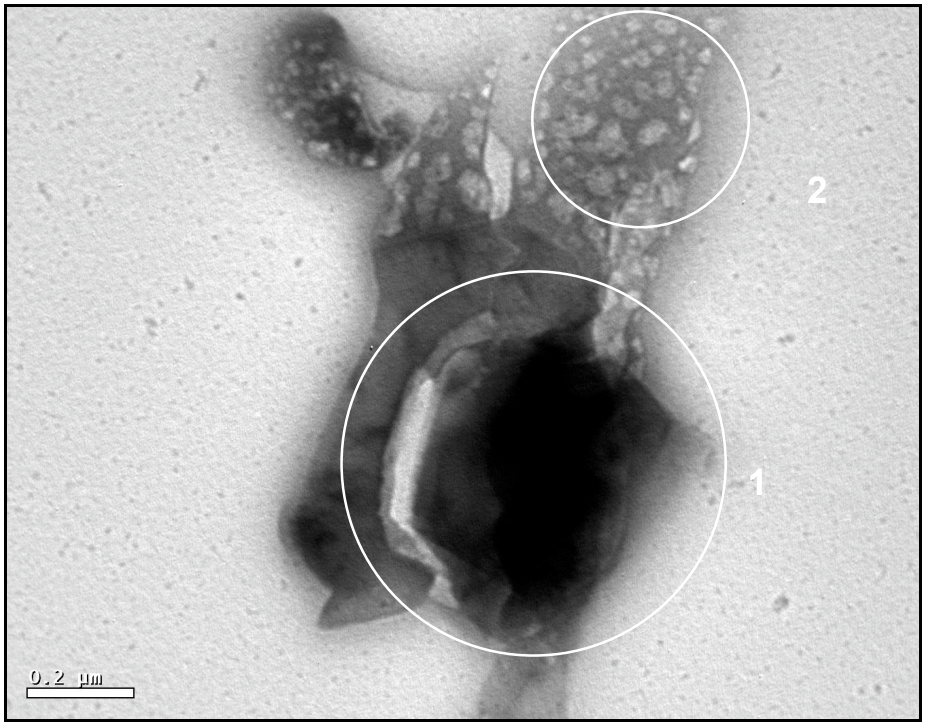


Figure 5-18: TEM bright field image of the glass-ceramic specimen sintered at 850^{o}C (x80,000). Area 1 is crystalline, area 2 is a residual amorphous phase.

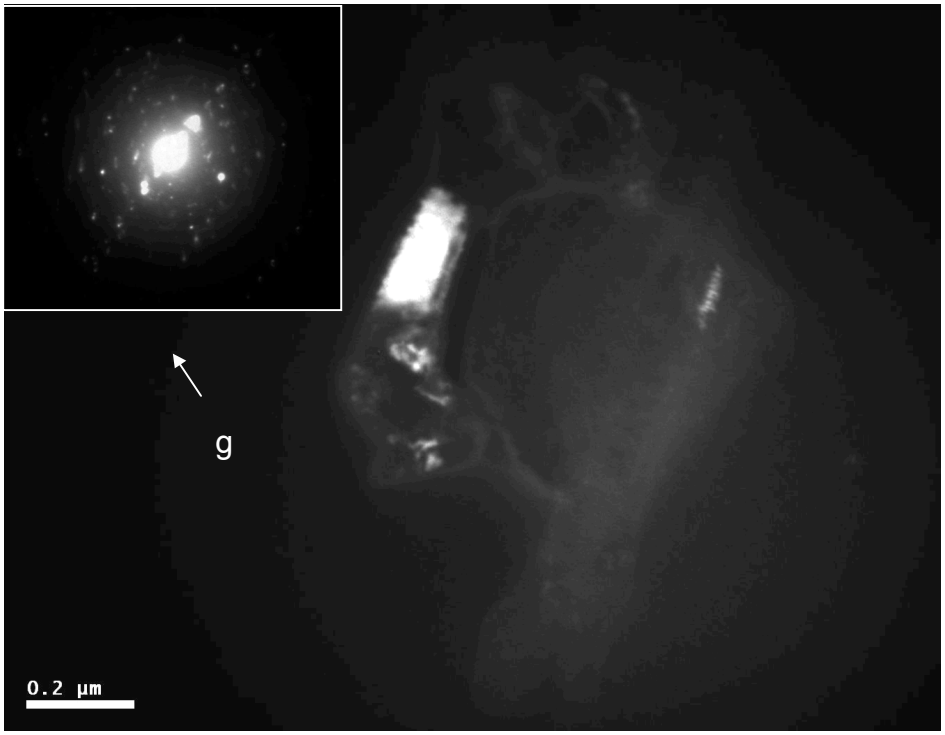


Figure 5-19: TEM morphology of crystal particles using centre dark field technique with - $\vec{g}$ diffraction beam. Diffraction pattern inset.

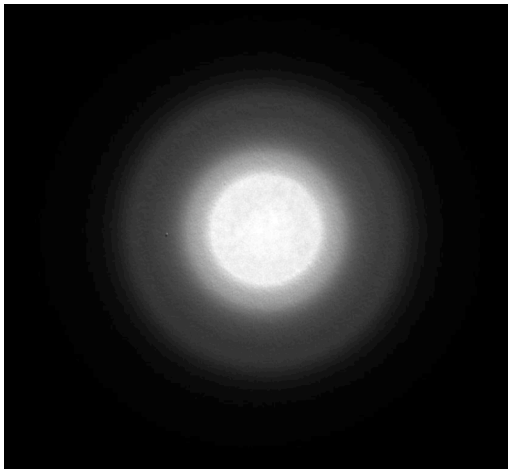


Figure 5-20: Selected area diffraction pattern from region 2 in Figure 5-18 showing the amorphous structure of the glassy phase.

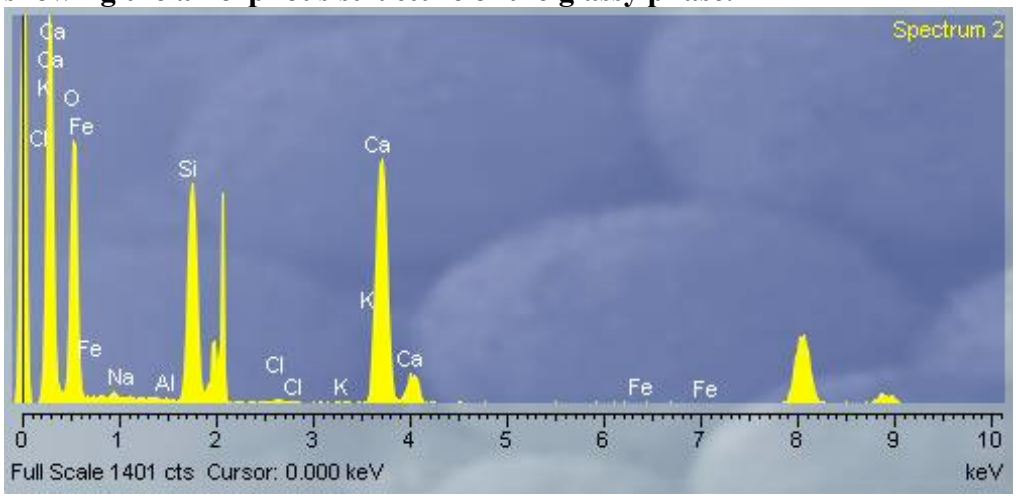


Figure 5-21: EDX spectrum of Ca and Si rich crystalline area 1 indicating the presence of substituted elements.

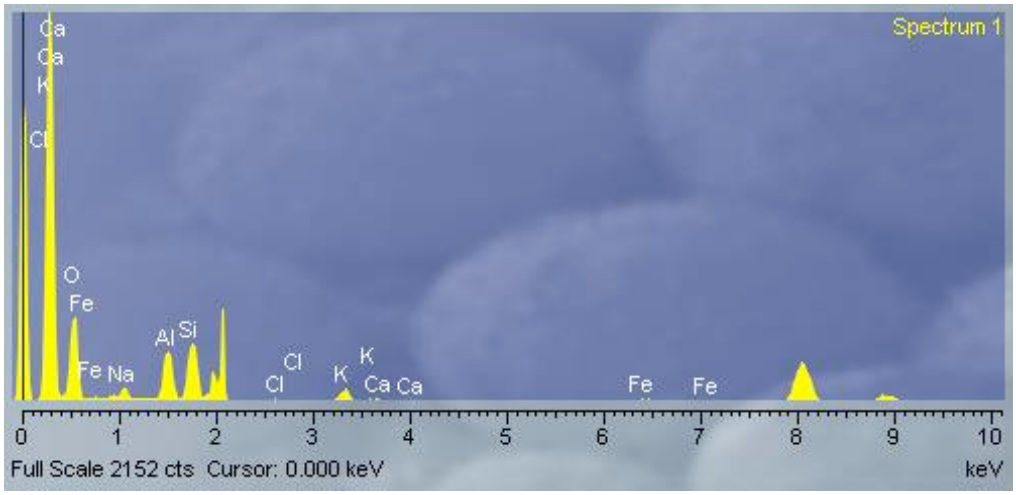


Figure 5-22: EDX spectrum of amorphous area 2 depleted in Si and Ca.

5.6.2 TEM analysis of sintered glass-ceramic

TEM analysis was carried out on the sintered glass-ceramic to obtain more detailed information on the microstructure that might not have been visible using SEM techniques. Two areas of interest were observed, as highlighted in Figure 5-18. Area 1 shows crystalline particles embedded in a glassy matrix. EDX analysis (Figure 5-21) showed that the crystalline particles were rich in calcium, silicon and oxygen, as expected for wollastonite. Lesser amounts of potassium, sodium, aluminium, iron and chlorine were detected.

Area 2 is an amorphous area with phase separation that was not observed previously by any means due to the sub-micron structure. The amorphous phase was confirmed by the diffraction pattern in Figure 5-20. It was not possible to determine the chemical composition of the separate glass phases due to the width of the beam needed to achieve strong x-rays being larger than the scale of the features. The amorphous phase contained the same elements as detected in the crystalline phase (Figure 5-22) elements but was depleted in silicon and calcium as these elements had been incorporated into the crystalline phase.

5.7 Mechanical and physical properties

5.7.1 Bending strength

The modulus of rupture of the sintered glass-ceramic was measured using bar shaped samples by means of a three-point bend test as described in chapter 3. The value

measured was 65 ± 4MPa producing a linear stress v strain plot exhibiting brittle fracture. However, the modulus of rupture for the sintered glass-ceramic was the same as for its parent glass, GB6 which was unexpected. There may not have been an increase in bending strength due to the porosity and lower density of the sintered samples compared to the parent glass. This value is however, favourably comparable to that of other glass-ceramics formed from wastes. Fume abatement and feldspar mining wastes were used by Bernado *et al* [128] to form a glass-ceramic by sintering of a parent glass with a bending strength of 60MPa. Two sintered glass-ceramics were fabricated by Appendino *et al* [26] from glasses formed from bottom ashes from two different municipal waste incinerators at 950^{o}C to achieve a bending strength of 52MPa and 61MPa.

5.7.2 Modulus of elasticity

The modulus of elasticity (E) was measured on bar shaped sintered samples using an impulse excitation technique as explained in chapter 3. The value of E was 70 ± 6GPa. This value is similar to that of sintered glass-ceramics from glasses of a similar waste composition; 70GPa [128].

5.7.3 Density and porosity

The bulk density measurements for sintered samples held at 850^{o}C for 1, 2, and 3 hours were 2600 kg.m^{-3}. The true density of the sintered glass-ceramic was 3000 kg.m^{-3} with a porosity of 14%. The true density of the glass-ceramic was as expected

as the density of Wollastonite and gehlenite are 2900 $kg.m^{-3}$ and 3000 $kg.m^{-3}$, respectively. The bulk density is comparable to other sintered glass-ceramics of similar waste compositions. A sintered glass-ceramic from vitrified bottom ash achieved a bulk density of 2600 $kg.m^{-3}$ with a porosity of 11% [26]. However, porosity of the present material was higher than that reported in the literature for a glass-ceramic fabricated from fume abatement residues and glass waste; 2700 $kg.m^{-3}$ with a porosity of 3% [128].

5.7.4 Leach test of sintered glass-ceramic

Table 5-8 shows the distilled water leach test results obtained by ICP-AES for the sintered glass-ceramic material. The concentration of each element did not exceed the leachate levels for inert and hazardous waste as set out in the Landfill Regulations 2004 [11, 124].

Table 5-8: ICP-AES analysis of sintered glass-ceramic leach test samples.

Element	Concentration ppm Standard deviation [ ]	Landfill leachate limits non-hazardous waste ppm [11]
Aluminium	0.62 [0.07]	-
Barium	0.19 [0.01]	45
Chromium	0.79 [0.04]	5
Copper	0.04 [0.02]	45
Lead	<0.01 [0]	6
Manganese	<0.01 [0]	-
Zinc	0.02 [0.01]	30

5.7.5 Wear resistance and Microhardness

A pin on disc wear resistance test was carried out to compare the wear resistance of a disc sample of sintered glass-ceramic to that of alumina and float glass samples. Table 5-9 shows that the wear resistance and Vickers microhardness values for the sintered glass-ceramic sample and comparison samples of alumina and float glass. It can be seen that the of the sintered glass ceramic is far better than the float glass and similar to that of the sintered alumina. It is important to note that the mechanical properties of the samples are very different. The alumina sample's mechanical properties were nearly three times better than those of the glass ceramic whilst the float glass had a microhardness value close to that of the glass-ceramic sample. Factors such as crystal grain size and porosity will impact upon a materials wear resistance and microhardness [1].

Table 5-9: ware speed values (Wd) obtained from each sample tested.

Sample	Vickers Microhardness (GPa)	Wd (μm/rev)
1. Glass Ceramic PC	4.0 [0.1]	0.8
2. Float Glass	4.9 [0.1]	19.9
3. Alumina	13.2 [0.3]	0.3

Standard deviations in parenthese.

5.7.6 XRD analysis

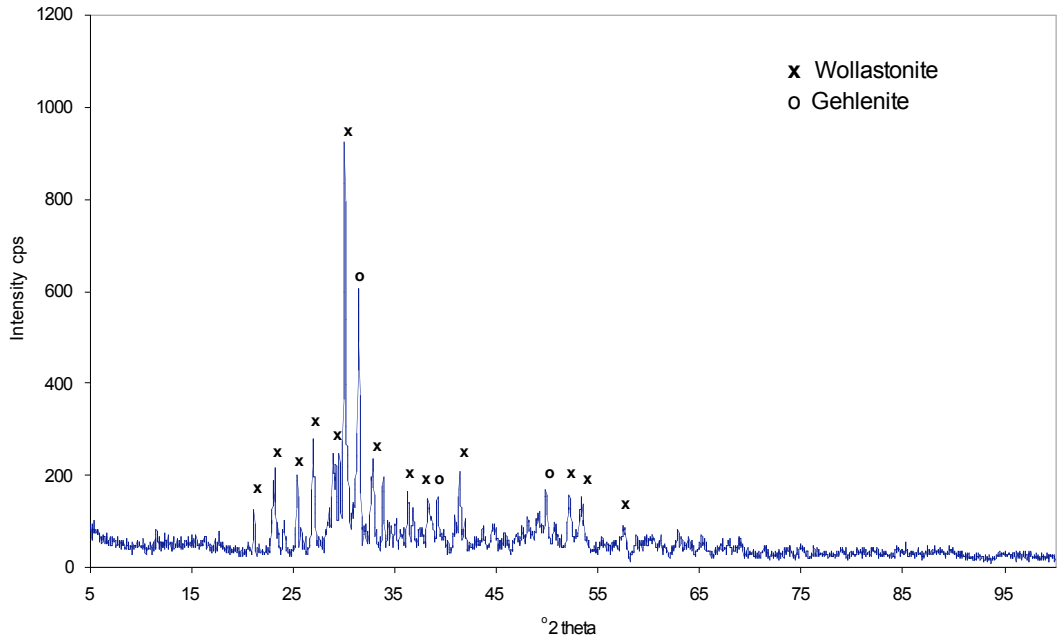


Figure 5-23: XRD pattern showing crystalline phases within glass-ceramic from glass GB6 sintered at 850°C, heating rate:5°C/min, hold time: 2hrs.

The main crystalline phases present in the glass-ceramic produced from glass GB6 were wollastonite and gehlenite, as determined by XRD (Figure 5-23). This was expected as the same phases were formed within the sintered material produced from WAPC residue, EP dust and glass cullet. This is desirable as the phases had previously been seen to offer properties suitable for exploitation such as high hardness, density and fine microstructure (section 4.3).

5.8 Bulk crystallisation

Glass GB6 showed a capability to crystalise in bulk as well as in powdered form. The DTA trace (Figure 5-24) of glass GB6 shows well defined exothermic peaks of

crystallisation for powdered and bulk samples occurring at approximately 800^{o}C and 1000^{o}C, respectively.

5.8.1 Nucleation and crystallisation analysis of glass GB6

The short hold time of 15 minutes allowed for the observation of the stages of nucleation and crystallisation and to investigate the influence of temperature on these stages. Figure 5-25 shows a digital macrograph of bulk GB6 samples after thermal treatment at temperatures of 850^{o}C, 900^{o}C and 1000^{o}C (15 minute hold at temperature). The upper row shows the cross sections of fractured samples whilst the lower row shows the outer surfaces. The varying degree of devitrification at the different temperatures can be observed with the naked eye. Figure 5-25 in combination with Figure 5-26 elucidates the process of crystallisation for parent glass GB6. At 850^{o}C it is clearly visible that surface crystallisation has commenced from the outer surface, progressing inwards. The inner part of the sample appears to the eye to be glassy.

5.9 Microstructure of bulk glass-ceramic

SEM images (Figure 5-26 a-c) of polished surfaces of the glass-ceramic show that nucleation has commenced within the bulk of the specimen. Spherulitic growth of small primary crystals near the surface was also visible (Figure 5-26 a). These primary crystal growths are shown in more detail in Figure 5-27, which shows high magnification, polished and etched surfaces of the sample. The crystals formed at

850°C range in size from approximately 5µm to 25µm. Barbieri *et al* observed spherulitic wollastonite crystal phase after bulk crystallisation at 900°C of glass containing fly ash, cullet and other waste additives [129]. However, they determined that psuedowollastonite also formed due to contaminant elements from the incineration residues.

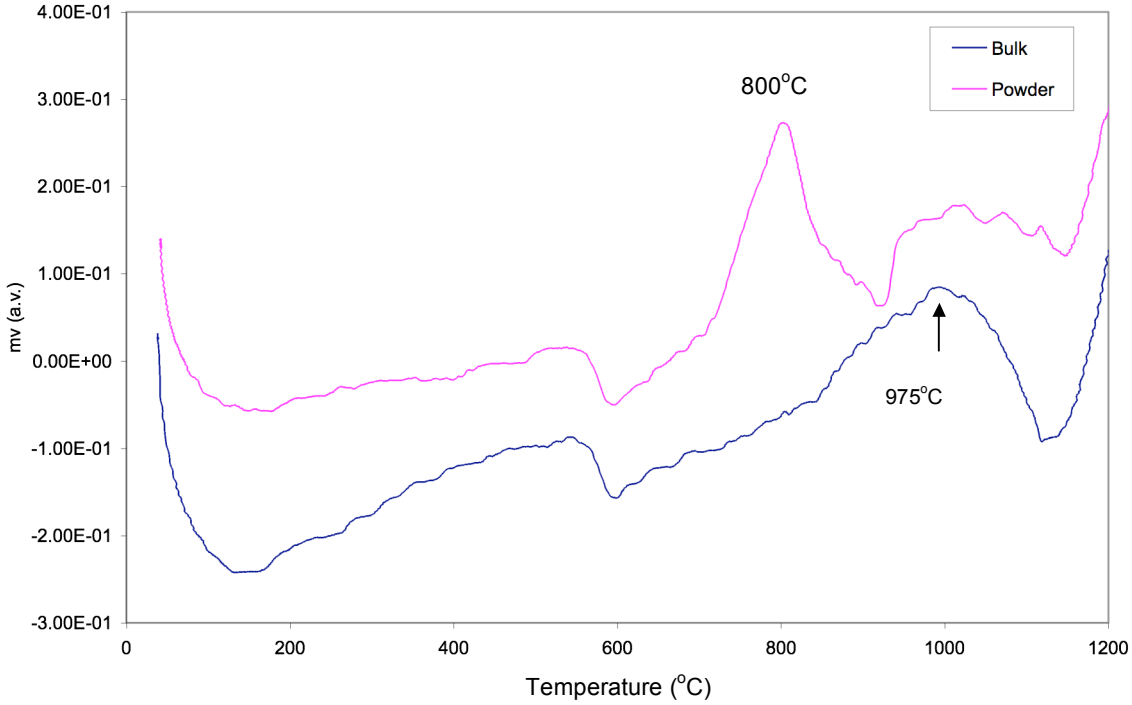


Figure 5-24: DTA traces of powdered and bulk glass GB6 showing crystallisation peaks.

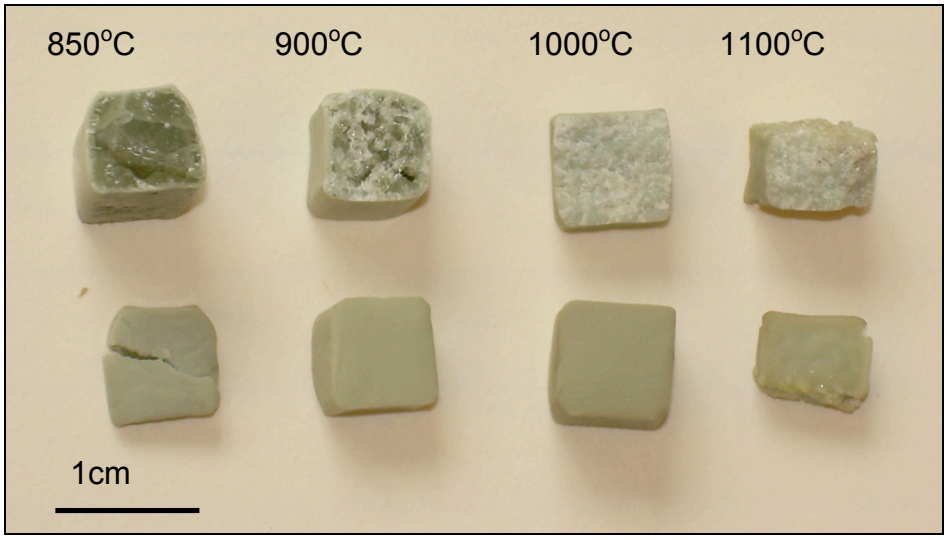


Figure 5-25: Macrograph of bulk glass-ceramics heated at 1°C/min 15 min dwell. Upper row showing internal fracture surfaces, lower row showing external surfaces.

Cracking of the sample was observed due to the incomplete devitrification and the thermal expansion differences of the glass and the crystalline phases. At 950°C a glassy phase is still visible but the crystalline phases make up a higher proportion of the sample. The SEM micrograph shows that the sizes of the crystals within the bulk of the sample have increased. Surface crystallisation has progressed inwards and the crystals have increased in size. At a temperature of 1000°C the sample appears fully crystallised to the eye and the SEM image shows that there is a well-developed crystalline phase. The crystalline phase formed at 1000°C has developed a 'house of cards' structure. Spherulitic and 'house of card' structures are typical of chain silicates, such as wollastonite ($CaSiO_3$) [82].

It can be seen in Figure 5-28 that the crystal phase wollastonite makes up the largest proportion of the crystalline phases formed during the bulk heat treatment of glass

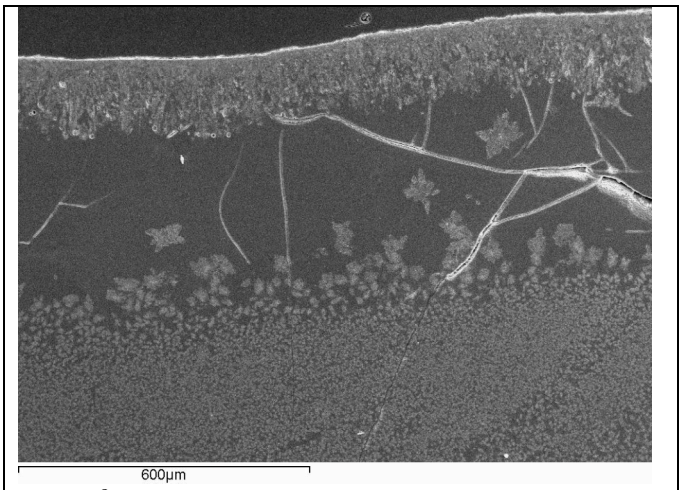
GB6. Gehlenite ($Ca_2Al_2Si_7$) and calcium borate silicate are minor phases formed during the devitrification of glass GB6. The XRD patterns for heat treatment at different temperatures clearly shows the increase in the proportion of crystalline phases relative to the glass phase with increasing temperature. At 1100^oC the crystalline phases began to melt and the sample became deformed as visible in Figure 5-25. Glass-ceramics containing wollastonite or gehlenite have been produced from incineration fly ashes from other countries [37, 130]. Other crystal phases produced in glass-ceramics from incineration fly ashes and APC residues have included diopside and augite [31, 37, 131].

Bulk samples of GB6 glass held at temperature for 1 hour at 850^oC and 900^oC did not exhibit any marked difference in appearance or crystallinity compared to those held at temperature for 15 minutes and so dwell times were increased to 4 hours. However, polygonal, almost cubic crystals were visible in glass-ceramic samples treated at 1000^oC for 1 hour (Figure 5-29). Samples held at temperature for 4 hours appeared to be fully crystallised to the naked eye and when analysed by SEM (Figure 5-30). The cubic shaped crystals were, as before, only observed in the samples heat treated at 1000^oC for 1 hour or more but were well formed and defined compared to samples held for 1 hour. The polygonal crystals when observed in their earlier stage of development, after 1 hour at temperature, tended to originate from the centre of the spherulitic formations (Figure 5-29). This suggests that the spherulitic crystals, which form more rapidly at a lower temperature, may have provided a nucleation point for the secondary tetragonal crystal phase, gehlenite with a cubic appearance. A similar phenomenon was observed by, Rincon, Romero and Boccaccini [33], who identified pyroxene and spinel as main crystal phases in a waste derived glass-ceramic. Mapping

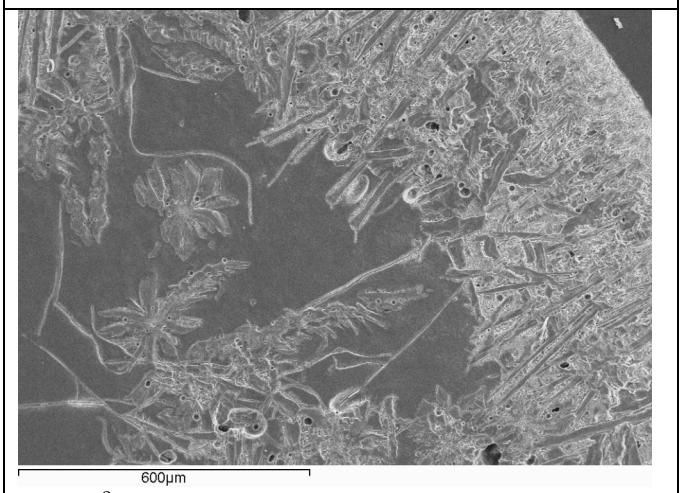
and point analysis of the surfaces of the sample using EDX techniques (Figure 5-31) showed that the cubic crystal phase is a calcium aluminate silicate, identified by XRD as gehlenite.

It is possible that the crystal phase could be attributed to the calcium borate silicate as it is not possible to detect boron with EDX techniques. However, a bulk glass-ceramic produced from fly ash by Karoly et al observed that although gehlenite was detected in samples formed below 1000^{o}C, above 1000^{o}C large easily distinguished areas of gehlenite formed [132]. EDX analysis also indicated that elemental substitutions had occurred for Zn, Na, Fe, Mg in the gehlenite phase. Incorporation of elements including Mg, Zn, Fe and Ti into a gehlenite phase has also been observed in a glass-ceramic produced from a Korean fly ash via bulk crystallisation by Kim and Kim [37].

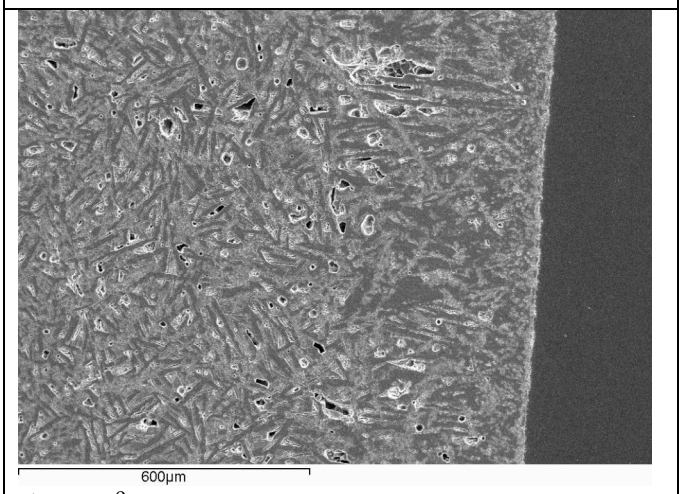
It was found that the wollastonite phase did not contain any elemental substitutions when analysed by EDX point analysis. Some smaller unevenly shaped crystal phases were observed in relatively lesser amounts between some of the wollastonite 'blades' (Figure 5-31). These crystalline phases were also calcium aluminate silicates but they also contained Ti and K as well as Fe, Zn, Mg and Na as detected in the other gehlenite phase by EDX.



a) 850°C



b) 900°C



c) 1000°C

Figure 5-26: SEM micrographs of the glass-ceramic heated to 850°C, 900°C and 1000°C, 15 minute dwell (polished surfaces) magnification x100.

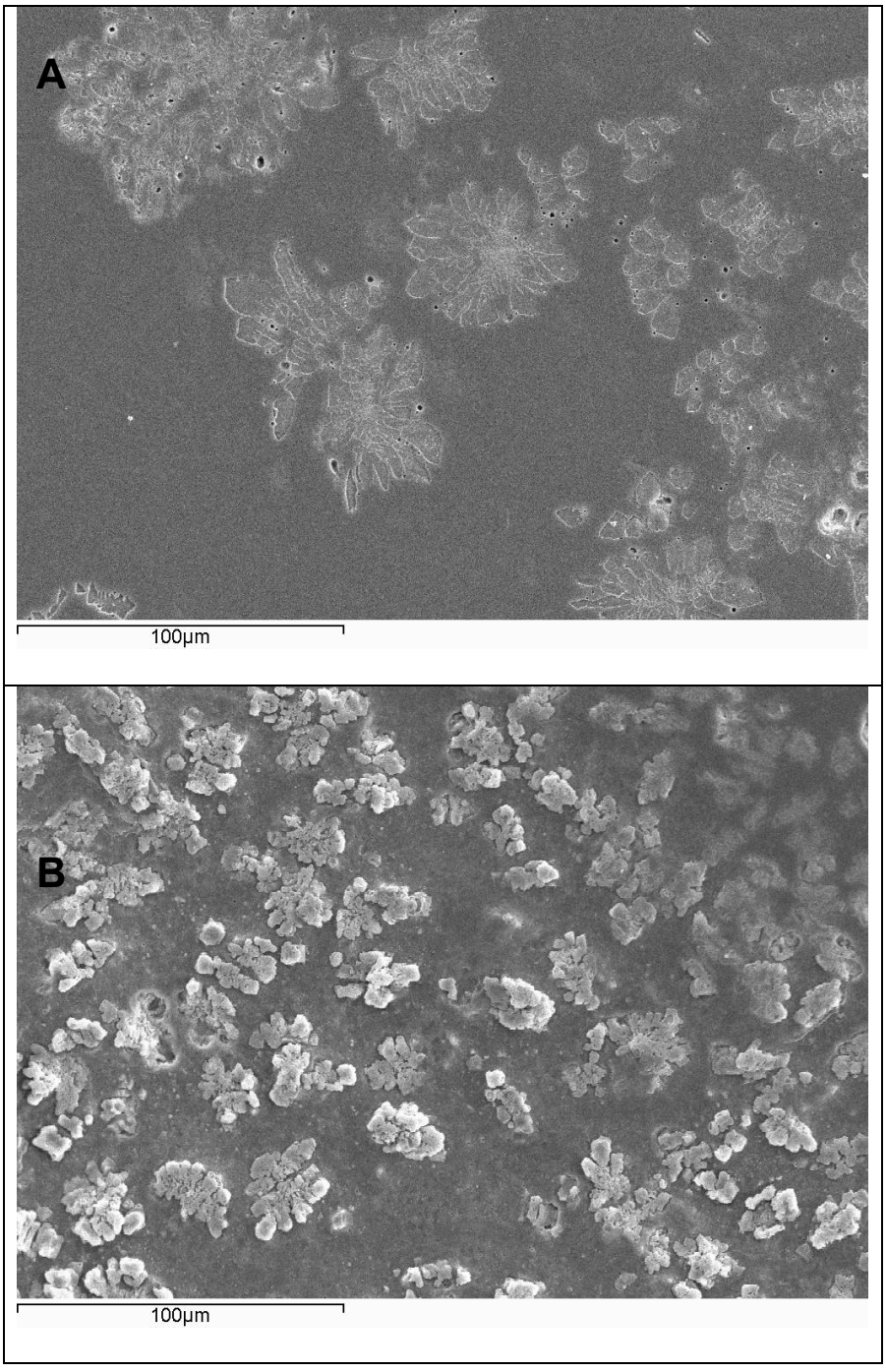


Figure 5-27: SEM micrographs showing the crystalline phase forming in the glass-ceramic, heat treated at 850°C. A) polished surface B) polished and HF acid etched, magnification x500.

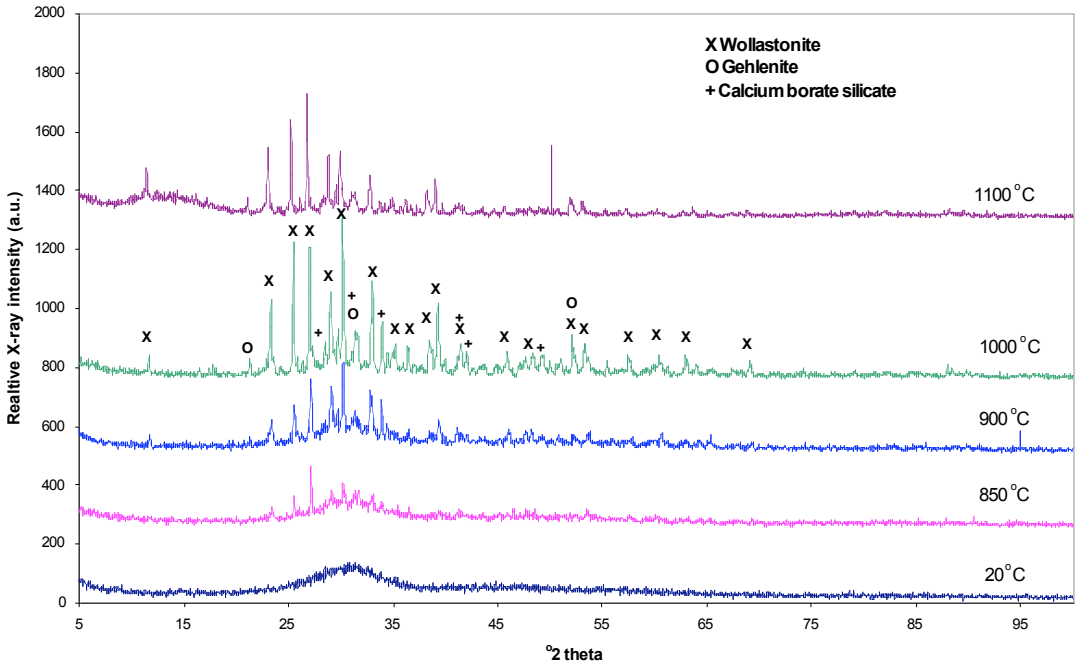


Figure 5-28: XRD patterns of glass GB6 after heat treatment at indicated temperatures with a heating rate of 1°C/minute for a hold time of 15 minutes.

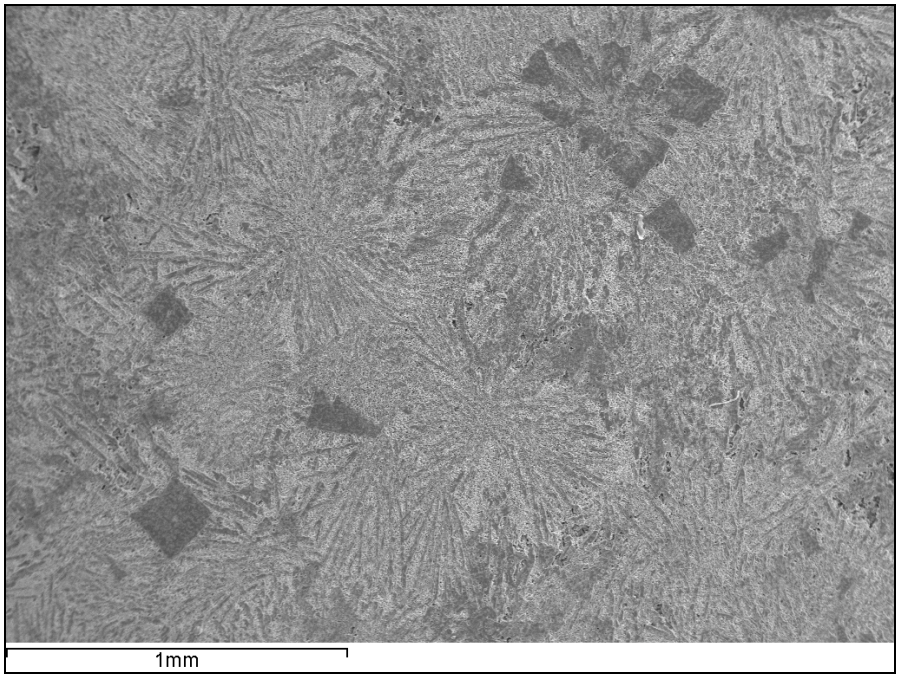


Figure 5-29: Secondary electron micrograph of the bulk glass-ceramic heat treated at 1000°C for 1 hour.

At a higher magnification (Figure 5-31) it was observed that the spherultic crystal phase, identified as wollastonite, was penetrating the cubic crystal phase and there was what appeared to be phase separation within the boundaries of the cube shaped phase. EDX point analysis was able to detect three different element spectrums. Figure 5-31 shows the polished cross section of the bulk glass-ceramic sample treated at 1000^{o}C for 4 hours also showing the EDX point analysis sites.

Figure 5-32 (A) shows a backscattered electron SEM micrograph of a polished surface section of the bulk glass-ceramic sample. Large, elongated wollastonite crystals are visible radiating from a central point towards the bottom of the micrograph. At this point there is an area of residual glass phase. EDX spectrum point analyses were carried out at two points labelled on the image (Figure 5-32 (B)). For each spectrum the unlabelled peaks correspond to gold as a gold coating was used to improve image quality, as it was known not to overlap or interfere with the elements of interest within the sample. Spectrum 1 indicates that the glass phase has been depleted of most of its original elements but is rich in calcium and silicon with lesser amounts of fluorine and chlorine. No chlorine or fluorine peaks were detected in spectrum 2, nor the EDX analyses made in Figure 5-31. This suggests that the chlorine and fluorine were immobilised within the glass matrix. Other elements, including heavy metals were incorporated, by substitution, into the gehlenite phase.

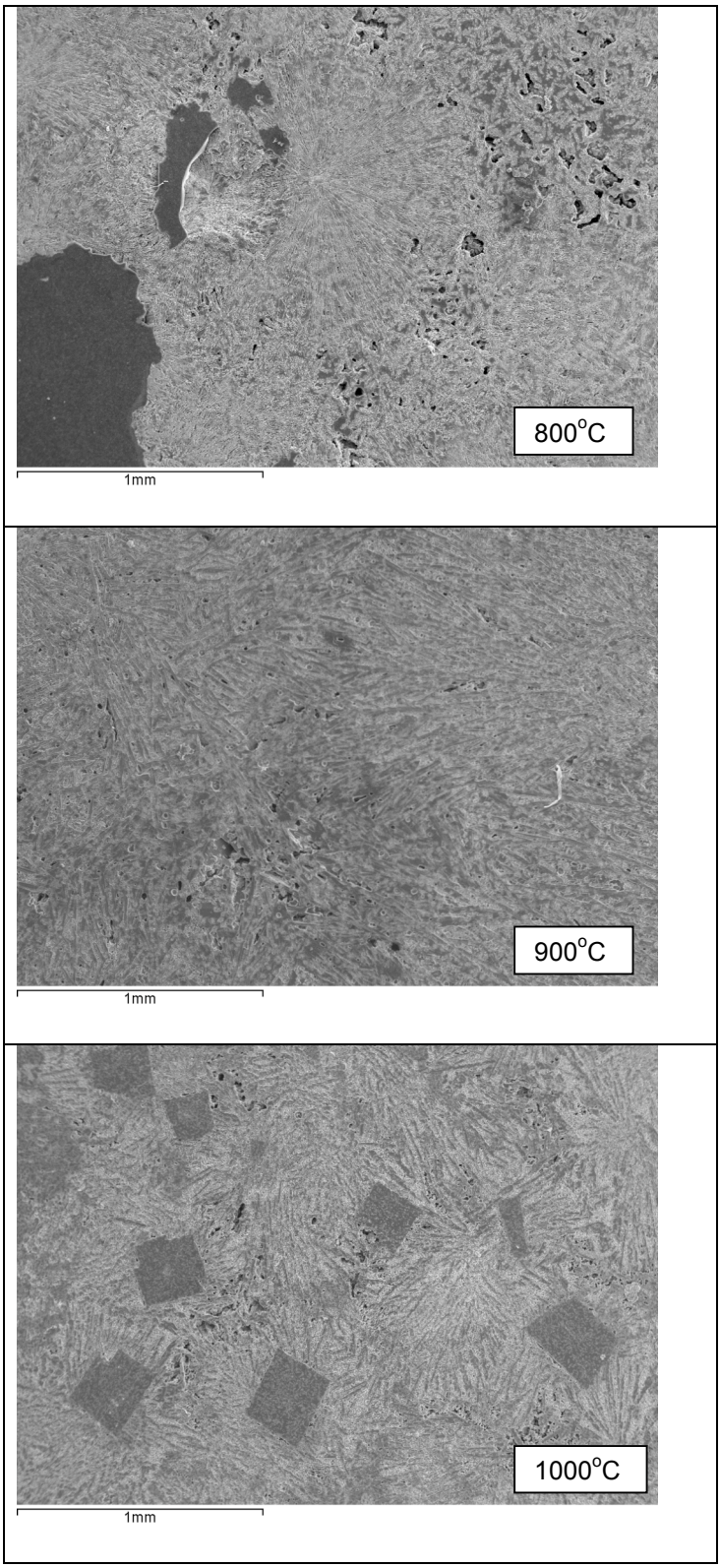
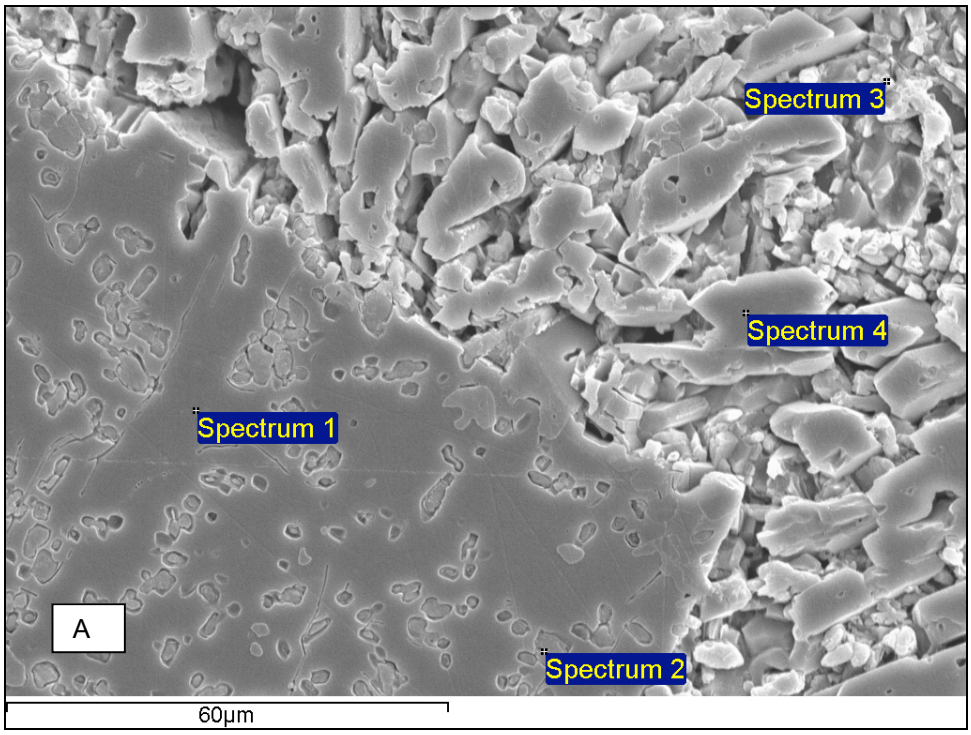
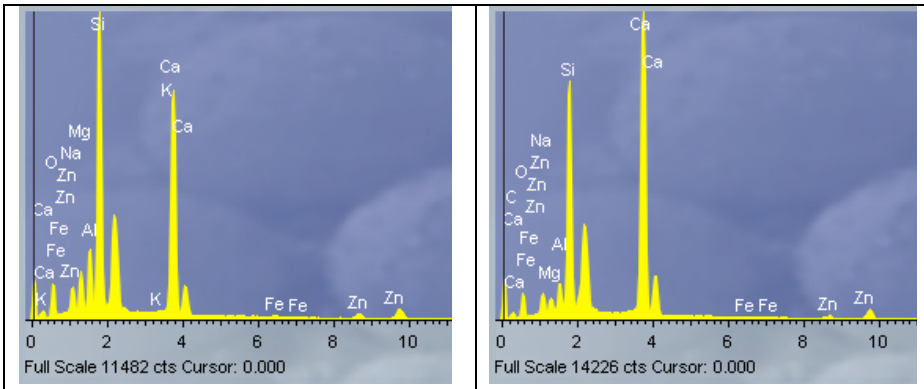


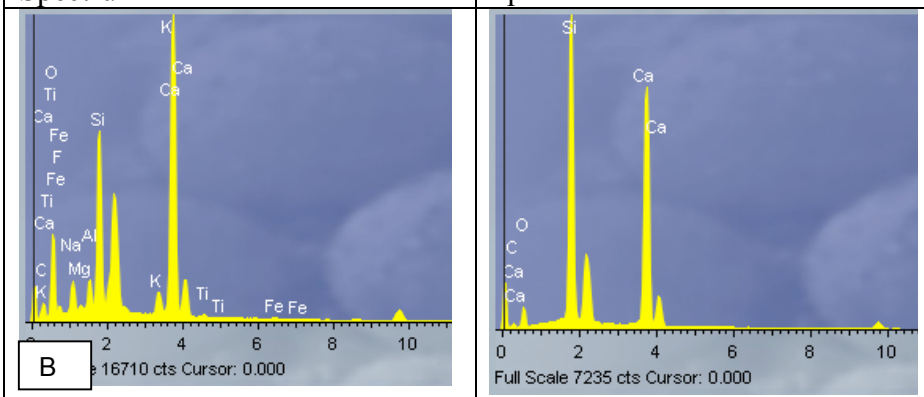
Figure 5-30: SEM micrographs of polished surfaces of the bulk glass-ceramic heat treated at stated temperatures for 4 hours (x50) showing the effect of temperature on crystalline morphology.





Spectrum 1

Spectrum 2



Spectrum 3

Spectrum 4

Figure 5-31: Secondary electron SEM micrograph showing the polished surface of a glass-ceramic treated at 1000°C for 4 hours (A) showing positions of EDX point analysis (B).

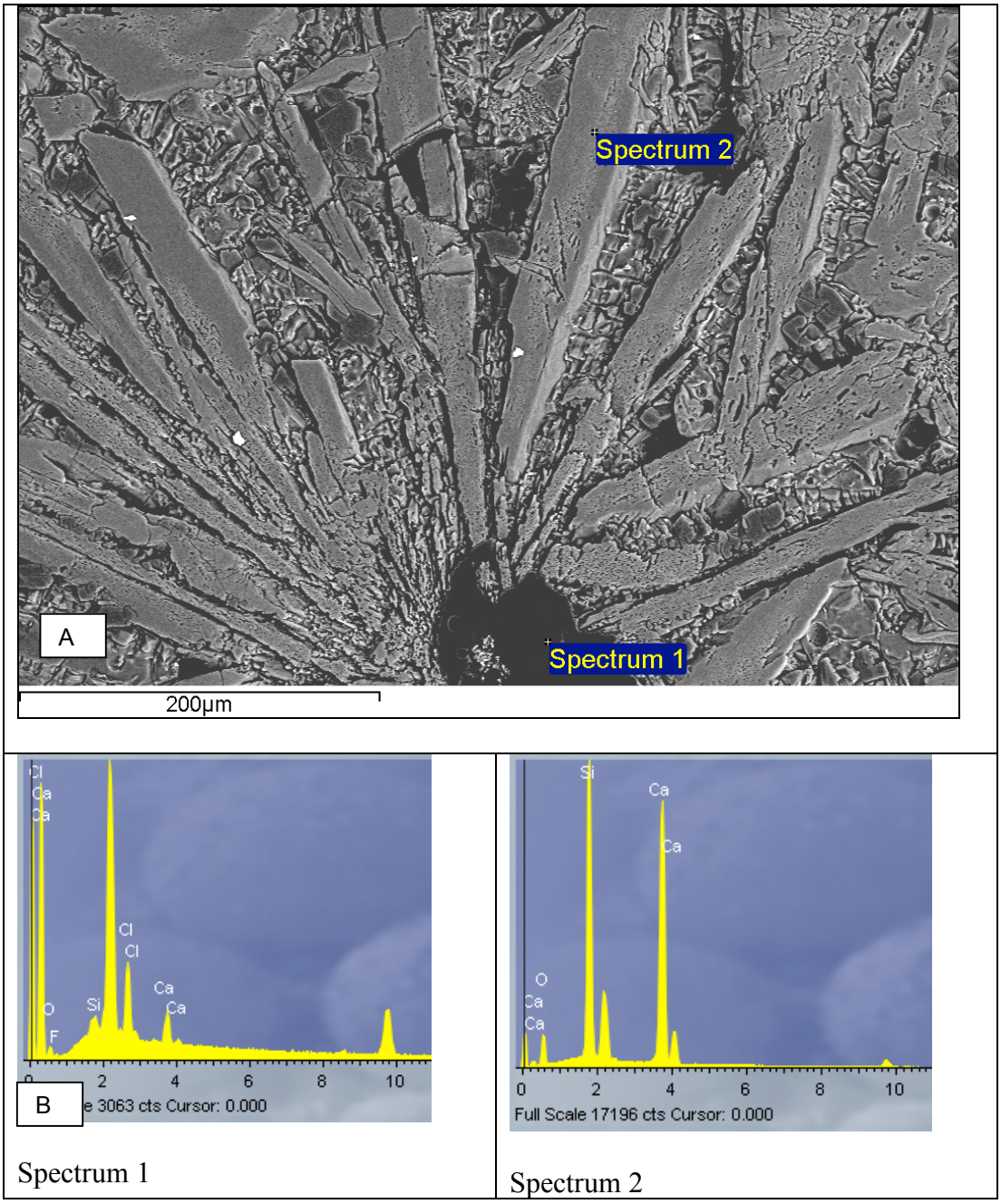


Figure 5-32: Backscattered SEM micrograph of bulk glass-ceramic (1000°C) (A) showing EDX point analysis and associated element spectrums (B).

5.10 Mechanical and physical properties

5.10.1 Microhardness

Vicker's microhardness testing was the only mechanical test carried out on polished samples of bulk glass-ceramics devitrified at different temperatures.

Table 5-10: Microhardness values for bulk glass-ceramics.

	800°C	900°C	1000°C
Microhardness (GPa)	4 [1]	4 [1]	4 [1]

Standard deviations in parenthesis.

The microhardness values were seen to remain constant regardless of heat treatment temperature (Table 5-10), with a value of 4GPa for the optimum temperature for devitrification of 1000°C. All samples, regardless of temperature, exhibited large standard deviations. It was observed that the highest individual microhardness values were obtained from the cubic gehlenite crystals (1000°C) and the large bladed wollastonite crystals (900°C and 1000°C). Measurement indentations that fell between these areas produced lower values and led to the wide variation of data. At 800°C devitrification was incomplete, with areas of glassy phase and finer bladed wollastonite crystal formation. This meant that high hardness values from indentations made on the large crystals were less likely to occur.

5.10.2 Density and porosity

The true density of the bulk glass-ceramic heat treated at 1000°C for 4 hours, as measured by pycnometry, was 2930 $kg.m^{-3}$, with a porosity of 4%. Some porosity was expected due to the crystalline phases having a more ordered structure than the parent glass. The low level of porosity is visible in Figure 5-30. The density is comparable to that of bulk glass-ceramics produced from coal fly ash with and without the addition of silicate waste, possessing densities of 3320 $kg.m^{-3}$ and 2710 $kg.m^{-3}$, respectively [104].

5.11 Chapter Summary

It was possible to incorporate up to 60wt% WAPC residues combined with glass cullet to produce a silicate glass at 1400°C. The addition of 30wt% EP dust to the glass batch mix led to improved mechanical and physical properties of the glass (labelled GB6), which compared favourably to similar glasses from wastes.

Leach testing showed that glass GB6 stabilised the WAPC residues. It was also confirmed (by heat treating different WAPC residues) that the batch mix for glass GB6 can be used to produce glass from APC residues sourced from different UK EfW facilities.

It was possible to produce a sintered glass-ceramic exhibiting isotropic shrinkage behaviour and good densification from the parent glass at a temperature of 850°C. The sintered glass-ceramic consisted of wollastonite and gehlenite phases with elemental

substitution occurring in the gehlenite phase. Elements were stabilised within the glass-ceramic, being resistant to leaching.

TEM analysis indicated that phase separation within the glassy phase of the sintered glass-ceramic had occurred. The optimised glass-ceramic possessed good mechanical properties (Hv=4GPa, E= 70GPa and bending strength = 64MPa) making it a candidate for use as a building material, e.g. for floor and wale tile manufacturing.

A further, limited investigation showed that a bulk glass-ceramic could be produced from Glass GB6 at a temperature of 1000^{o}C. The bulk glass-ceramic contained wollastonite, calcium borate silicate and an elementally substituted gehlenite crystalline phase, which allows incorporation of other elements found in APC residues.

This chapter has discussed the production of glasses and glass-ceramics by two different methods from hazardous APC residues in combination with other wastes. A number of other small scale investigations could be carried out in order to more fully understand and exploit the findings of the research project. Suggestions for this are outlined in the next chapter.

6 Conclusions

- This work has successfully demonstrated that it is possible to reuse hazardous APC residues via thermal treatment, based on existing technologies at relatively low temperatures to produce useful materials. The materials produced exhibit physical, chemical and mechanical properties (refer to Table 6-1) that make them candidates for commercial applications.

- Characterisation of APC residues determined that the chemical composition was low in glass forming oxide SiO_2 and rich in glass modifier CaO. Therefore, additives were required to produce a glass or a ceramic material. A combination of glass cullet and EP dust was used as additives to provide a source of SiO_2 and B_2O_3, respectively.

- The addition of borates (as EP dust and Neobor®) is beneficial, lowering processing temperatures whilst enhancing hardness and densification of materials.

- Washing of APC residues was required to remove soluble chlorides. Up to 93% of soluble chlorides were removed by the simple washing procedure at a liquid to solid ratio of 20. The washing procedure permitted thermal treatment of the WAPC residues without emission of chlorine gases.

- A dense sintered material containing wollastonite and gehlenite phases was produced by a powder processing route combining WAPC, cullet and EP dust.

Microstructure analysis showed the presence of Ti-rich nanocrystalline phase and a fine-grained microstructure of low porosity.

- It was determined that the commercial product Neobor® could be used as an alternative source of borate in place of EP dust, to produce a sintered material with high density and hardness, low water absorption, and resistance to leaching. The sintered material was composed of a wollastonite crystalline phase in a glass matrix. A crack deflection mechanism, detected by investigating fracture surfaces indicates the material should possess a high fracture toughness and low brittleness.

- It was possible to incorporate up to 60wt% WAPC residues combined with glass cullet to produce a silicate glass at 1400^{o}C. The addition of borate in the form of 30wt% EP dust (approximately 10wt% B_2O_3) to the glass batch mix led to improved mechanical and physical properties of the glass which compared favourably to similar glasses from wastes. The borate-containing glass was used to produce glass-ceramics as it exhibited the ability to readily devitrify in both powder and bulk form. Leach testing showed that glass GB6 stabilised the WAPC residues.

- The glass batch composition is robust enough to be used to produce glass from APC residues sourced from different UK EfW facilities which is extremely important for the application of the process in a commercial situation.

- It was possible to produce a sintered glass-ceramic, from the parent glass GB6, exhibiting isotropic shrinkage behaviour and good densification at a temperature

of 850^{o}C. The sintered glass-ceramic consisted of wollastonite and gehlenite phases with elemental substitution occurring in the gehlenite phase. Elements were stabilised within the crystalline phases of the glass-ceramic, being resistant to leaching which is critical for commercial use or disposal. The optimised glass-ceramic possessed good mechanical properties (Hv=5GPa, E= 70GPa and bending strength = 65MPa) making it a candidate for use as a construction material, e.g. for floor and wall tile manufacturing.

- A bulk glass-ceramic was produced from Glass GB6 at a temperature of 1000^{o}C. Surface and bulk nucleation mechanisms were observed during devitrification. The bulk glass-ceramic contained wollastonite, calcium borate silicate and an elementally substituted gehlenite crystalline phase that allowed incorporation of other elements found in the APC residues. This effect is considered relevant in terms of the chemical durability of the material.

- This research provides an excellent stepping-stone towards the use of APC residues, providing a solution to the problem of disposal in hazardous landfill and permanent storage.

Table 6-1: Summary of properties of the products produced from thermal treatment of APC residues in combination with other wastes.

	Material				
Property	Sintered material SB2	Sintered material containing Neobor	Glass GB6	Sintered glass-ceramic	Bulk glass-ceramic
Bulk density $kg.m^{-3}$	2600	2300	2800	2600	2800
True density $kg.m^{-3}$	-	2800	2800	3000	2900
Porosity %	-	18	0	14	4
Hardness GPa	4.5	5.4	6	5	4
Modulus of rupture MPa	-	-	65	65	-
Young's modulus GPa	-	-	83	70	-
Fabrication temperature ^{o}C	950	1150	1400	850	1000

7 Further Work

In the following paragraphs recommendations are made for further work that could be carried out to support the findings in this research project. Some recommendations may be suitable as individual small-scale projects.

7.1 Optimisation of APC residue washing pre-treatment

The washing pre-treatment of APC residues is an essential process in the formation of sintered or vitreous materials to avoid harmful gaseous emissions. However, it would be of benefit to further investigate optimisation of the washing treatment or an alternative process capable of producing equal or better extraction of soluble phases from the APC residues with a reduction in the water required. This is of importance as the washing procedure in itself produces a secondary waste stream, which requires minimisation. An evaporation process of the wash water could be investigated to recover the dissolved salts for storage or use in other applications. It may be possible to encapsulate the chloride-containing salts (potassium chloride, sodium chloride and calcium chloride) in a sintered material (or combination of materials) which should sinter at a temperature below their temperature of decomposition (approximately 770^{o}C). Another option would be to store the salts in unused salt mines, as already used for wastes such as APC residues. This approach is obviously less desirable than reuse however this process would result in a large volume reduction (60wt%) in the fraction of APC residue being disposed of.

7.2 Large scale production

A future step would be to scale up the processes to assess the potential of producing larger volumes of material. Problems can occur when larger quantities of glass and glass-ceramics are produced which may not be foreseen without testing, such as changes in melting behaviour of the glass and problematic pressing of powder compacts. Defects may also become more apparent in larger samples such as non-homogenous glass-ceramic microstructures, microcracks and shape distortion.

Issues related to the social acceptance of the products need to be addressed. In this regard, cell culture and toxicity investigations, beyond the classical chemical leaching tests, must be carried out in order to certify the safety of the materials, which will be in direct contact with humans.

7.3 Mechanical properties of sintered material containing Neobor®

The sintered materials produced from waste powders with the addition of Neobor® possessed promising physical and mechanical properties that make it a candidate for exploitation as a building material. Further characterisation is required to fully assess its suitability as a building material. Suggested tests would include; wear resistance, bending strength, Young's modulus, fracture strength and compressive strength. Other applications of the materials, e.g. for fabrication of wear or abrasion resistant components, are possible due to the hardness values achieved, and should be considered.

7.4 Porous aggregate

During the powder sintering experimentation a spherical, highly porous sintered material was produced with a bulk density of 1200 $kg.m^{-3}$. The material was not investigated further as a dense, sintered material of low porosity was the desired aim of the present research project. However, the porous material would be of interest for use as a lightweight aggregate such as Lytag® produced from sintered fly ash for applications in concrete and as filler. Optimisation of the sintering process could be carried out with an assessment of reproducibility and leaching analysis.

7.5 The use of glass in solid oxide fuel cell technology

Preliminary investigations were made into the use of glass GB6 as a potential seal between the anode and electrolyte layer within a solid oxide fuel cell. Crofer steel has a thermal expansion coefficient of $11.2x10^{-6}$ 1/°C whilst the nickel oxide layer has a value of $13x10^{-6}$ 1/°C. Therefore, the sealant material that joins these two layers should possess a thermal expansion coefficient that lies between the two values, in order to prevent their disassociation during heating and cooling which could occur due to large thermal expansion coefficient mismatch. A glass derived from a waste will not have a composition that will remain consistent enough for application in a precision application such as a fuel cell however; the chemical composition of Glass GB6 could be used to produce a similar glass of consistent composition from pure chemicals.

7.6 Thermal shock of glass and glass-ceramics

The optimised glass, GB6 and the glass-ceramic produced from it by powder sintering could potentially be used in applications involving fluctuations in temperature. Thermal shock resistance tests would give valuable information of the working environment that the glass-ceramic can withstand without a detrimental effect on its strength. Thermal cycling investigation would also be of value for assessing the suitability of the materials for a range of applications involving hot oxidising environments (e.g. hot air).

7.7 Economic viability of processes and large scale production trials

The research has shown that useful materials can be produced from hazardous problematic waste at the lab scale. The methodologies developed in this research project are based on well-established technologies but it is important that the economic viability is determined as thermal processes are energy intensive and involve high cost. The cost of the processing must be below a certain boundary otherwise it would price the product out of its intended market. Nevertheless in the cost/viability calculation, also issues related to the environmental and economic benefit of fabricating products from waste, e.g. diverting it from landfill, must be included.

References

1. McMillan, P.W., *Glass-Ceramics*. 2nd ed. 1964, London & New York: Academic Press Inc.
2. Defra. *Municipal waste management statistics 2007/08*. [Website] 2007/08 6 November 2008 [cited 2009 20 March 2009]; Available from: http://www.defra.gov.uk/environment/statistics/wastats/archive/mwb200708_statsrelease.pdf.
3. Defra. *Municipal waste management survey 2002/03*. [Website] 2004 11 August 2004 [cited 2005 4 March 2005]; Available from: http://www.defra.gov.uk/environment/statistics/wastats/mwb0203/index.htm.
4. Tchobanoglous, G., H. Theisen, and S.A. Vigil, *Integrated Solid Waste Management*, in *Civil Engineering*, B.J. Clark, Morriss, J. M., Editor. 1993, McGraw-Hill Book Co. p. 361-540.
5. ESA. *Environmental Services Association*. [Web page] 2005 [cited 2005 July 2005]; Web site]. Available from: http://www.esauk.org/.
6. Environment Agency. *Environment Agency Web site*. 2007 unknown [cited 2008 15 November 2008]; Available from: http://www.environment-agency.gov.uk/.
7. Environmental Services Association. *Draft APC Residue Case Study*. [cited 2005 March 2005]; Available from: http://www.defra.gov.uk/environment/waste/hazforum/pdf/hwf-3-5iv.pdf.
8. DEFRA. *Landfill Directive Briefing Paper*. 2005 19 July 2005 [cited 2005 15 November 2005]; Available from: http://www.defra.gov.uk/environment/waste/topics/landfill-dir/pdf/landfilldir.pdf.
9. *Landfill Directive*, in *(1999/31/EC)*. 1999.
10. *European Waste Catalogue*, in *(2000/532/EC)*. 2000.
11. Environment Agency. *Environment Agency Web site*. 2005 unknown [cited 2005 15 November 2005]; Available from: http://www.environment-agency.gov.uk/.
12. *Directive 2008/98/EC of the European parliament and of the Council of 19 November 2008 on waste and repealing certain Directives* E. Parliament, Editor. 2008, Official Journal of the European Union.
13. Rani, A.D., A.R. Boccaccini, D. Deegan, and C.R. Cheeseman, *Air pollution control residues from waste incineration: Current UK situation and assessment of alternative technologies.* Waste Management, 2008. **28**(11): p. 2279-2298.
14. Environment Agency. *Waste Data Update 2006*. 2006 [cited 2008 26th October 2008]; Available from: www.environment-agency.gov.uk/wastedata2006.
15. Williams, P.T., *Waste Treatment and Disposal*. 1998, John Wiley & Sons Ltd.
16. Porteous, A., *Energy from Waste: A Wholly Acceptable Waste-management Solution.* Applied Energy, 1997. **58**(4): p. 177-208.
17. Denison, R.A. and J. Ruston, in *Recycling and Incineration: Evaluating the Choices*. 1990, Environmental Defense Fund Inc. p. 58-64, 201-212.

18. Environmental Services Association. *Legislation and Policy*. [Website] 2005 unknown [cited 2005 15 November 2005]; Available from: http://www.esauk.org/waste/legislation/.
19. DEFRA. *EC Directive on Promotion of Cogeneration (Combined Heat and Power) in the Internal Energy Market*. 2005 10 January 2005 [cited 2005 15 November 2005]; Available from: http://www.defra.gov.uk/environment/energy/internat/ec-cogen.htm#1.
20. South East London Combined Heat and Power. *Website*. 2005 [cited 2005 23rd May 2005]; Available from: www.SELCHP.com.
21. SELCHP, *Welcome to SELCHP - Recovering energy from waste*. p. 12.
22. Abanades, S., G. Flamant, B. Gagnepain, and D. Gauthier, *Fate of heavy metals during municipal solid waste incineration.* Waste Management & Research, 2002. **20**(1): p. 55-68.
23. Sakai, S., S.E. Sawell, A.J. Chandler, T.T. Eighmy, D.S. Kosson, J. Vehlow, H.A. vanderSloot, J. Hartlen, and O. Hjelmar, *World trends in municipal solid waste management.* Waste Management, 1996. **16**(5-6): p. 341-350.
24. Van Gerven, T., D. Geysen, L. Stoffels, M. Jaspers, G. Wauters, and C. Vandecasteele, *Management of incinerator residues in Flanders (Belgium) and in neighbouring countries. A comparison.* Waste Management, 2005. **25**(1): p. 75-87.
25. Sakai, S. and M. Hiraoka, *Municipal solid waste incinerator residue recycling by thermal processes.* Waste Management, 2000. **20**(2-3): p. 249-258.
26. Appendino, P., M. Ferraris, I. Matekovits, and M. Salvo, *Production of glass-ceramic bodies from the bottom ashes of municipal solid waste incinerators.* Journal of the European Ceramic Society, 2004. **24**(5): p. 803-810.
27. Cheeseman, C.R., S. Monteiro da Rocha, C. Sollars, S. Bethanis, and A.R. Boccaccini, *Ceramic processing of incinerator bottom ash.* Waste Management, 2003. **23**(10): p. 907-916.
28. Kula, I., A. Olgun, V. Sevinc, and Y. Erdogan, *An investigation on the use of tincal ore waste, fly ash, and coal bottom ash as Portland cement replacement materials.* Cement and Concrete Research, 2002. **32**(2): p. 227-232.
29. C-Tech Innovation, *Thermal Methods of Municipal Waste Treatment*. 2003.
30. Boccaccini, A.R., J. Schawohl, H. Hern, B. Schunck, J.M. Rincon, and M. Romero, *Sintered glass ceramics from municipal incinerator fly ash.* Glass Technology, 2000. **41**(3): p. 99-105.
31. Boccaccini, A.R., M. Kopf, and W. Stumpfe, *Glass-Ceramics from Filter Dusts from Waste Incinerators.* Ceramics International, 1995. **21**(4): p. 231-235.
32. Romero, M., J.M. Rincon, R.D. Rawlings, and A.R. Boccaccini, *Use of vitrified urban incinerator waste as raw material for production of sintered glass-ceramics.* Materials Research Bulletin, 2001. **36**(1-2): p. 383-395.
33. Rincon, J.M., M. Romero, and A.R. Boccaccini, *Microstructural characterisation of a glass and a glass-ceramic obtained from municipal incinerator fly ash.* Journal of Materials Science, 1999. **34**(18): p. 4413-4423.
34. Barbieri, L., A. Corradi, I. Lancellotti, G.C. Pellacani, and A.R. Boccaccini, *Sintering and crystallisation behaviour of glass frits made from silicate wastes.* Glass Technology, 2003. **44**(5): p. 184-190.
35. ESA. *Environmental Services Association*. [Web page] 2008 [cited 2008 November 2008]; Web site]. Available from: http://www.esauk.org/.

36. Environment Agency. *Hazardous Waste - Brief Guide. Air Pollution Control Residues*. [cited 26th October 2008]; Available from: http://www.environment-agency.gov.uk/commondata/acrobat/hw_bg_apc_fnl_850520.pdf.
37. Kim, J.M. and H.S. Kim, *Glass-ceramic produced from a municipal waste incinerator fly ash with high Cl content.* Journal of the European Ceramic Society, 2004. **24**: p. 2373-2382.
38. Geysen, D., C. Vandecasteele, M. Jaspers, and G. Wauters, *Comparison of immobilisation of air pollution control residues with cement and with silica.* Journal of Hazardous Materials, 2004. **107**(3): p. 131-143.
39. Quina, M.J., J.C.M. Bordado, and R.M. Quinta-Ferreira, *Treatment and use of air pollution control residues from MSW incineration: An overview.* Waste Management, 2008. **28**: p. 2097-2121.
40. Lewis, P., C. Dimech, Editor. 3rd November 2005, SELCHP. p. Email.
41. Defra. *Draft APC Residue Case Study*. [cited 2005 March 2005]; Available from: http://www.defra.gov.uk/environment/waste/hazforum/pdf/hwf-3-5iv.pdf.
42. Grundon. 2007 May 2007 [cited 208 November 2008]; Customer Information]. Available from: http://www.grundon.com.
43. Minosus. *Minosus Ltd.* 2008 [cited 2008 November 2008]; Available from: http://www.minosus.co.uk/.
44. Hjelmar, O., *Disposal strategies for municipal solid waste incineration residues.* Journal of Hazardous Materials, 1996. **47**(1-3): p. 345-368.
45. Alba, N., E. Vazquez, S. Gasso, and J.M. Baldasano, *Stabilization/solidification of MSW incineration residues from facilities with different air pollution control systems. Durability of matrices versus carbonation.* Waste Management, 2001. **21**(4): p. 313-323.
46. Barna, R., Z. Rethy, A. Imyim, Y. Perrodin, P. Moszkowicz, and L. Tiruta-Barna, *Environmental behaviour of a construction made of a mixture of hydraulic binders and air pollution control residues from municipal solid waste incineration Part 1. Physico-chemical characterisation and modelling of the source term.* Waste Management, 2000. **20**(8): p. 741-750.
47. Barna, R., Z. Rethy, Y. Perrodin, P. Moszkowicz, and L. Tiruta-Barna, *Environmental behaviour of a construction made of a mixture of hydraulic binders and air pollution control residues from municipal solid waste incineration Part 2. Simulation tests and validation of the source term modelling.* Waste Management, 2000. **20**(8): p. 751-759.
48. Todorovic, M. and H. Ecke, *Demobilisation of critical contaminants in four typical waste-to-energy ashes by carbonation.* Waste Management, 2006. **26**(4): p. 430-441.
49. Lampris, C., J.A. Stegemann, and C.R. Cheeseman, *Solidification/stabilisation of air pollution control residues using Portland cement: Physical properties and chloride leaching.* Waste Management, 2008(Article in Press).
50. Pacific Northwest Pollution Prevention Resource Center, *Stabilized Incineration Residue in Shore Protection Devices*. 1999. p. 2.
51. Rouchotas, E., *Metal removal from air pollution control residues by a water/acid extraction process*, in *Civil and Environmental Engineering*. 2001, Imperial College London.

52. Wang, K.S., K.Y. Chiang, K.L. Lin, and C.J. Sun, *Effects of a water-extraction process on heavy metal behavior in municipal solid waste incinerator fly ash.* Hydrometallurgy, 2001. **62**(2): p. 73-81.
53. Chimenos, J.M., A.I. Fernandes, A. Cervantes, L. Miralles, M.A. Fernandes, and F. Espiell, *Optimizing the APC residue washing process to minimize the release of chloride and heavy metals.* Waste Management, 2005. **25**(7): p. 686-693.
54. Abbas, Z., A.P. Moghaddam, and B.M. Steenari, *Release of salts from municipal solid waste combustion residues.* Waste Management, 2003. **23**(4): p. 291-305.
55. Wexell, D. *Vitrification of Ash from Waste-to-Energy Incinerators, Part II. Cold Crown Melting and Parameters for Scale-up*. [Website database] 1994 September 1999 [cited 2005 05/08/2005]; Available from: http://www.pprc.org/pprc/rpd/statefnd/nyschwm/vitrific.html.
56. Lee, P.H., V. Nasserzadeh, J. Swithenbank, J.V. Laming, J. Goodfellow, C. McLeod, B.B. Argent, D. Lawrence, and N. Garrod, *Sintering of the APC residue from municipal waste incinerators.* Process Safety and Environmental Protection, 1999. **77**(B4): p. 212-218.
57. Hollander, H.I., A.L. Plumley, and R.S. DeCesare, *ASME/US Bureau of Mines investigative program on vitrification of combustion ash residue: Findings and conclusions.* Journal of Hazardous Materials, 1996. **47**(1-3): p. 369-381.
58. Quina, M.J., M.A. Almeida, R.C. Santos, J.C.M. Bordado, and R.M. Quinta-Ferreira, *Prediction of solid waste incineration residues quantity for valorization in lightweight aggregates*, in *Advanced Materials Forum Iii, Pts 1 and 2*. 2006. p. 1731-1735.
59. De Casa, G., T. Mangialardi, A.E. Paolini, and L. Piga, *Physical-mechanical and environmental properties of sintered municipal incinerator fly ash.* Waste Management, 2007. **27**(2): p. 238-247.
60. Menzler, N.H., H. Mortel, R. Weissmann, and V. Balek, *Examination of two glass compositions for the vitrification of toxic products from waste incineration.* Glass Technology, 1999. **40**(2): p. 65-70.
61. Menzler, N.H., H. Mortel, and R. Weissmann, *Comparative studies of the corrosion and long-term stability of vitrified e-filter dust from waste incinerators, granules from high-temperature waste incineration plants and a model glass.* Glass Science and Technology-Glastechnische Berichte, 1999. **72**(8): p. 266-272.
62. Sorensen, M.A., E.P.B. Mogensen, K. Lundtorp, D.L. Jensen, and T.H. Christensen, *High temperature co-treatment of bottom ash and stabilised fly ashes from waste incineration.* Waste Management, 2001. **21**: p. 555-562.
63. Nzihou, A. and P. Sharrock, *Calcium phosphate stabilization of fly ash with chloride extraction.* Waste Management, 2002. **22**(2): p. 235-239.
64. Takeda, D., K. Matusita, and M. Koide, *Thermal properties of CaO-Al2O3-SiO2 glass containing chlorine.* Journal of the Ceramic Society of Japan, 2003. **111**(5): p. 339-342.
65. Donald, I.W., B.L. Metcalfe, and R.N.J. Taylor, *The immobilization of high level radioactive wastes using ceramics and glasses.* Journal of Materials Science, 1997. **32**(22): p. 5851-5887.
66. Metcalf, B.L. and I.W. Donald, *Candidate wasteforms for the immobilization of chloride-containing radioactive waste.* Journal of Non-Crystalline Solids, 2004. **348**: p. 225-229.

67. Donze, S., L. Montagne, G. Palavit, M. Zeyer, and C. Jager, *Structural analysis of the thermal conversion of metal chlorides into phosphate glasses.* Journal of Non-Crystalline Solids, 2000. **263&264**: p. 132-138.
68. Siwadamrongpong, S., M. Koide, and K. Matusita, *Prediction of chloride solubility in CaO-Al2O3-SiO2 glass systems.* Journal of Non-Crystalline Solids, 2004. **347**: p. 114-120.
69. Ikeda, Y., Y. Takashima, H. Kobayashi, and H. Igarashi, *Conversion reactions of metal chlorides into oxides with boric acid - Applicability to the vitrification of molten salt wastes generated in pyro-reprocessing process.* Journal of Nuclear Science and Technology, 1995. **32**(11): p. 1138-1145.
70. Berfeldt, B., K. Jay, H. Seifert, J. Vehlow, T.H. Christensen, D.L. Baun, and E.P.B. Mogensen, *Thermal treatment of stabilized air pollution control residues in a waste incinerator pilot plant. Part 1: fate of elements and dioxins.* Waste Management & Research, 2004. **22**(1): p. 49-57.
71. Weber, R., T. Sakurai, and H. Hagenmaier, *Formation and destruction of PCDD/PCDF during heat treatment of fly ash samples from fluidized bed incinerators.* Chemosphere, 1999. **38**(11): p. 2633-2642.
72. Mizukoshi, H., M. Masui, N. Namiki, J.C. Kim, and Y. Otani, *Suppression of solidification of calcium-rich incinerator fly ash during thermal treatment for decomposition/detoxification of dioxins.* Advanced Powder Technology, 2007. **18**(2): p. 143-154.
73. Ward, D.B., Y.R. Goh, P.J. Clarkson, P.H. Lee, V. Nasserzadeh, and J. Swithenbank, *A novel energy-efficient process utilizing regenerative burners for the detoxification of fly ash.* Process Safety and Environmental Protection, 2002. **80**(B6): p. 317-326.
74. Hsi, H.C. and T.H. Yu, *Evaluation of the leachability of polychlorinated dibenzo-p-dioxins and dibenzofurans in raw and solidified air pollution control residues from municiple waste incinerators.* Chemosphere, 2007. **67**: p. 1434-1443.
75. Hsi, H.C., L.C. Wang, and T.H. Yu, *Effects of injected activated carbon and solidification treatment on the leachability of polychlorinated dibenzo-p-dioxins and dibenzofurans from air pollution control residues of municipal waste incineration.* Chemosphere, 2007. **67**(7): p. 1394-1402.
76. Pfaender, H.G., *Schott Guide To Glass*. 3rd ed, ed. H. Schroeder. 1980, London: Van Nostrand Reinhold Company Inc.
77. Borax Consolidated Limited, *Glasses*. 3rd Ed ed. 1965, London: Borax Consolidated London. 83.
78. Ashby, M.F. and D.R.H. Jones, *Engnering Materials 2: An Introduction to Microstructures, Processing and Design.* 1986, UK: Pergammon Press, Oxford.
79. Holloway, D.G., *The Physical Properties of Glass*, ed. P.S.N. Mott. 1973, London: Taylor & Francis Ltd.
80. Shelby, J.E., *Introduction to Glass Science and Technology*. 2nd ed. 2005, Cambridge: The Royal Society of Chemistry.
81. McColm, I.J., *Chapter 4*, in *Ceramic Science for Materials Technologists.* 1983, Leonard Hill. p. 204-234.
82. Holand, W. and G. Beall, in *Glass-Ceramic Technology*. 2002, The American Ceramic Society, USA. p. 57-72.
83. Callister, W., *Materials Science and Engineering an Introduction*. 1997.

84. Boccaccini, A.R., M. Bucker, J. Bossert, and K. Marszalek, *Glass matrix composites from coal flyash and waste glass.* Waste Management, 1997. **17**(1): p. 39-45.
85. Barbieri, L., I. Lancellotti, T. Manfredini, I. Queralt, J.M. Rincon, and M. Romero, *Design, obtainment and properties of glasses and glass-ceramics from coal fly ash.* Fuel, 1999. **78**(2): p. 271-276.
86. Olgun, A., Y. Erdogan, Y. Ayhan, and B. Zeybek, *Development of Ceramic Tiles from Coal Fly Ash and Tincal Ore Waste.* Ceramics International, 2005. **31**: p. 153-158.
87. Shao, H., K. Liang, F. Peng, F. Zhou, and A. Hu, *Production and properties of cordierite-based glass-ceramics from gold tailings.* Minerals Engineering, 2005. **18**(6): p. 635-637.
88. Catarino, L., J. Sousa, I.M. Martins, M.T. Vieira, and M.M. Oliveira, *Ceramic products obtained from rock wastes.* Journal of Materials Processing Technology, 2003. **143**: p. 843-845.
89. Pisciella, P., S. Crisucci, A. Karamanov, and M. Pelino, *Chemical durability of glasses obtained by vitrification of industrial wastes.* Waste Management, 2001. **21**: p. 1-9.
90. Rozenstrauha, I., J.P. Wu, and A.R. Boccaccini, *Processing of Latvian silicate waste into glass-ceramics by powder technology and sintering.* Glass Technology, 2005. **46**(3): p. 248-254.
91. Yun, Y.H., C.H. Yoon, Y.H. Kim, C.K. Kim, S.B. Kim, J.T. Kwon, B.A. Kang, and K.S. Hwang, *Glass-ceramics prepared by waste fluorescent glass.* Ceramics International, 2002. **28**(5): p. 503-505.
92. Ferreira, C., A. Ribeiro, and L. Ottosen, *Possible applications for municipal solid waste fly ash.* Journal of Hazardous Materials, 2003. **96**(2-3): p. 201-216.
93. Boccaccini, A.R., M. Petitmermet, and E. Wintermantel, *Glass-Ceramics from Municipal Incinerator Fly Ash.* American Ceramic Society, 1997. **Bulletin 76**(11): p. 75-78.
94. Park, Y.J. and J. Heo, *Conversion to glass-ceramics from glasses made by MSW incinerator fly ash for recycling.* Ceramics International, 2002. **28**: p. 689-694.
95. Park, Y.J. and J. Heo, *Vitrification of fly ash from municipal solid waste incinerator.* Journal of Hazardous Materials, 2002. **91**(1-3): p. 83-93.
96. Romero, M., R.D. Rawlings, and J.M. Rincon, *Development of a new glass-ceramic by means of controlled vitrification and crystallisation of inorganic wastes from urban incineration.* Journal of the European Ceramic Society, 1999. **19**(12): p. 2049-2058.
97. Romero, M., R.D. Rawlings, and J.M. Rincon, *Crystal nucleation and growth in glasses from inorganic wastes from urban incineration.* Journal of Non-Crystalline Solids, 2000. **271**(1-2): p. 106-118.
98. Cheng, T.W., *Effect of additional materials on the properties of glass-ceramic produced from incinerator fly ashes.* Chemosphere, 2004. **56**(2): p. 127-131.
99. Karamanov, A., M. Pelino, M. Salvo, and I. Metekovits, *Sintered glass-ceramics from incinerator fly ashes. Part I. The influence of the heating rate on the sinter-crystallisation.* Journal of the European Ceramic Society, 2003. **23**(10): p. 1609-1615.

100. Cheng, T.W., T.H. Ueng, Y.S. Chen, and J.P. Chiu, *Production of glass-ceramic from incinerator fly ash.* Ceramics International, 2002. **28**: p. 779-783.
101. Karamanov, A., M. Aloisi, and M. Pelino, *Sintering Behaviour of a Glass Obtained from MSWI Ash.* Journal of the European Ceramic Society, 2004.
102. Barbieri, L., A. Corradi, and I. Lancellotti, *Bulk and sintered glass-ceramics by recycling of municipal incinerator bottom ash.* Journal of the European Ceramic Society, 2000. **20**: p. 1637-1643.
103. Wu, J.P., A.R. Boccaccini, and R.D. Rawlings, *Glass-Ceramics: Their Production from Wastes. A Review.* Journal of Materials Science, 2006. **41**(3): p. 733-761.
104. Erol, M., S. Kucukbayrak, and A. Ersoy-Mericboyu, *Production of glass-ceramics obtained from industrial wastes by means of controlled nucleation and crystallization.* Chemical Engineering Journal. **In Press, Corrected Proof**.
105. Francis, A.A., R.D. Rawlings, and A.R. Boccaccini, *Glass-ceramics from mixtures of coal ash and soda-lime glass by the petrurgic method.* Journal of Materials Science Letters, 2002. **21**(12): p. 975-980.
106. Rio Tinto Borax. *Rio Tinto Borax website*. [Website] 2004 [cited 2005 18 March 2005]; Available from: http://www.borax.com/.
107. Karasu, B., G. Kaya, and M. Karalar, *Use of concentrator wastes of Etibor Kirka Borax company in soft porcelain opaque glazes as an alternative fluxing agent*, in *Euro Ceramics Viii, Pts 1-3*. 2004. p. 2497-2500.
108. Ediz, N., A. Issi, and H. Yurdakul, *Effect of tincal waste addition to replace silica sand in wall tile production*, in *Euro Ceramics Viii, Pts 1-3*. 2004. p. 2465-2468.
109. Bernardo, E., R. Castellan, and S. Hreglich, *Sintered glass-ceramics from mixtures of wastes.* Ceramics International. **In Press, Corrected Proof**.
110. CERAM. *CERAM Website*. [cited 2006 17th January 2006]; Available from: www.CERAM.co.uk.
111. Dodd, J.W. and K.H. Tonge, *Thermal Methods - Analytical Chemistry by Open Learnings.* 1987, Chichester: John Wiley & Sons.
112. British Standards, *Characterisation of waste - Leaching - Compliance test foe leaching of granular waste materials and sludges - Part 4 One stage batch test at a liquid to solid ratio of 10 l/kg for materials with particle size below 10mm (without or with size reduction)*. 2002.
113. American Water Works Association, *Standard Methods for the Examination of Water and Wastewater*. 21st ed, ed. L.S.C. Andrew D. Eaton, Eugene W. Rice and Arnold E. Greenberg. 2005: American Public Health Association, Water Environment Federation, and American Water Works Association. Baltimore.
114. *The Landfill (England and Wales) (Amendment) Regulations 2005*. 2005: England
Wales.
115. Lundtorp, K., D.L. Jensen, M.A. Sorensen, T.H. Christensen, and E.P.B. Mogensen, *Treatment of waste incinerator air-pollution-control residues with FeSO4: Concept and product characterisation.* Waste Management & Research, 2002. **20**(1): p. 69-79.

116. He, P.-J., H. Zhang, C.-G. Zhang, and D.-J. Lee, *Characteristics of Air Pollution Control Residues of MSW Incineration Plant in Shanghai.* Journal of Hazardous Materials, 2004. **B116**: p. 229-237.
117. Cheeseman, C.R., C.J. Sollars, and S. McEntee, *Properties, microstructure and leaching of sintered sewage sludge ash.* Resources, Conservation and Recycling, 2003. **40**(1): p. 13-25.
118. Tsai, C.-C., K.-S. Wang, and I.-J. Chiou, *Effect of SiO2-Al2O3-flux ratio change on the bloating characteristics of lightweight aggregate material produced from recycled sewage sludge.* Journal of Hazardous Materials, 2006. **134**(1-3): p. 87-93.
119. *Guidance on Sampling and Testing of Wastes To Meet Landfill Waste Acceptance Procedures*, E. Agency, Editor. 2005, Environment Agency.
120. Rawlings, R.D. and F.L. Mathews, *Composite Materials: Engineering and Science*. 1995, Chapman and Hall: London. p. 342-348.
121. Boccaccini, A.R. and V. Winkler, *Fracture surface roughness and toughness of Al2O3-platelet reinforced glass matrix composites.* Composites: Part A, 2002. **33**: p. 125-131.
122. Boccaccini, A.R., *Machinability and Brittleness of Glass-Ceramics.* Journal of Materials Processing Technology, 1997(65): p. 302-304.
123. Park, Y.J., S.O. Moon, and J. Heo, *Crystalline phase control of glass ceramics obtained from sewage sludge fly ash.* Ceramics International, 2003. **29**: p. 223-227.
124. *The Landfill (England and Wales) (Amendment) Regulations 2004*. 2004.
125. Boccaccini, A.R. and P.A. Trusty, *In situ characterisation of the shrinkage behaviour of ceramic powder compacts during sintering by using heating microscopy.* Materials Characterization, 1998. **40**: p. 1-13.
126. Pascual, M., A. Duran, and L. Pascual, *Sintering process of glasses in the system Na2o-B2O3-SiO2.* Journal of Non-Crystalline Solids, 2001(306): p. 58-69.
127. Boccaccini, A.R., W. Stumpfe, D.M.R. Taplin, and C.B. Ponton, *Densification and crystallization of glass powder compacts during constant heating rate sintering.* Materials Science and Engineering A, 1996. **219**(1-2): p. 26-31.
128. Bernardo, E., M. Varrasso, F. Cadamuro, and S. Hreglich, *Vitrification of wastes and preparation of chemically stable sintered glass-ceramic products.* Journal of Non-Crystalline Solids, 2006. **352**(38-39): p. 4017-4023.
129. Barbieri, L., A. Karamanov, A. Corradi, I. Lancellotti, M. Pelino, and J.M. Rincon, *Structure, chemical durability and crystallisation behaviour of incinerator-based glassy systems.* Journal of Non-Crystalline Solids, 2008(354): p. 521-528.
130. Cheng, T.W. and Y.S. Chen, *Characterisation of glass ceramics made from incinerator fly ash.* Ceramics International, 2004. **30**(3): p. 343-349.
131. Erol, M., U. Demirler, S. Kucukbayrak, A. Ersoy-Mericboyu, and M.L. Ovecoglu, *Characterization investigations of glass-ceramics developed from Seyitomer thermal power plant fly ash.* Journal of the European Ceramic Society, 2003. **23**(5): p. 757-763.
132. Karoly, Z., I. Mohai, M. Toth, F. Weber, and J. Szepvolgyi, *Production of glass-ceramics from fly ash using arc plasma.* Journal of the European Ceramic Society, 2007. **27**: p. 1721-1725.

8 Appendix 1

The optimum sintering temperature for pressed powder compacts was determined using a number of test samples at incremental temperatures. A starting temperature of 800^{o}C was used, as this was the lowest processing temperature reported in the literature for thermal treatments of APC residues (refer to Chapter 1, Table 1-3). Powder compacts were sintered at temperatures in increments of 100^{o}C. If samples became deformed due to too high a temperature then no further increase in temperature was necessary. Once the sintering temperature 'window' had been identified increments of 50^{o}C were used to further optimise the sintering temperature. Dwell times at temperature for 1 hour, 2 and 3 hours were used.

Samples were examined upon cooling. Linear and bulk density measurements were taken. Those samples that appeared to be sintered *i.e.* could not be easily crushed by hand or left a powder residue when handled were analysed by SEM to observe the degree of densification and crystal growth. Vickers microhardness measurements were also carried out. Those samples that possessed a desirable combination of appearance, high density, low porosity, high microhardness value were determined to have been sintered at optimum temperature and dwell time.